Molecular Dynamics Simulation of Lead Germanate Glasses

Elham Ghobadi

A Thesis
in
The Department
of
Chemistry and Biochemistry

Presented in Partial Fulfillment of the
Requirements for the Degree of
Doctor of Philosophy (Chemistry) at
Concordia University
Montreal, Quebec, Canada

January 2008

Your file Votre référence
ISBN: 978-0-494-37723-9
Our file Notre référence
ISBN: 978-0-494-37723-9

Abstract

Molecular Dynamics Simulation of
Lead Germanate Glasses

Elham Ghobadi, Ph.D.
Concordia University, 2008

In recent years, there has been a great deal of focus on the development of glass materials with low transmission loss in optical fibers. Although the glass forming ability and efficiency of lead germanate glasses, $PbO.GeO_2$, for such applications have already been established, little is known about the structure of these glasses. Germanate glasses tend to exhibit anomalous properties as a function of their composition, referred to as 'germanate anomaly.' There is a controversy in the literature concerning the dominant coordination of germanium ions in these glasses at different lead oxide compositions and the structural mechanism by which 'germanate anomaly' occurs. In spite of numerous Raman, Infra-red (IR), neutron, and X-ray Absorption Fine Structure (EXAFS) studies of lead germanate glasses, a full understanding of short-range and medium-range order of these glasses is still lacking.

Using Molecular Dynamics (MD) simulation with a two-body potential model, a composition study was performed on $xPbO.(1-x)GeO_2$ glasses with x=0.05-0.50 in order to investigate the structure of the lead

germanate glasses at different lead oxide concentrations. The structural features of the germanate framework and the lead environment are calculated and represented by pair and cumulative distribution functions, ring statistics, bond angle distributions, and percentage of non-bridging oxygens (NBOs) at each lead oxide composition. The results of the MD simulations show no evidence of the germanate anomaly in the simulated lead germanate glasses and indicate that the germanate framework consists predominantly of GeO_4 units. Continuous formation of NBOs is observed with the addition of lead oxide. Through connectivity studies, the presence of a secondary lead framework is predicted.

To further enhance the potential model, lattice dynamics simulation using shell-model and a combination of two- and three-body potential model was used to generate crystal properties of α-quartz-like GeO_2 (infrared frequencies, lattice energy, bulk modulus, elastic constants, static dielectric constants, high frequency dielectric constants, and heat capacity at constant volume). This study suggests that it is possible not only to model, but also to predict various crucial properties of crystals by the use of appropriate potential models and computer modeling codes. The potential was also capable of reproducing the infrared frequencies, and elastic constants of rutile-like GeO_2 crystal.

Acknowledgements

First and foremost, I would like to extend my deepest appreciation and gratitude to my thesis supervisor, Dr. John A. Capobianco for his tireless guidance, support, and patience in this endeavour.

I would like to offer my warmest thanks to the members of my research committee, Dr. Peter H. Bird and Dr. Heidi Muchall for their contributions to this thesis and their continued support.

I wish to express gratitude to Dr. Julian Gale for allowing me to use the GULP code for the lattice dynamics simulations.

I would also like to acknowledge Dr. Robert Kilgour for serving on my thesis examination committee.

Special gratitude is also presented to the external thesis examiner, Dr. Grant S. Henderson, for his time, expertise, and input. I learned a lot from Dr. Henderson during my thesis examination.

Finally, I would like to thank my family and friends for their encouragement, support, and love.

Table of Contents

List of Figures

List of Tables

Chapter 1

1.1 Introduction

Although glass is one of the early materials used in the history of civilization, the scientific research for a long time has paid little attention to these materials due to their higher structural complexity. It is only in recent decades that progress has been made towards developing theories of glasses. This progress has been made possible by the application of theoretical and experimental methods of solid-state physics and chemistry to explain macroscopic properties of glasses on the basis of their molecular structure.

It is important to distinguish between glass and crystal. A perfect crystal exhibits a structure in which the atoms are arranged in periodically repeating groups. Glasses are considered non-crystalline, vitreous or amorphous solids obtained by rapid cooling of molten material. This rapid cooling ensures that a regular crystal lattice does not form.

The volume–temperature relationship involved in crystal and glass formation is illustrated in Figure 1.1.1. The process starts with a liquid at high temperatures (point *A* in Figure 1.1.1). Upon cooling the melt along line *AB*, the volume decreases with constant volumetric thermal expansion coefficient, α_L. The volumetric thermal expansion coefficient represents the

variation of volume with respect to temperature. Crystallization occurs at the melting temperature, T_m, when the rate of cooling is slow enough. Crystallization can further be characterized by a sharp decrease in volume along line *BE* (discontinuous change of α_L) which will undergo additional volume decrease as it is further cooled along line *EF*.

A glass is formed when the melt undergoes supercooling below T_m along the line *BC* (continuous change of α_L). Crystallization does not occur along the line *BC*, since the supercooled system remains liquid below T_m such that the nucleation sites necessary for crystallization are not accessible. As this system is further cooled, its viscosity rises rapidly. At the glass transition temperature, T_g, the material's viscosity has risen to the point that the liquid is unable to establish equilibrium, and a liquid-solid transition occurs. The resulting glassy state has a viscosity greater than 10^{12} poise [1] and is resistant to deformation.

Formation of a crystal is thermodynamically controlled and is energetically more favoured over the melt below T_m. On the other hand, formation of a glass is kinetically controlled. In this case, the glass does not have the required kinetic energy to pass over the potential energy barrier and is classified as a metastable phase, whereas crystal represents a stable thermodynamic phase.

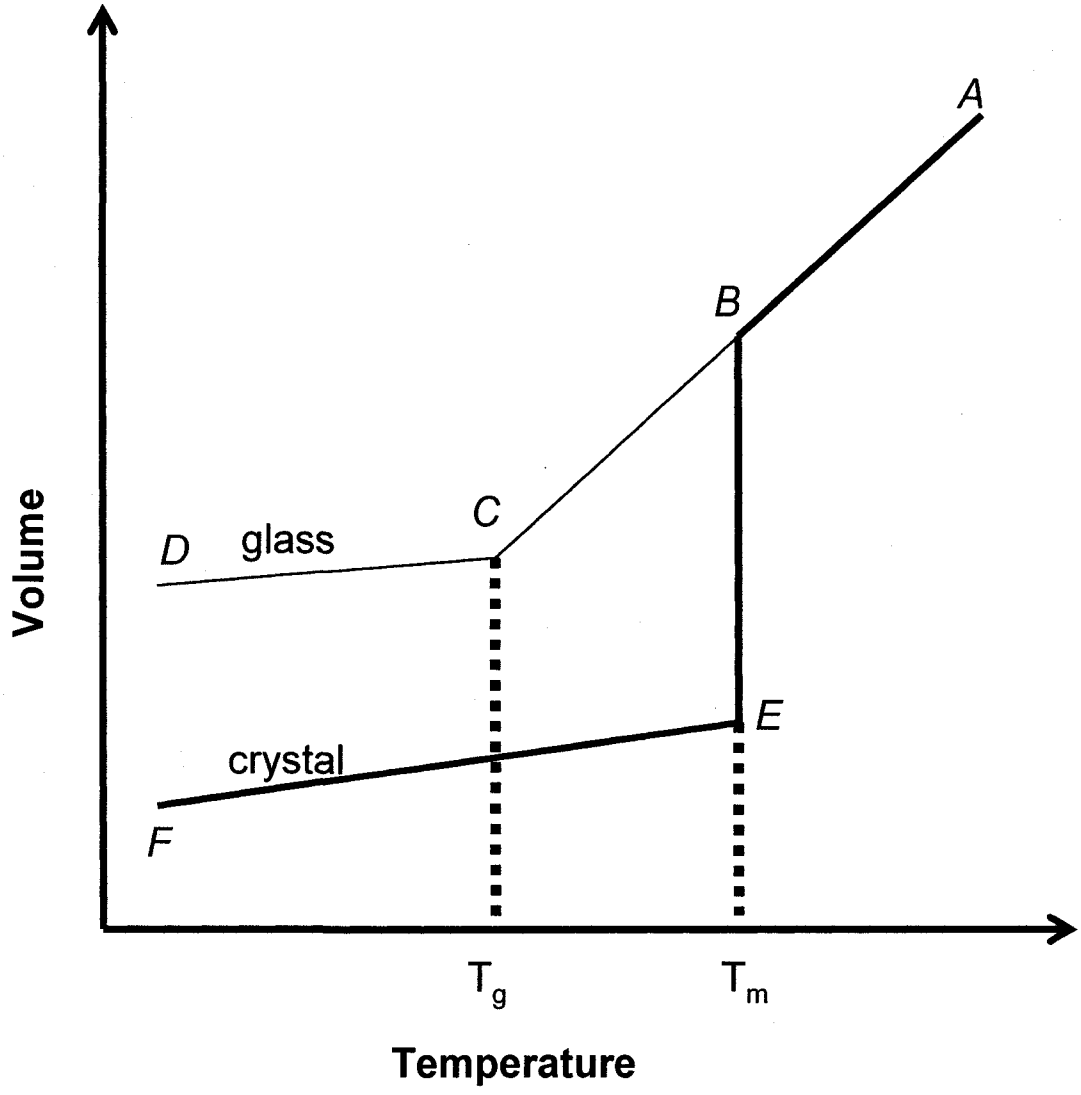

Figure 1.1.1 Process of glass and crystal formation (further discussed in reference 2).

As for the overall structure, a crystal exhibits both short and long range order, whereas atoms in a glass exhibit random positions with short range order. Short range order describes the first coordination shell and nearest-neighbour bonding environment of each atom (radial distance of up to 2Å)[3] such as the GeO_4 units in α-quartz-like GeO_2 crystal, and long range order represents the periodic repetition of these nearest-neighbour units. The long range order defines a radial distance of greater than 10-20Å.[3] A concise review of the description of short, medium, and long range ordering in glass is given by Henderson *et al.*[3]

The diagrams of α-quartz-like GeO_2 crystal and GeO_2 glass generated from simulations of this study are presented in Figures 1.1.2 and 1.1.3. The blue and green spheres represent germanium and oxygen ions, respectively.

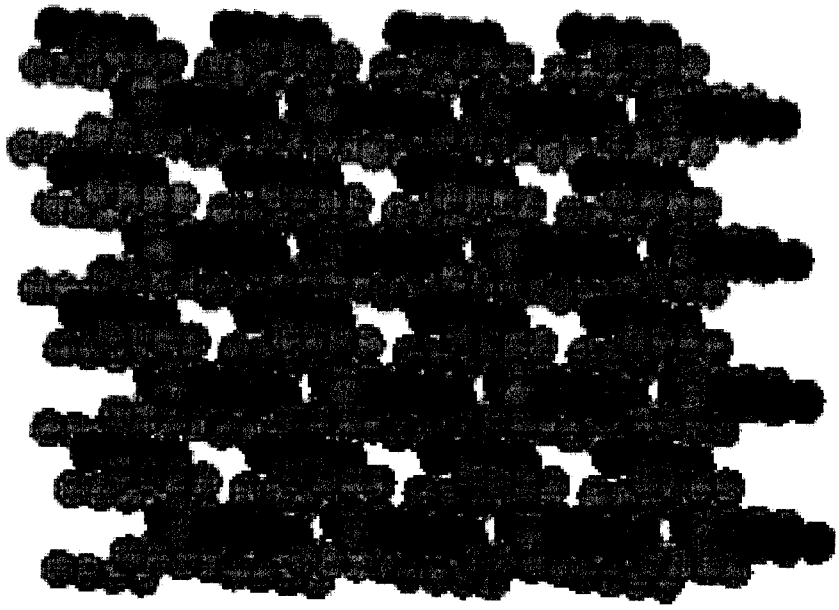

Figure 1.1.2 Pictorial representation of α-quartz-like GeO_2 crystal.

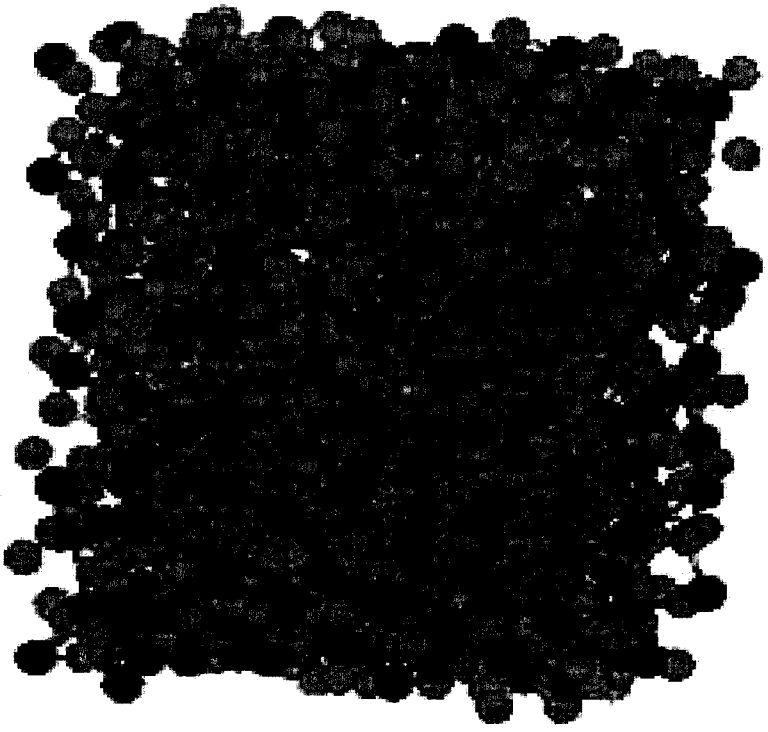

Figure 1.1.3 Pictorial representation of GeO_2 glass.

There has been a great deal of focus in recent years on the development of glass materials with small light scattering in order to improve the transmission loss in optical fibres (thin, flexible and long strands of glass material set in bundles for transmission of light signals over long distances). Oxide glasses show mechanical strength, chemical durability and temperature stability which play a significant role in the development of rare-earth doped optical fibres. In this class of materials, germanium dioxide, GeO_2, containing glasses have demonstrated their importance in the telecommunications and optics industries for use in devices operating at wavelengths greater than 3 μm with signal losses as low as 0.01 dB/km.[4] In recent years, GeO_2 has sparked further interest due to the existence of polymorphism in its liquid state, where a structural transition from tetrahedral to octahedral framework has been observed.[5-7]

Germanate glasses tend to exhibit anomalous properties as a function of their composition, referred to as the 'germanate anomaly.'[8] This phenomenon was first observed in alkali germanate glasses and characterized by sharp maxima in the density and the refractive index and a minimum in the molar volume between 15 and 20 mol % alkali content.[8] The origin of this anomalous behaviour is not fully understood. To explain these observations one theory[9] suggests that, with increasing alkali content, a partial Ge-O coordination change from the four to six occurs,

increasing the packing efficiency of the framework and the density. It should be noted that the common practice among researchers is to refer to a germanium ion connected to four and six oxygen ions as four- and six-coordinated Ge^{4+} ions, respectively. GeO_4 and GeO_6 units are other terminologies used in this context. Above 15 to 20 mol% a decrease in density of the glass due to formation of non-bridging oxygens (NBO) occurs with re-conversion of six- to four-coordinated Ge^{4+}. [9] Henderson *et al.*[10] have proposed an alternative model based on the formation of three-membered GeO_4 rings without the creation of six-coordinated Ge^{4+} ions.

Figure 1.1.4 shows a three-membered GeO_4 ring[11] consisting of a closed path connecting three germanium ions via bridging oxygens (BO). A bridging oxygen is defined in this thesis as an oxygen that is connected to two germanium ions (Ge-O-Ge); on the other hand, in this thesis a non-bridging oxygen (NBO) is referred to an oxygen that is connected to a germanium ion and another ion such as lead in the case of lead germanate glasses (Ge-O-Pb).

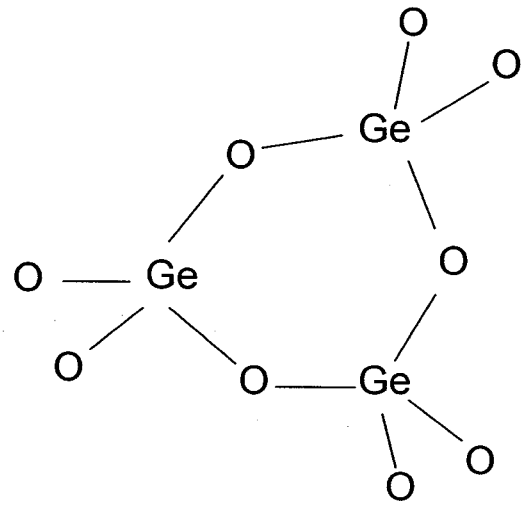

Figure 1.1.4 Pictorial representation of a three-membered GeO_4 ring.

Lead germanate glasses exhibit several important properties such as high densities, high refractive indices, and low softening temperatures.[4] Their remarkably high Raman scattering makes them good candidates for use in fibre optical amplifiers.[4, 12] These glasses also exhibit excellent transmission in the IR region up to 4.5 μm.[13]

Although, glass forming ability[14, 15] and efficiency of lead germanates have already been established, little is known about the structure of these glasses. In spite of numerous Raman[16], IR[17], neutron[18], EXAFS[17, 19-21], and X-ray scattering[22] studies of lead containing glasses in germanate systems, a full understanding of short-range and medium-range order of

lead germanate glasses and direct evidence of the structural change with respect to Ge^{4+} ions in these glasses is still lacking. There is a controversy in the literature concerning the dominant coordination of Ge^{4+} ions in these glasses at different lead oxide compositions and the mechanism by which the 'germanate anomaly' occurs. Different studies have proposed, or supported, different mechanisms for the structural anomaly in lead germanate glasses, and a satisfactory explanation is still not available (details presented in literature review section). This is mostly due to the complex nature of glass structure and lack of suitable experimental studies for a definitive structure determination.

In practice, it is possible to determine the structure of a crystalline material absolutely. In the case of glass materials, even with perfect diffraction data, it is impossible to obtain the structure of the amorphous solid explicitly. Since the optical properties of the glass depend not only on the composition but also on the structure and coordination state of the ions, it is essential to investigate the structural properties of these glasses.

Chapter 2

2.1 Current State of Knowledge

2.1.1 Structure of GeO_2

Germanium dioxide exists in two stable crystalline modifications of rutile-like and α-quartz-like phases at ambient pressure. The rutile modification (tetragonal phase consisting of six-coordinated Ge^{4+} ions) exists at temperatures below 1000°C and transforms to the β–quartz-like structure at about 1049°C. The rutile-like phase has an average Ge-O interatomic distance of 1.89Å, Ge-Ge interatomic distances of 2.86 and 3.42 Å, and Ge-O-Ge angles of 98 and 130°. [23-26]

The α–quartz-like modification (hexagonal phase) is obtained by cooling of β-quartz-like GeO_2 below 1020°C.[24, 27] The α–quartz-like modification consists of four-coordinated Ge^{4+} ions and Ge-O interatomic distance of 1.74 Å [28, 29], Ge-O-Ge bond angle of 130.1° , and O-Ge-O angles ranging from 106.3°-113.1°. A diagram of the tetrahedral O-Ge-O, ϕ, and inter-tetrahedral Ge-O-Ge angle, θ, is shown in Figure 2.1.1.1.

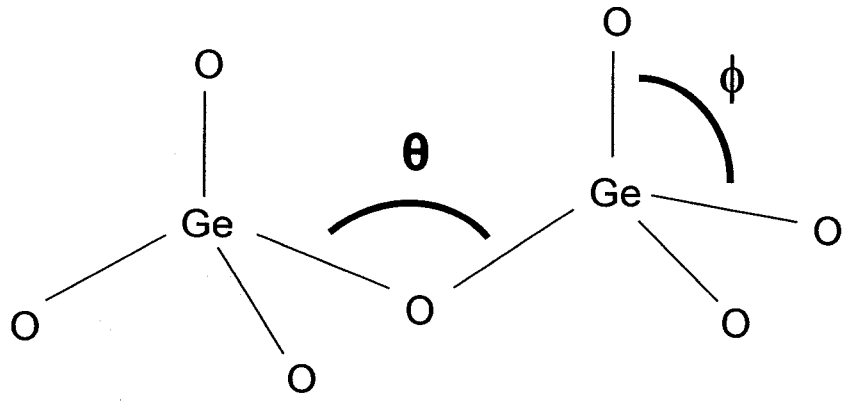

Figure 2.1.1.1 Pictorial representation of tetrahedral, ϕ, and inter-tetrahedral, θ, angles. This diagram is for illustration purposes, actual angles in the glass framework may vary.

From high pressure studies, it has been shown that α–quartz-like GeO_2 transforms to rutile-like GeO_2 at a temperature of 417 K and pressure of 1.8-2.2 GPa.[30] A trigonal phase with a cristobalite-like structure and four-coordinated Ge^{4+} ions has also been reported.[31] A melting temperature (T_m) of 1378K [32] and glass transition temperatures (T_g) ranging from 800 to 1010K [33, 34] have been determined for GeO_2.

The structure of GeO_2 glass has been studied by EXAFS, neutron diffraction, and X-ray diffraction techniques (see Table 2.1.1.1) with the conclusion that Ge^{4+} exhibits a coordination number of four with respect to oxygen atoms similar to the hexagonal crystal phase with Ge-O, Ge-Ge,

and O-O interatomic distances of 1.70-1.78 Å, 3.15-3.45 Å, and 2.82-2.85 Å, respectively.

An average Ge-O-Ge bond angle of 130.1° and O-Ge-O bond angle distribution of 106.3°-113.1° have also been reported. Neutron diffraction[35] further indicates that the structure of vitreous GeO_2 contains a large number of three-membered GeO_4 rings. The results of the aforementioned experimental studies on GeO_2 glass are presented in Table 2.1.1.1.

Table 2.1.1.1 Structural features of GeO_2 glass

Study *(ref.)*	**Interatomic Distance (Å)**			**Coordination Number**			**Bond Angle**
	Ge-O	Ge-Ge	O-O	Ge-O	Ge-Ge	O-O	Ge-O-Ge
Neutron							
(36)	1.72	3.45	2.85	4.0			
(37)	1.739	3.185	2.838	3.9	4.0	6.0	130.1°
(38)		3.21					
(39)	1.744	3.155	2.84	4.0	4.0	6.0	
(40)	1.733		2.822	3.99		6.0	
(41)	1.73	3.16	2.83				132° ± 5°
X-ray							
(42)	1.70						
(43)	1.74	3.18					133
(44, 45)	1.73	3.17	2.85				129° -139°
(46)	1.74	3.15					
(47)	1.74						123.5° -136.5°
(48)	1.73	3.17					133° ± 8.3°

The medium-range order of vitreous GeO_2 (10-20Å scale structure[3] present in glass affecting the optical, electronic, and mechanical properties of the material)[49] has most commonly been described by continuous random-network (CRN) model proposed by Zachariasen [50] and describes the formation of a three-dimensional framework that lacks long range order. For the oxide glasses, disorder is introduced by variations in bond angles and rotations of neighbouring units about their axes. In general, the average Ge-O-Ge angle of 133° is found to contain a narrower distribution compared with the average 144° and 120-180° bond angle distributions found in the silica glass.[51]

Another model for describing the structure of oxide glasses is the microcrystalline model, which describes the glass as an array of microcrystals.[52–54] One common feature in both the microcrystalline and CRN model is the probability of closed rings in the structure of oxide glasses. In the CRN model, the germanate glass framework consists mostly of six-membered GeO_4 rings with a high proportion of three-membered GeO_4 rings. The occurrence of a large number of three-membered, non-planar GeO_4 rings has been justified due to the favourable 130.5° of this ring structure compared with the average inter-tetrahedral angle of 133°.[23] It is worth mentioning that in the case of vitreous silica, planar three-membered rings have been predicted and observed by

Raman spectroscopy.[55] In the microcrystalline model, six-membered rings dominate both the SiO_2 and GeO_2 glasses and the formation of small rings found in the CRN model is discounted.[54]

The structure of GeO_2 has also been subject of theoretical studies.[56, 57] The potential models used in these calculations contain a long range Coulombic part and a short range repulsive part. Simulation of glass and liquid phase of GeO_2 by Micoulaut *et al.*[56] has been successful where Ge-O and O-O interatomic distances of 1.72 and 2.81Å are reported, respectively. A larger Ge-O-Ge bond angle of 159° is reported in this study due to an overestimation of the Ge-Ge interatomic distance.

Another recent study on glass and liquid GeO_2 by Hoang[57] calculates a Ge-Ge interatomic distance of 3.21Å with improved bond angles of 108° and 133° for O-Ge-O and Ge-O-Ge, respectively, using a Morse-like potential. Hoang reports slightly underestimated values for the Ge-O and O-O interatomic distances of 1.69Å and 2.78 Å, respectively.

2.1.2 Structure of $PbO.GeO_2$

PbO exists in two polymorphs, tetragonal red PbO is stable at room temperature, and orthorhombic yellow PbO is stable only at temperatures above 488°C. The orthorhombic phase can be stabilized at room temperature by the presence of small amounts of impurities.[58] The Pb-O and Pb-Pb interatomic distances are 2.34Å and 3.70-3.90Å for the tetragonal phase[59] and 2.21-2.42Å and 3.47-3.63Å for the orthorhombic phase[60], respectively.

$PbO.GeO_2$ glasses can be prepared up to 45 mol% PbO by air quenching and up to 60-65mol% PbO by water quenching.[8] No crystallization occurs between 0-60 mol% PbO[61], and a glass/crystal mixture is obtained between 60-75 mol % PbO by water quenching.[49]

In the lead germanate system, no anomaly in refractive index has been observed.[62] The thermal expansion coefficient of $PbO.GeO_2$ glass exhibits broad minima between 0-20 mol% PbO.[8] Evstropiev *et al.*[63] reported a sharp increase for the variation of density with composition at 30 mol % PbO which was later disputed by Topping *et al.*[14] (see Figures A1 - A4 in appendix). Topping *et al.*[14] concluded that the variations in the density and molar volume are mainly determined by the amount of lead, and possible structural changes concerning the germanate framework are effectively

masked due to the high polarizability (distortion of the electron cloud around lead in the presence of an external electric field) and large mass of Pb^{2+}. On the other hand, a decrease in molar volume is observed at 35-40 mol% PbO, and was taken as evidence for a coordination change.[64] The shift to higher modifier contents (30 - 40 mol%) in the case of lead germanate compared to alkali germanate (15 - 20 mol%) glasses has been explained with the network-forming ability of Pb^{2+} which competes with Ge^{4+} for the oxygen, consequently lowering the rate of the formation of six-coordinated germanium ions. [64]

In essence, two structural models have been proposed for lead germanate glasses: The first model was inferred from structural changes observed in alkali germanate glasses and assumes a partial Ge^{4+} coordination change from four to six with increasing lead oxide content. The second model involves a continuous formation of NBOs and a breakdown of the 3-dimensional germanate framework. Within the second model, the minimum in the molar volume is attributed to a constriction of the germanate framework around the Pb^{2+} ions occupying interstitial sites. The increase in the molar volume above 40 mol% is postulated to result from the participation of PbO_4 pyramids in the framework and creation of NBOs.[17]

Raman spectra of alkali germanate glasses show well resolved bands between 600 and 700 cm^{-1} that were assigned to GeO_6 stretching vibrations.[61] In lead germanates, no distinct peaks are observed in this region, indicating that no GeO_6 is formed. However, Canale *et al.*[61] pointed out that lead containing glasses are highly polarizable exhibiting broad features. Hence, Raman bands associated with GeO_6 might be hidden behind other observed bands. On the other hand, GeO_4 vibrational frequencies involving NBOs are observed at lower modifier contents in lead germanates than in alkali germanates[64] indicating that in lead germanates less (or no) GeO_6 is forming upon addition of PbO. Numerous other Raman and IR studies have not been able to unambiguously determine the formation of GeO_6 units upon addition of PbO to GeO_2 glasses. [16, 65-68]

A neutron scattering study[18] showed a shift of the Ge-O interatomic distance from 1.872 Å to 1.902 Å and a gradual increase in the Ge-O coordination number from 4 to 4.7 at 40 mol% PbO which this study relates to conversion of 33% of GeO_4 units to GeO_6 at 40 mol% PbO.

X-ray scattering results[22] did not show whether the short-range order of $PbO.GeO_2$ glasses consisted only of GeO_4 or a mixture of GeO_4 and GeO_6 units.

EXAFS[17, 19] studies on lead germanate glasses revealed a shift of Ge-O interatomic distances to higher values. However, in one paper this effect is ascribed to the partial coordination change for Ge^{4+} ions [19], in the other study it is attributed to the presence of NBOs.[17] The occurrence of GeO_6 units besides GeO_4 could not be unambiguously deduced from these studies. A recent EXAFS[20] study indicates that an average of 3.6 oxygen atoms surround a germanium ion with the addition of up to 33 mol% PbO which is attributed to formation of GeO_3 and GeO_4 units. At PbO contents higher than 33 mol%, only GeO_4 units are reported. The average Ge-O interatomic distance is reported to be independent of glass composition.[20] A recent combined EXAFS and Molecular Dynamics (MD) studies[21] using a 2-body Born-Mayer-Huggins (BMH) potential model of lead germanate glass indicates that the average Pb-O interatomic distance is independent of the glass composition. This EXAFS/ MD study reports the predominance of PbO_4 units at PbO contents of less than 20 mol% and the additional occurrence of PbO_3 units at higher PbO content. With the addition of up to 40 mol% PbO, the Ge-O interatomic distance shifts from 1.74 Å to 1.75Å. The Ge-O coordination increases gradually from 3.5 to 4.0 with the addition of 10 to 50 mol% PbO.[21]

It appears that at concentrations higher than 40 mol%, the lead ions increasingly act as network formers and creating PbO_4 tetragonal

pyramids[17] as was also found for other glasses such as lead silicates[69] and lead borates.[70] A network-former (such as Si, Ge, B, As, and P) is a cation which contributes to network-building polyhedra. At low PbO contents (below 40 mol%) the lead ions seem to act as network-modifier by occupying interstitial sites and ultimately breaking down the germanate framework, but whether NBOs and/or GeO_6 units are created is still being debated. A network-modifier is a cation that can transform the framework, such as alkaline and alkaline earth metals. A schematic diagram[71] of sodium atoms acting as network-modifiers in a sodium silicate glass is shown in Figure 2.1.2.1.

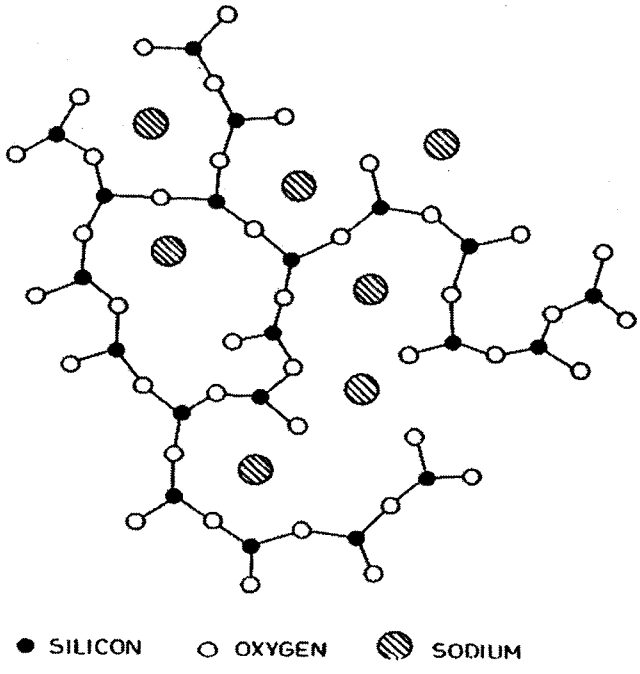

Figure 2.1.2.1 Illustration of sodium acting as a network-modifier in sodium silicate glass (reproduced from reference 71).

Henderson *et al.*[72] have shown that the interpretations of previous studies on alkali germanate glasses were tentative, and that no real experimental proof for the change in coordination number of Ge^{4+} ions exists in these systems. According to their studies on alkali germanate glasses, "the structural mechanism responsible for the anomaly remains inconclusive, but appears to involve a complex interaction between the formation of five-fold Ge, generation of Q^3 and Q^2 species, and formation of small three-membered GeO_4 rings. Further work, particularly high resolution neutron scattering on low alkali compositions before the anomaly, as well as high alkali compositions beyond 33 mol%, are needed to resolve many of the inconsistencies between different experimental results".[73]

The Q^n species describes the distribution of germanate tetrahedra, where n is the number of bridging oxygens. Figure 2.2.1 and 2.2.2 illustrate Q^0 and Q^4 species, respectively.

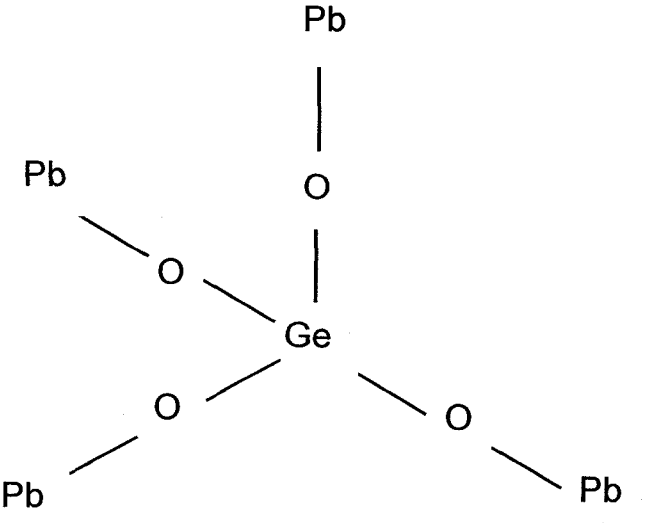

Figure 2.2.1 Representation of Q^0 species.

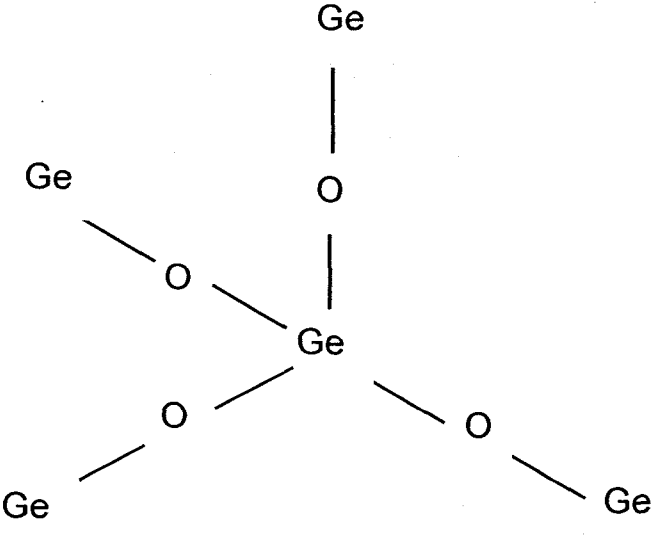

Figure 2.2.2 Representation of Q^4 species.

Other studies have either authenticated[74] the explanation presented by Henderson *et al.* or have questioned the validity of the coordination model.[75]

In disordered systems, ions do not experience identical fields, resulting in the absence of properties of symmetry. Consequently, in such materials it is harder to draw a conclusion on the local structure by means of spectroscopic measurements. Limitations of experimental techniques such as neutron diffraction are such that only averaged structural information is provided, whereas EXAFS should give information about local structure. However, none of these aforementioned methods yield accurate structural details at the atomic level, and have failed to provide sufficient evidence of short range structure changes in lead germanate glasses. The drawback of the structural determination of glasses based solely on vibrational studies has been demonstrated for alkali germanates where distinction between five- or six-coordinated Ge^{4+} atoms is said to be unsuccessful and the authors caution against explanation of the 'germanate anomaly' based on an occurrence of six-coordinated Ge^{4+} ions.[76]

To remedy these difficulties, other studies have opted for MD simulations of disordered structures.[77, 78] In an MD study on sodium

germanate glass by Karthikeyan *et al.*[77], the Ge-O coordination number was found to increase from 4 to 5 with the addition of up to 18 mol% alkali oxide. Further addition of alkali oxide led to formation of NBOs and a decrease in Ge-O coordination number. A recent model for Ge-O coordination in germanate glasses by Hannon *et al.*[79] also supports the interpretation that the predominant higher coordination of germanium is five-fold, and not six-fold.

In a recent publication, Henderson states that "before full understanding of the structural mechanism responsible for the germanate anomaly can be achieved the discrepancies and contradiction between the findings obtained by different techniques must be resolved" and the affirms future need of "numerical models exploring what drives the anomalous behaviour, the small ring formation, the alkali dependence, and the conversion of $^{[IV]}$Ge to $^{[V]}$Ge." [72]

The field of computer simulation is developing towards an increasingly realistic and predictive description of complex systems; which is facilitated both by the continuing growth in computational power and advances in computational techniques.[80] The use of computer modeling techniques such as MD allows for a more detailed model of the glass structure, and provides information on the short and intermediate range

order of the glass. This technique can calculate average structural, thermodynamic and transport properties of a given material. Once the average simulated structural features, interatomic distance and bond angles to name a few, match those observed experimentally, then specific structures creating those averages can be explicitly obtained by the simulation rather than just inferred from the experimental data. From these simulations, the best structures are reproduced, the statistical data are collected, and spectroscopic properties of materials can be calculated. The success and benefits of MD simulations have already been demonstrated by our research group. Cormier has successfully simulated the structure of Eu^{3+} doped SiO_2 and $Na_2O.SiO_2$ glasses.[81] Peres performed MD simulation of Eu^{3+}, Er^{3+} and Yb^{3+} doped $PbO.SiO_2$ glass [82], and the MD simulation of metaphosphate glasses has been performed by Sourial.[83] For details of these studies, the reader is referred to the respective theses.

2.2 Statement of Problem and Research Goals

To date, the direct evidence for the formation of six-coordinated Ge^{4+} in lead germanate glasses is missing. The observation of an increase in the Ge-O interatomic distance with increasing mol% PbO could support a conversion of four- to six-fold Ge^{4+} ions, however there are inconsistencies between the structural data, as pointed out by Henderson *et al.* in the case of alkali germanates.[72] In addition, a number of questions still remain unanswered and cannot be explained by the proposed Ge-O coordination change. For example, EXAFS[19] indicates that the Ge-O interatomic distance remains constant at lead germanate contents beyond 40 mol% PbO which is contradictory to the second part of the coordination hypothesis that would require the Ge-O interatomic distance to decrease if GeO_6 were converting to GeO_4. In this study,[19] the Ge-O coordination number shows its highest change from 4.0 to 4.2 at 20 mol% PbO, but the anomaly maximum has been reported for addition of 30-40 mol% PbO.[14, 84] It must also be stated that an average coordination change from 4.0 to 4.2 does not necessarily imply formation of six-coordinated Ge^{4+} ions.

The present thesis has been motivated by the need to shed additional light on the structure of lead germanate glasses using MD. The specific goal of this thesis is to perform MD simulations of $xPbO.(1-x)GeO_2$

glasses with x = 0.05 - 0.50 to investigate the structural features of the germanate framework and the lead environment, including interatomic distances, coordination numbers, bond angle distributions, ring statistics, and percentage of NBOs at each composition.

To further enhance the potential model, lattice dynamics simulation using shell-model and a combination of two- and three-body potential model is used to generate crystal properties of α-quartz-like GeO_2 (infrared frequencies, lattice energy, bulk modulus, elastic constants, static dielectric constants, high frequency dielectric constants, and heat capacity at constant volume). This study suggests that it is possible not only to model, but also to predict various crucial properties of crystals by the use of appropriate potential models and computer modeling codes. The potential is also capable of reproducing the infrared frequencies, and elastic constants of rutile-like GeO_2 crystal.

Chapter 3

3.1 Research Design and Methods

3.1.1 Overview of Approach

As mentioned earlier, a full understanding of the fine features of short-range and medium-range order of lead germanate glasses is still missing. The problem with the existing experimental studies on lead germanate glasses is that the proposed mechanism of the 'germanate anomaly' is based on average structural data (see chapter 2). Computer simulations act as a link between theory and experiment. The starting point is a model which involves a simplified description of a system to help understand the actual system. A model gives rise to theory and simulation where a simulation represents the computational results of a detailed model, and a theory is an explanation of facts and observations. Simulation has the potential and ability to test the predictions of theory. In recent years, computer simulations have become an invaluable and predictive tool when actual experimental results are lacking or ambiguous. The simulations are not only able to give average simulated structural features, but also determine specific structures creating those averages.

One of the goals of this thesis is to simulate lead germanate glasses at different PbO concentrations. The purpose of such simulations is to obtain a better understanding of the structure of glass with respect to both germanate framework and the lead environment, the role of lead in the glass network, the dominant coordination of Ge^{4+} ions in these glasses at different lead oxide compositions.

The initial steps when performing simulations of a given system involves the choice of computational method, accurate description of the interactions in the system, determination of the potential functions, and the derivation of suitable potential parameters governing interactions in the system. The choice of the computational method for this thesis is MD which provides an analysis of the local environment of individual atoms. It is concerned with simulating the motion of atoms and thus generating a glass by calculating the pairwise interionic forces of a large array of ions. From the net force on each ion, the velocity and position at each time step can be obtained. The new interionic forces can then be recalculated using the new positions. This process is repeated until equilibrium is reached where the average properties of the glass structure will no longer change with time. The equilibration temperature provides the ions with considerable mobility and results in complete randomization in a very short period of time. After equilibration, the simulated glass is cooled to room

temperature by removing the kinetic energy in several steps and thus slowing down the motion of the ions.

In simulations presented in this thesis, the initial configuration was melted by heating from 300K to 15,000K in a total of 60,000 time steps (Δt) of 1fs ($1x10^{-15}$ s). The melt was thermalized at 15,000K for 500,000 time steps. The size of the box was increased at higher temperature steps in order to simulate thermal expansion. The system was then cooled to room temperature in six successive temperature steps at 7500, 5000, 3000, 1250, 600 and 300K, each for 25,000 steps for a total quench time of 150,000 ns and quench rate of $3.0x10^{12}$ K/s. The simulations were carried out at constant volume for each temperature step. By adjusting the size of the simulation box at 300K, the density of simulated glass is determined and compared to the experimental glass density. 3.1.1.1 and 3.1.1.2 summarize the MD technique and computational details for simulation of the glass, respectively.

From the slope of total energy versus temperature plot, the glass transition temperature for the simulated glasses is observed and compared to that for the experimental glass. One important issue to consider is that the glass transition temperature of the simulated system has no resemblance to the experimental T_g, since the rate of quenching for an experimental glass is about 10^6 times slower. However, this difference is

not believed to alter the structural and thermodynamic properties of the simulated glass significantly compared to the laboratory glass since the heat capacity and thermal expansion coefficient of the framework glasses change very little when the structure is frozen.[85]

The algorithms responsible for moving particles in the simulations are Verlet [86] and fifth order Nordsieck-Gear predictor corrector.[87] Using the Verlet method, velocities are calculated from positions and particles are moved accordingly. The advantages of the Verlet algorithm are that it is straightforward and the storage requirements are modest. The disadvantage is that the algorithm is of moderate precision. The Nordsieck-Gear predictor corrector algorithm is more precise as accelerations are obtained from positions which give rise to force using Newton's equation. The algorithm then compares the new calculated force and corrects the position based on the new force and moves the particles accordingly.

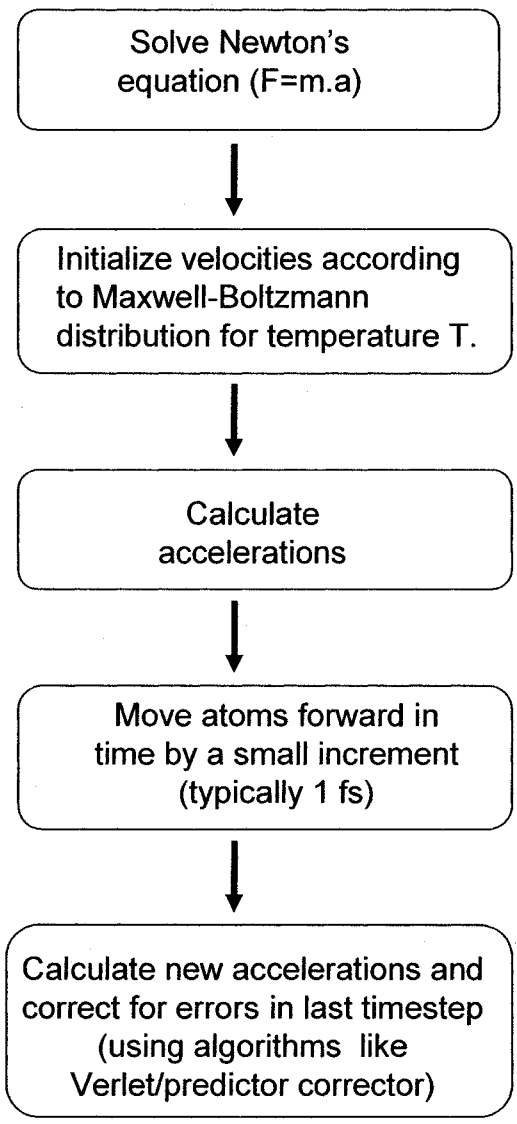

Figure 3.1.1.1 Steps involved in MD simulation (reproduced from reference 88).

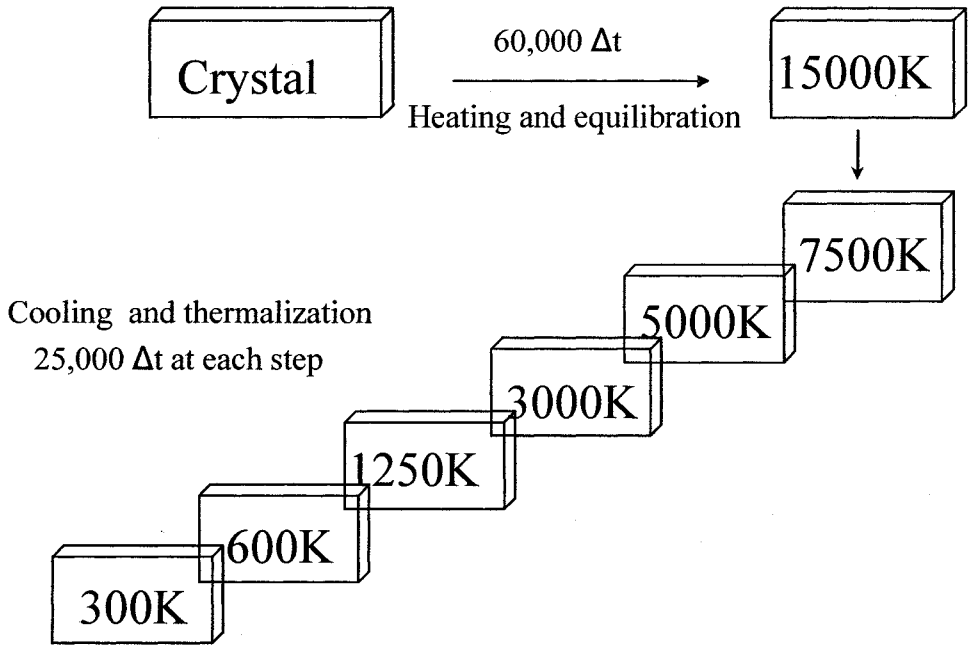

Figure 3.1.1.2 Schematic diagram of glass simulation procedure.

Before describing the potential energy function used in this thesis, it is important to say a few words regarding ab initio calculations. It is well known that the most crucial component of the predictive ability of a MD simulation is the applied potential energy function. Although, ab initio MD simulation is a promising and novel tool in computer simulation, this approach can for the most part be applied to systems of a few hundred

atoms only. Furthermore, the ab initio MD technique has also a limited time scale of a few tens of picoseconds. This is a serious limitation, since in this short time only a limited portion of the potential energy surface can be sampled. The essential motions of the system in long scales are needed in order to determine the relevant configurations of the system.

For these reasons, we chose to start the simulations with a simple 2-body simulation, next a 3-body bending term was added to the potential function to account for the partial covalency of the system. The third type of potential used in this study involves a combination of a 2- and 3- body potential with a shell-model introducing polarization in the interaction potential. This new potential function is very promising as was demonstrated in the publication on lattice dynamics simulation of α-quartz-like GeO_2[89] and will enable us to further validate the derived potential parameters by generating the vibrational spectra of the systems under study. Figure 3.1.1.3 is a schematic diagram of the research method for this thesis.[88]

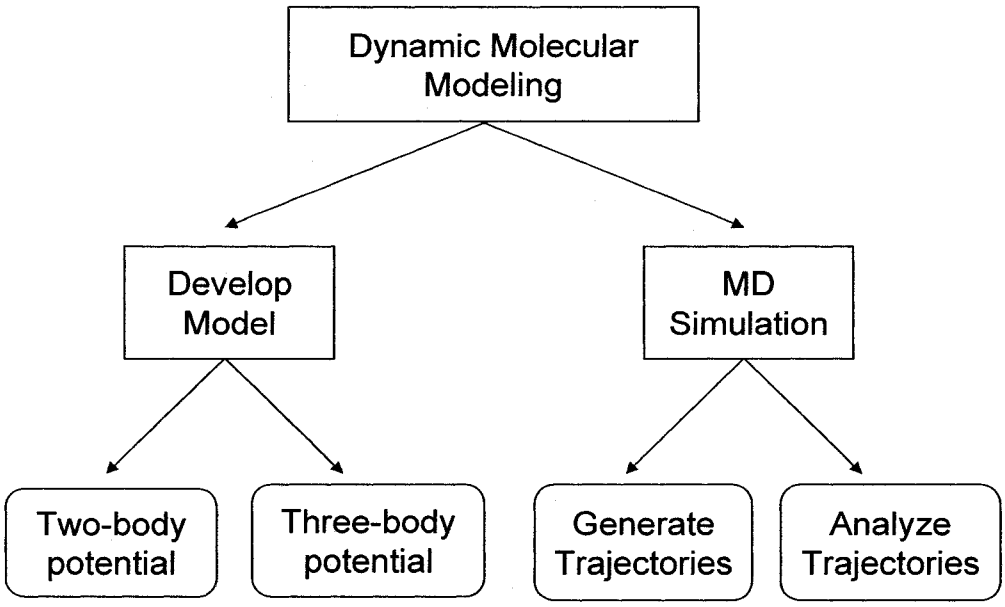

Figure 3.1.1.3 Schematic diagram of the research method (reproduced from reference 88).

3.2 Potential Models

3.2.1 Two-Body Potential

The first study involved the simulation of GeO_2 glass using the pairwise 2-body ionic potential described by Mitra et *al.*[90]:

$$V(r_{ij}) = \frac{q_i q_j e^2}{4\pi\varepsilon_0}\frac{1}{r_{ij}}\left[1 + sign(q_i q_j)\frac{(\sigma_i+\sigma_j)^n}{n+1}\frac{1}{r_{ij}^n}\right] \qquad 3.2.1.1$$

where q_i and q_j are the ionic charges, σ_i and σ_j are the radii of the ions i and j , n is a measure of the hardness of the repulsion, e is the electronic charge, ε_o is the permittivity of free space, and r_{ij} is the interatomic distance between atoms i and j . The *sign* function generates a value of -1 or +1 depending on the sign of the operand (q_iq_j). A hardness parameter of 8 was used to mimic the short-range order observed in the experimental glass. This potential model will be referred to as ***potential model 1*** from this point on.

As for the ionic radii, Shannon *et al.* proposed ionic and crystal radius of 39 and 53 pm for the four-coordinated Ge^{4+}, respectively.[91] Whittaker *et al.*[92] showed that similar to Si^{4+}, a Ge^{4+} radius intermediate between the ionic and crystal radius values of Shannon *et al.* provides the

best conformity for the use in crystal chemistry. They proposed a value of 48 pm for the radius of four-coordinated Ge^{4+}.[92] Although the discussion of the detailed method for determination of these radii is beyond the scope of this thesis, it is worth mentioning that Shannon's value for the ionic radius was derived assuming Pauling's quantum mechanically derived radius of 1.40Å for six-coordinated oxygen while their crystal radius was derived assuming a radius of 1.20Å for six-coordinated oxygen, a value that is based on the empirical difference between the radii of O^{2-} and F^-. Whittaker *et al.* on the other hand used a radius of 1.30Å for four-coordinated oxygen as a suitable mean value in their calculations.

It has already been established that Ge^{4+} ions exhibit a coordination number of four in GeO_2 glass (see Table 2.1.1.1). Since it is important to simulate a GeO_2 framework that is structurally in agreement with the experimental glass before attempting to study the effect of addition of PbO to the simulated glass, the role of Ge^{4+} radius in the coordination environment of the GeO_2 glass was investigated and the results are summarized in section 4.1.1 of this thesis.

Radii of 1.20Å for oxygen and 0.99Å for lead ions have already been successfully used in simulation of lead silicate glasses.[78] Therefore, all related 2-body simulations used ionic radii of 1.20Å and 0.99Å for oxygen and lead, respectively.

3.2.2 Three-Body Potential

One of the criticisms of the use of a 2-body potential model is that the lack of a multi-body bonding term might result in bond defects and discrepancies in the O-Ge-O bond angle distributions. Inclusion of a 3-body bending term might improve the short range of the GeO_2 glass. It has been shown that inclusion of angle-dependant parameters improves the simulation of the lead environment of $PbO.SiO_2$ glasses.[82] For this reason, we incorporated a combination of 2- and 3-body potential model in our simulation. The multi-body potential developed and successfully employed by Feuston *et al.*[93] was used in this simulation. The 2-body term in this potential model consists of a modified form of the Born-Mayer-Huggins (BMH) ionic potential:

$$V_{ij}^{(2)} = A_{ij} \exp\left(-\frac{r_{ij}}{\rho_{ij}}\right) + \frac{Z_i Z_j \ e^2}{r_{ij}} \operatorname{erfc}\left(\frac{r_{ij}}{\beta_{ij}}\right) \qquad 3.2.2.1$$

Where A_{ij} is the short range coefficient for the repulsion and is used to determine interatomic distances. It influences primarily the repulsive region of the potential curve, and contains information concerning radius, electrostatic repulsion and electron density of the atomic pair. β_{ij} reflects

the attractive part of the potential curve and provides information about the charge and distance of a given atomic pair, and the ρ_{ij} parameter influences the depth of the potential energy well (see Figure 3.2.2.1). r_{ij} is the distance between atoms i and j, and Z is the formal charge of the ions. The *erfc* is an error function designed to make appropriate corrections to the attractive part of the potential energy curve.

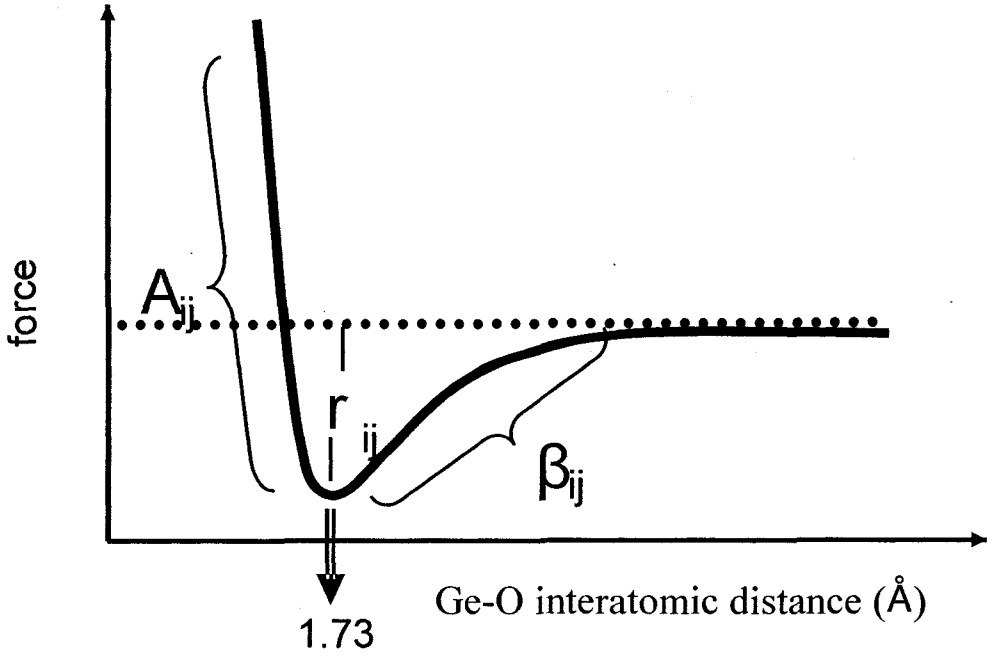

Figure 3.2.2.1 Potential energy curve for the Ge-O pair.

The 3-body potential energy term can be expressed as follows:

$$V_3(r_{ij}, r_{ik}, \theta_{ijk}) = \left[\lambda_i \exp\left(\frac{\gamma_i}{r_{ij} - r_i^c} + \frac{\gamma_i}{r_{ik} - r_i^c} \right) \left(\cos\theta_{ijk} - \cos\theta_{ijk}^c \right)^2 \right] \qquad 3.2.2.2$$

where *i* is the central atom with nearest neighbours *j* and *k*, and θ_{ijk} is the angle with vertex at i sustained by *rij* and *rik*. λ_i, γ_i, r_i^c, and θ_{jik}^c are constants. The bond bending term in the potential model is included in order to account for the directional covalent bonding in GeO_2. It is "designed to lower the total binding energy when the angle formed by a central atom and two of its covalently bonded neighbours differs from the perfect tetrahedral angle, thus ensuring the potential energy minimum is obtained for the optimum bonding configuration." [65] In the simulation of silicate glasses, it has been shown that the experimentally observed tetrahedral geometry is obtained for silicon ions when $\theta_{O\text{-}Si\text{-}O}$ is set equal to the tetrahedral angle of 109.47°. [82]

This potential model will be referred to as ***potential model 2*** from this point on.

3.2.3 Lattice Dynamics

In the past, the inclusion of polarizability did not receive much support due to the added computing time required versus the projected improvements in the results. This assumption is no longer valid due to advances in computer technology in recent years. The inclusion of polarizability allows for the calculation of additional structural information[94] and results in improved simulated properties that are closer to experimental results. Hence, a combination of 2- and 3-body potential with a shell-model in the interaction potential is used and enables us to generate the vibrational spectra of the simulated system.

For this study, the short-range interaction is described by the Buckingham potential. This potential is appropriate for the simulation of ionic and semi-ionic solids [94] and is given by:

$$V_{ij}(r) = \sum [A_{ij} \exp(- r_{ij} / \rho_{ij}) - C_{ij} / r_{ij}^6] \qquad 3.2.3.1$$

where the first and the second part of the above summation represent the repulsive and the attractive dispersion term between pairs of species, respectively. A_{ij} is a measure of the hardness of interaction and ρ_{ij} is

related to the relative sizes of the atoms. The complete potential model used in this study is given by the following equation:

$$V_{ij}(r) = \tfrac{1}{2} \sum_{i} \left(\sum_{j \neq i} (q_i q_j / r_{ij}) + \sum_{j \neq i} A_{ij} \exp(-r_{ij} / \rho_{ij}) - C_{ij} / r_{ij}^{6} + \sum_{j \neq i,\ l \neq \{i,j\}} k_{ijl} (\theta_{ijl} - \theta_{ijl}^{\circ})^{2} \right) \quad 3.2.3.2$$

where q_i and q_j are the charges on the atoms i and j , respectively. r_{ij} is the distance between atoms i and j. θ_{ijl}° is the equilibrium O-Ge-O angle, θ_{ijl} represents the angle between the bonds ij and il, and k_{ijl} is the 3-body force constant.

The shell model [95] used in this simulation describes the polarization in terms of the displacement of a massless shell from a core connected by a harmonic spring constant k. All the mass is concentrated in the core, and the shell simulates the valence-shell electrons with a charge Y. The polarizability on the free ion is given as Y^2 / k. "The shell model can simulate a covalent system using an ionic model due to similarity between polarization and covalency." [94]

This potential model will be referred to as ***potential model 3*** from this point on.

3.3 Data Analysis

From MD trajectories obtained at 300K, the pair (PDF) and cumulative (CDF) distribution functions, bond angle distributions, as well as ring statistics and % of BOs and NBOs are obtained for the glasses.

The pair distribution function (PDF) represents the probability of finding two atoms separated by a distance, $r \pm \Delta r$.

The cumulative distribution function (CDF) is defined as the average number of atoms of type j surrounding atoms of type i in a sphere of radius r. It gives valuable information about the atomic arrangement in the material and can be calculated by integrating the PDF.

The bond angle, θ_{ijk}, corresponds to the angular arrangement of atoms i, k and j with directionality vectors r_{ik} and r_{jk} (see Figure 3.3.1).

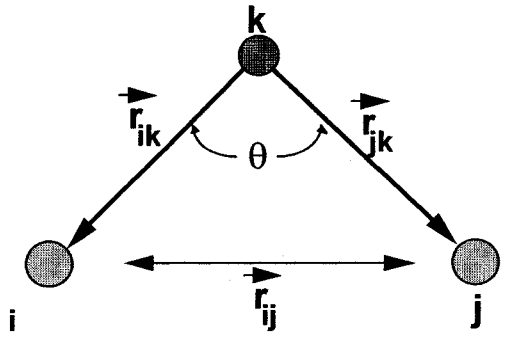

Figure 3.3.1 Schematic representation of the angle, θ_{ijk}.
(reproduced from reference 81).

To further study the germanate framework, the percentage of BOs, and NBOs are calculated. This analysis is done by counting the types of oxygen atoms present within the first Ge-O coordination shell. The distribution of Q^n species will also be determined to identify the types of bonded germaniums for each individual oxygen atom.

Chapter 4

4.1 Simulation of GeO_2 Glass using *Potential Model 1*

4.1.1 Ionic Radii Study

The starting point of the simulations was to generate a model of GeO_2 glass whose structural properties are in agreement with published experimental data on GeO_2 glass. Once a good model for GeO_2 glass was generated, the next step focused on simulation of $PbO.GeO_2$ glasses. As mentioned earlier in section 3.2.1, one of the adjustable parameters in *potential model 1* is the ionic radius for Ge^{4+}. Since the goal was to study the effect of addition of PbO on the structure of the simulated glass and shed light on the "germanate anomaly", it was essential to first investigate the role of the Ge^{4+} radius on the coordination environment of the GeO_2 glass and to simulate a GeO_2 framework that is structurally in agreement with the experimental glass (see Table 2.1.1.1).

MD simulations of vitreous GeO_2 using *potential model 1* (described in section 3.2.1) with Ge^{4+} radii of 39, 48, and 53 pm were performed to elucidate the influence of Ge^{4+} radii on the structural characteristics of the glass. From this point on, we'll refer to these glasses as 39, 48 and 53 GeO_2 glasses. The initial set of atomic positions used to simulate the glasses was obtained from the unit cell of crystalline α-quartz-like GeO_2.[96]

The glasses were simulated as summarized in Figure 3.1.1.2 and Table 4.1.1.1 using Verlet algorithm. From the positions obtained at 300K, the pair (PDF) and cumulative (CDF) distribution functions, and the bond angle distributions were calculated.

Table 4.1.1.1 Simulation parameters for GeO_2 glasses

		39	**48**	**53**
Hardness parameter, n :		8	8	8
Ionic radii, σ (Å) :	oxygen	1.20	1.20	1.20
	germanium	0.39	0.48	0.53
Ionic Charge (q):	oxygen	-2.0	-2.0	-2.0
	germanium	4.0	4.0	4.0
Number of Ions:	oxygen	750	750	750
	germanium	375	375	375
Simulated density (g/cm^3):		3.61	4.35	5.70
Length of box side (Å):		26.13	24.56	22.59

The room temperature equilibrated pair distribution functions for the germanium-oxygen pair are shown in Figure 4.1.1.1. The PDF of 39, 48 53 GeO_2 glasses are represented as black, red, and green curves, respectively. The average Ge-O interatomic distances were found to be 1.72Å with a full width half maximum (FWHM) of 0.16Å, 1.81Å with FWHM of 0.20Å and 1.87Å with FWHM of 0.21Å for the 39, 48, and 53 GeO_2

glasses, respectively. The PDFs for the Ge-O pair for all glasses are sharp and narrow. A good separation between the first and the second coordination shell is indicated by the observation that these PDFs return to a null value after the first maximum.

The results for the 39 glass corresponds to the α-quartz-like GeO_2 and is in good agreement with experimental neutron diffraction studies [36-41] which reported a Ge-O interatomic distance of 1.72 to 1.74Å. An X-ray study by Zarzycki[42] showed a Ge-O peak at 1.70Å, while another X-ray study by Leadbetter *et al* [43] reported a Ge-O interatomic distance of 1.74Å. The results for the 53 glass correspond to the rutile-like GeO_2 and are in good agreement with a high-pressure XAS study on crystalline GeO_2.[23] reporting a Ge-O interatomic distance of 1.89Å. The result for the 48 glass was found to represent a mid point between the α-quartz and rutile-like GeO_2.

From the cumulative distribution function of the Ge-O pair (Figure 4.1.1.2), the average number of oxygen around germanium ions at a cut-off distance of 2.6Å was determined to be 4.0, 5.0, and 5.4 for the 39, 48, and 53 GeO_2 glasses, respectively. The CDFs for all three ionic radii show a flat plateau region, which is indicative of the well-defined short-range environment for the germanium ions. Throughout this thesis, the cut-off distance for each atomic pair represents the cut-off point between the first

and second coordination shells for the atomic pair. The value of cut-off is chosen to reflect the atoms in the first coordination shell.

As mentioned earlier, one of the benefits of using a simulation technique such as MD is that specific details giving rise to average structural data can be determined from simulations. In order to get a better idea of the number of oxygen ions surrounding the germanium ions in the first coordination shell, the distribution of the Ge-O coordination for the simulated glasses was extracted from the simulations. The results of this calculation are illustrated in the form of a histogram (Figure 4.1.1.3) and show that for the 39 glass, 96% of the germanium ions are coordinated to four oxygen atoms, and 4.0% are six-coordinated. In the 48 glass, 26% of the germanium ions are four-coordinated, 50% are five-coordinated, and 24% are six-coordinated, whereas for the 53 glass, 8% are four-coordinated, 51% are five-coordinated, and 41.0% are six-coordinated. This analysis demonstrates that the 39 glass consist mainly of four-coordinated germanium ions corresponding to coordination of Ge^{4+} in the α-quartz-like structure, whereas the germanium ions in the 48 and 53 glasses are mainly five-coordinated, describing a rutile-like structure. The results presented for the 39 glass are in agreement with experimental studies listed in Table 2.1.1.1 reporting four-coordinated Ge^{4+} ions for the GeO_2 glass.

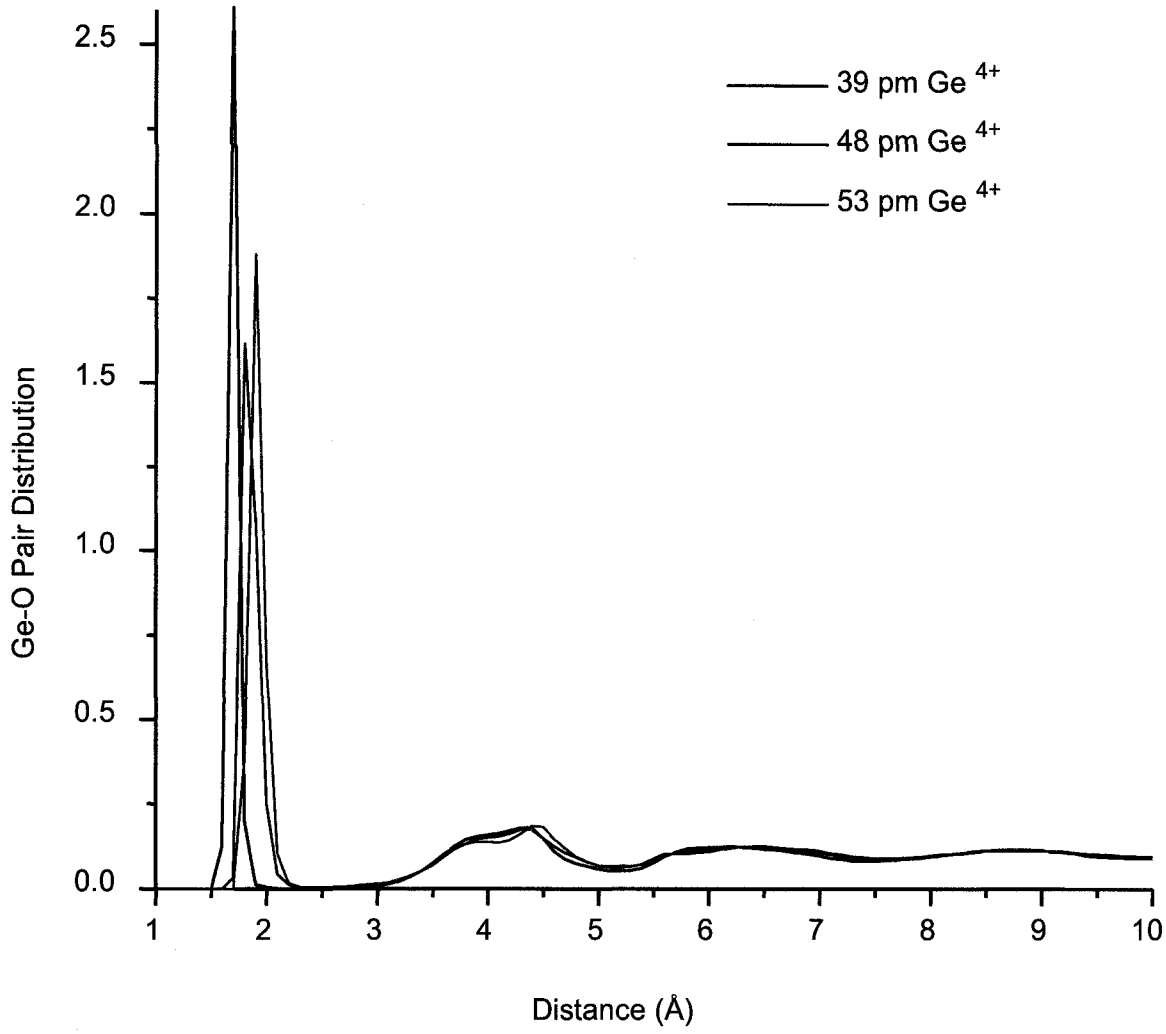

Figure 4.1.1.1 Pair distribution function of Ge-O atomic pair for the 39 (black curve), 48 (red curve), and 53 (green curve) simulated GeO_2 glasses.

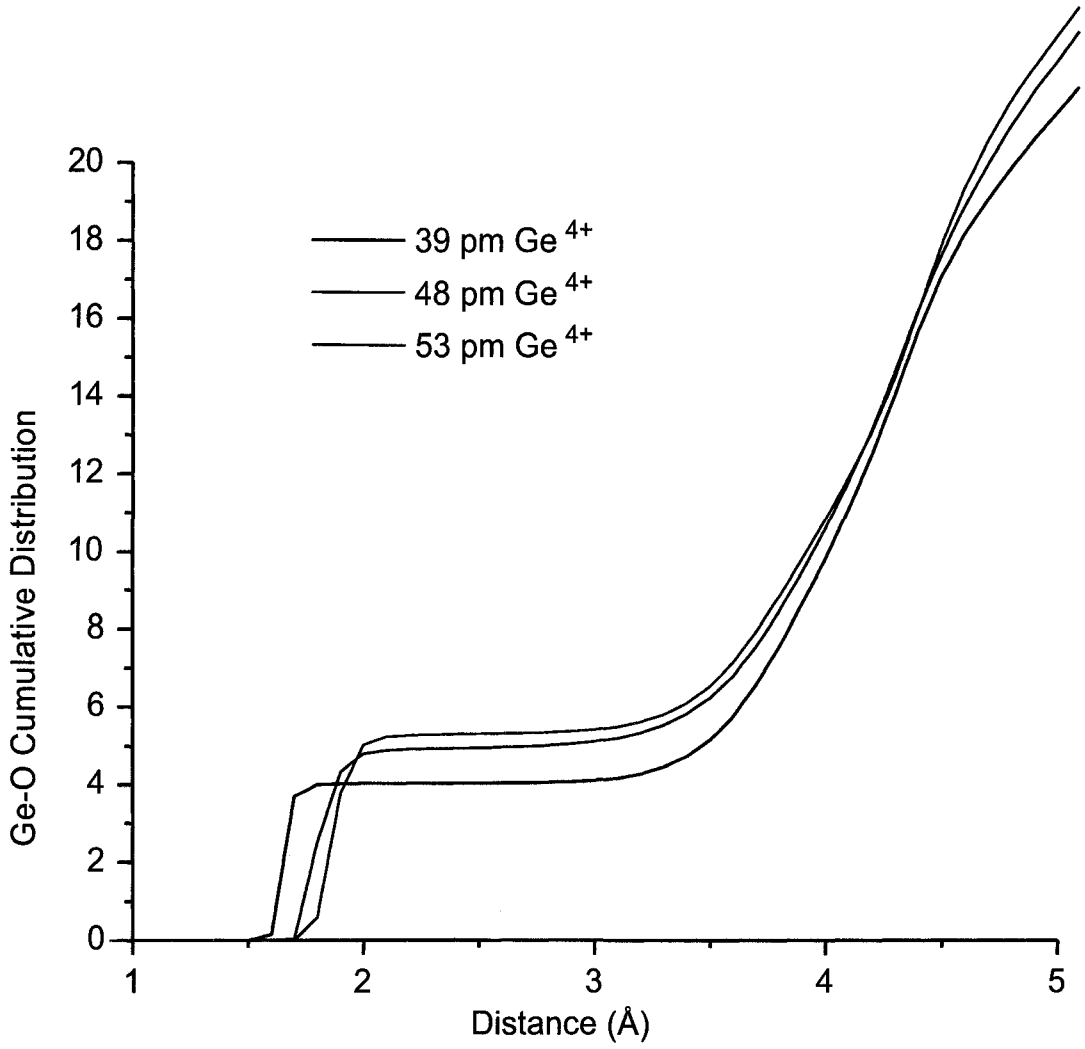

Figure 4.1.1.2 Cumulative distribution function of Ge-O atomic pair for the 39 (black curve), 48 (red curve), and 53 (green curve) simulated GeO_2 glasses.

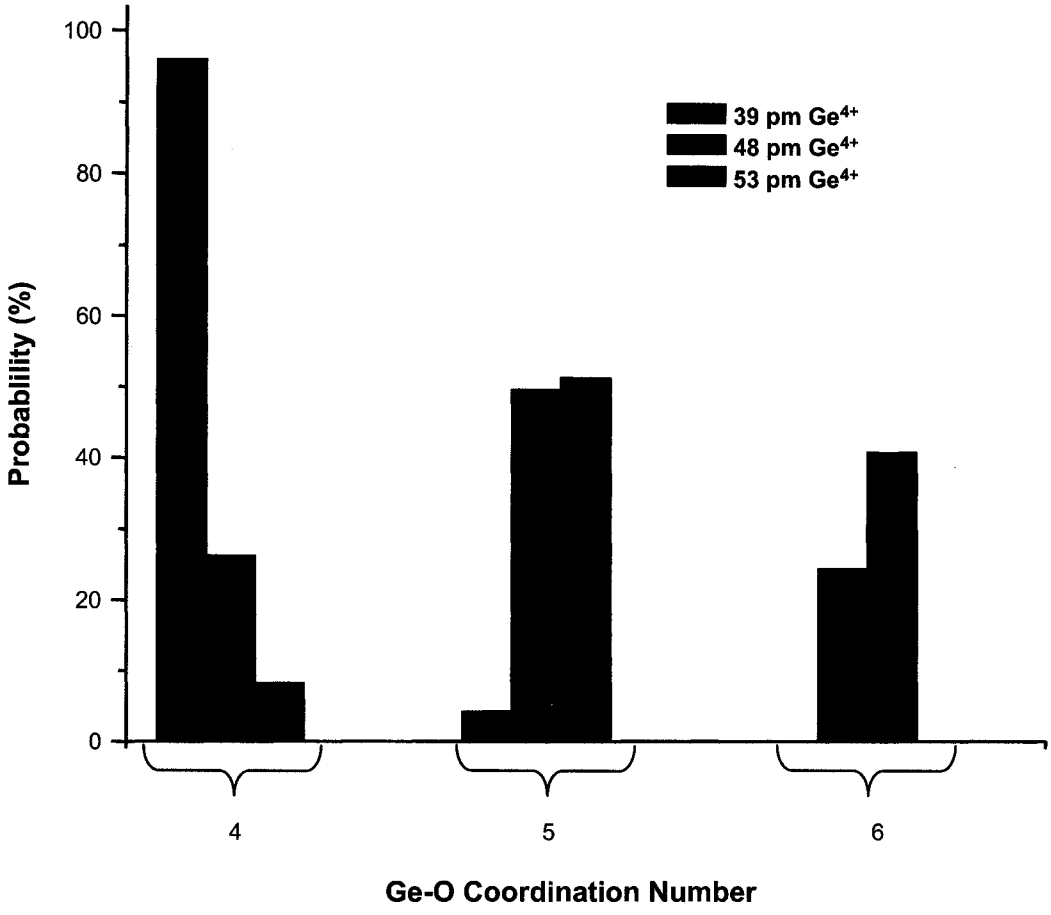

Figure 4.1.1.3 Percentage of different types of Ge-O coordination present in 39 (black bar), 48 (red bar), and 53 (green bar) simulated GeO_2 glasses.

The average interatomic distance for the oxygen-oxygen pair was found to be 2.80 Å with FWHM of 0.36 Å, 2.69 Å with FWHM of 0.36 Å, and 2.65Å with FWHM of 0.37Å for the 39, 48 and 53 GeO_2 glasses, respectively. The average number of oxygen-oxygen neighbours at a cut-off distance of 3.7Å was found to be 5.60 for the 39 glass, 5.70 for the 48 glass, and 6.04 for the 53 glass. The oxygen-oxygen interatomic distance for the simulated 39 glass is in good agreement with experimental results of 2.82 - 2.85Å (see Table 2.1.1.1). The PDFs for all glasses show a small tail, which is an indication of the presence of odd coordinated species in the structure. In addition, neither of the PDFs for the O-O pair returns to a null value, indicating that there is not a good separation between the first and the second coordination shell, that is, the short-range order is not as well defined for the O-O pair. The CDFs for both glasses increase continuously without the presence of a plateau, which supports the lack of a short-range environment with respect to the O-O pair.

The average interatomic distance for the germanium-germanium pair was found to be 3.25Å with FWHM of 0.29Å, 3.30Å with FWHM of 0.29Å, and 3.35Å with FWHM of 0.30Å for the 39, 48, and 53 GeO_2 glasses, respectively. The average number of germanium neighbours was found to be 3.73, 4.10, and 4.47 at a cut-off distance of 3.2 Å for the 39, 48, and 53 glasses, respectively. The PDFs for the 48 and 53 glasses show a small

tail indicative of the presence of odd coordinated species in the structure. This tail is not seen for the 39 glass. The PDFs for the Ge-Ge pair do not return to a null value after the maximum suggesting that there is substantial overlap between the first and the second coordination shells, that is, the short-range order is not as well defined for the Ge-Ge interatomic pair. For the 48 and 53 glasses, a significant shoulder was observed in the first Ge-Ge peak at 2.90 Å and 2.81 Å, respectively. The presence of a shoulder agrees well with the properties of a rutile-like structure, which is reported to exhibit Ge-Ge nearest neighbour distances of 2.86Å and 3.42Å.[25] The Ge-Ge interatomic distance for the simulated 39 glasses is in the range of experimental values listed in Table 2.1.1.1. The CDFs for all glasses increase continuously without the presence of a flat region, indicating that the short-range environment with respect to the Ge-Ge interatomic pair is not as well defined. Table 4.1.1.2 summarizes the structural details for 39, 48, and 53 GeO_2 glasses obtained from MD simulations.

Table 4.1.1.2 Structural parameters derived from the pair and cumulative distribution functions for GeO_2 glass

Atomic pair	First peak maxima (Å)			FWHM (Å)			Coordination number *		
	39	48	53	39	48	53	39	48	53
O-O	2.80	2.69	2.65	0.36	0.36	0.37	5.60 (3.7)	5.70 (3.7)	6.04 (3.7)
Ge-O	1.72	1.81	1.87	0.16	0.20	0.21	4.04 (2.6)	5.03 (2.6)	5.42 (2.6)
Ge-Ge	3.25	3.30	3.35	0.29	0.29	0.30	3.73 (3.2)	4.10 (3.2)	4.47 (3.2)
Ge-Ge**	----	2.90	2.81	-------	0.69	0.72	----------		

* The number in parenthesis refers to the interatomic distance (in Å) at which the average coordination number is calculated.

** Indicates the location of a shoulder in the first atomic pair peak.

The average O-Ge-O bond angles (Figure 4.1.1.4) for the simulated glasses were found to be 109° with FWHM of 19.2° for the 39 GeO_2 glass. The 48 and 53 glasses show an average O-Ge-O angle of about 90° with FWHM of 21°. A less intense peak is observed at 170° for the 48 and 53 glasses. Experimentally, a O-Ge-O bond angle distribution of 106.1°-113.1° has been reported.[35] A value of approximately 90° is representative of square planar and/or distorted octahedral geometries,

whereas a value of approximately 109° corresponds to a tetrahedral angle. Therefore, the O-Ge-O angles obtained from the simulations are in good agreement with the four-coordinated Ge^{4+} ions in 39 and six-coordinated species found in both the 48 and 53 GeO_2 glasses.

The Ge-O-Ge bond angle distributions (Figure 4.1.1.5) show a maximum of about 97° and 134° with FWHM of 12.9° and 25.7° with respect to the 48 and 53 GeO_2 glasses, and 135° with FWHM of 30.6° for the 39 glass. For the 39 glass, corresponding to α-quartz-like structure, several X-ray and neutron diffraction experiments [36–48] found the Ge-O-Ge angle to be 129° - 139° for α-quartz-like structure. It is worth mentioning that the observation of narrower bond angle distributions in the GeO_2 glass compared to the SiO_2 glass (FWHM 38°) [97] has been reported in the literature [51] and observed from simulations presented in this thesis. For a rutile-like structure, Ge-O-Ge angles of 98° and 130° are expected [23], which is in agreement with the simulated 48 and 53 GeO_2 glasses. According to the aforementioned results, the GeO_2 glass with α-quartz-like structure (39 glass) consists of corner-sharing polyhedra, whereas both edge-sharing and corner-sharing polyhedra are expected for the rutile-like structure and are observed in the simulated 48 and 53 glasses. The pictorial representations of an edge-sharing (two-membered GeO_4 ring) and a corner-sharing tetrahedra are shown in Figures 4.1.1.6 and 4.1.1.7,

respectively. In the case of corner-sharing polyhedra, the oxygen is connected by one corner which results in greater mobility and a larger Ge-O-Ge bond angle.

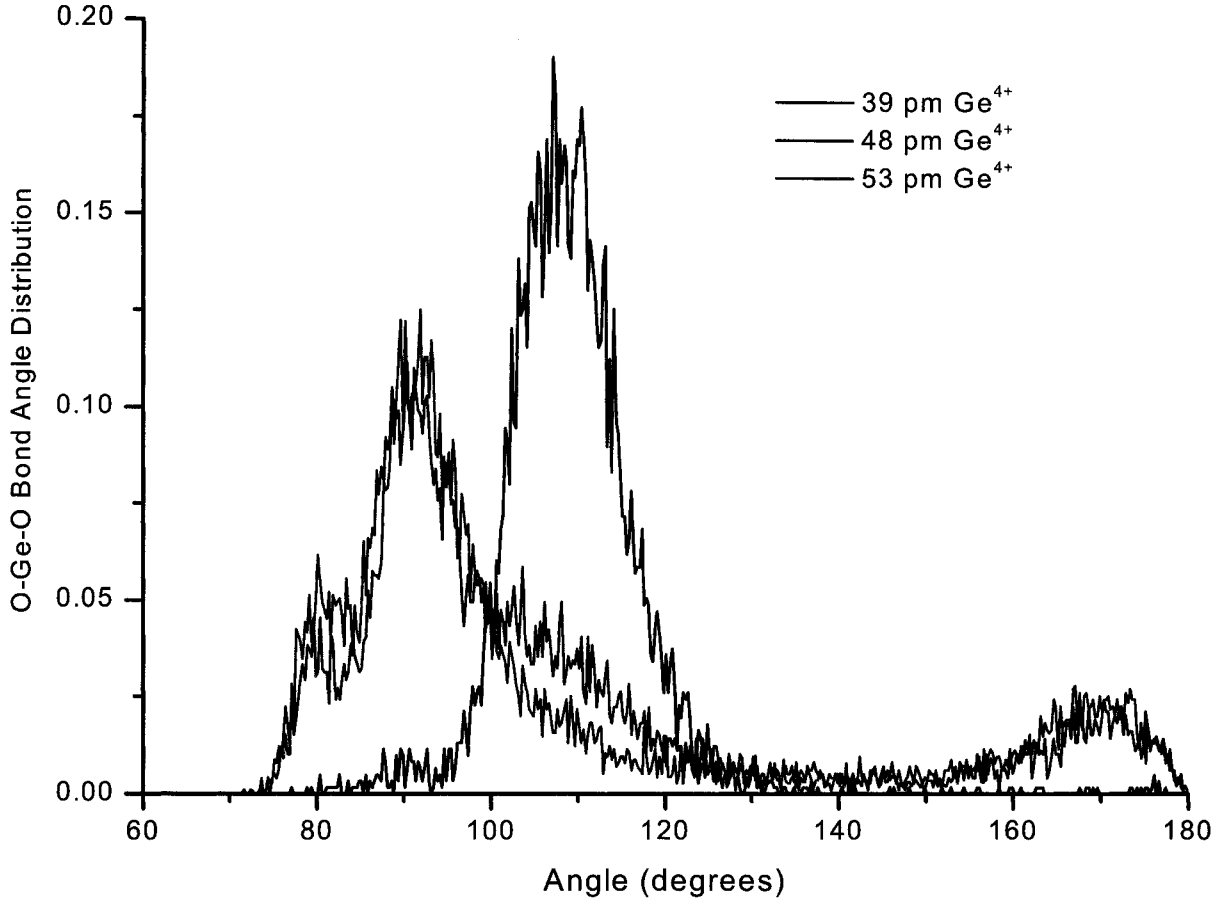

Figure 4.1.1.4 O-Ge-O bond angle distribution for the 39 (black curve), 48 (red curve), and 53 (green curve) simulated GeO_2 glasses.

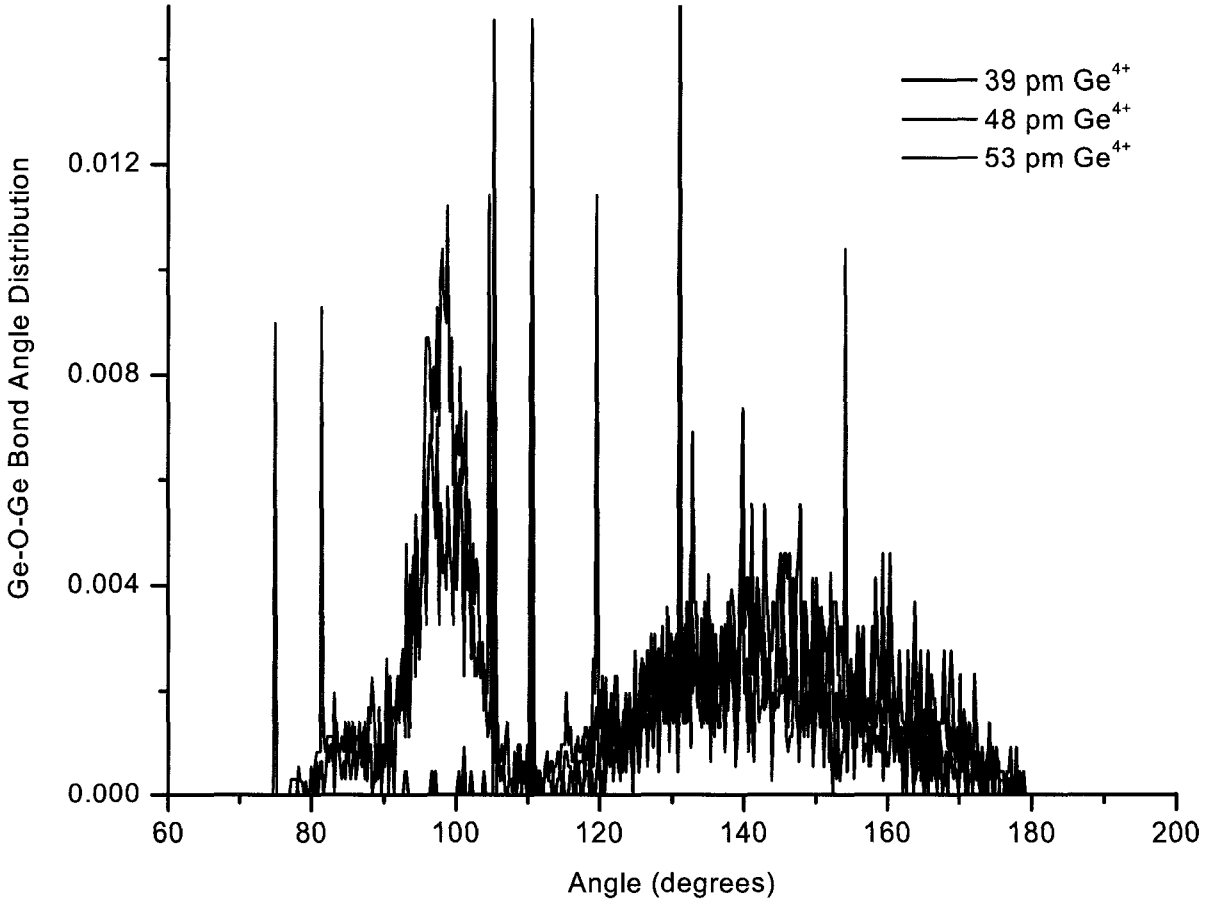

Figure 4.1.1.5 Ge-O-Ge bond angle distribution for the 39 (black curve), 48 (red curve), and 53 (green curve) simulated GeO_2 glasses.

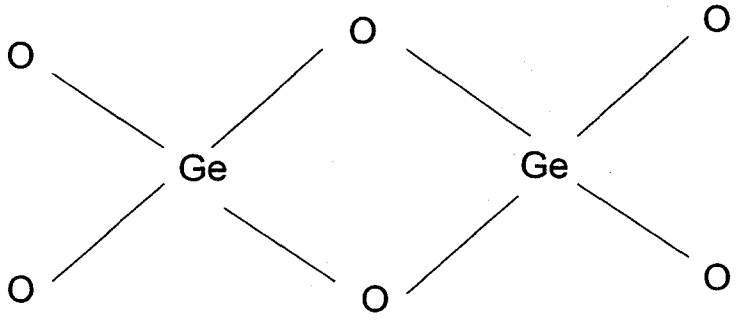

Figure 4.1.1.6 Pictorial representation of edge-sharing tetrahedra.

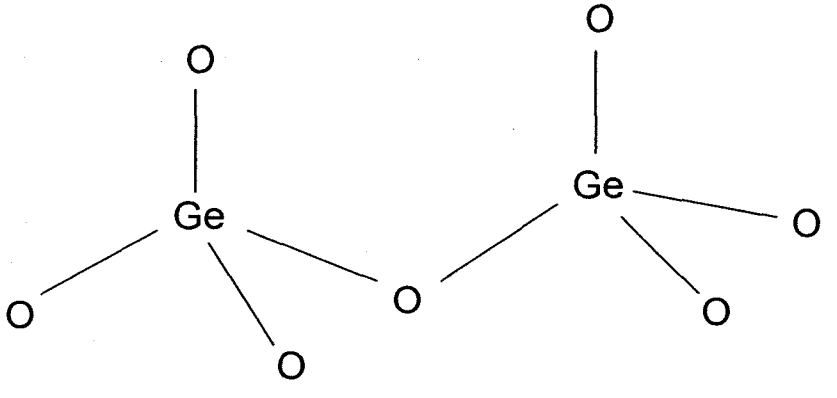

Figure 4.1.1.7 Pictorial representation of corner-sharing tetrahedra.

In order to investigate the medium-range structure and connectivity of the simulated glasses, a ring analysis was performed. Based on these results, the simulated GeO_2 glasses consisted mostly of five- and six-membered GeO_4 rings. The present MD simulation shows low percentage of three-membered GeO_4 rings in the simulated GeO_2 glass. This result is in accordance with the microcrystalline model [54] which predicts occurrence of large number of six-membered rings in GeO_2 glass and discounts the formation of small rings found in the CRN model.

Further validity of the simulated glass structures is given in the simulated densities of the two GeO_2 glasses. The simulations resulted in a density of 3.61 g/cm^3 for the 39 glass, in good agreement with the reported α-quartz-like GeO_2 glass density of approximately 3.65 g/cm^3 by Leadbetter *et al.* [43] The simulated density of 5.70 g/cm^3 obtained for the simulated 53 GeO_2 glass compares more with a density of approximately 6.28 g/cm^3 reported for the rutile-like GeO_2 crystal.[25]

In conclusion, the properties of the simulated glasses (interatomic distances from PDF, coordination numbers from CDF, and bond angles) were compared to results of EXAFS, neutron diffraction, and X-ray diffraction. The best Ge^{4+} radius capable of reproducing the experimental GeO_2 glass was determined to be 39 pm and will be used for simulation and composition studies of $PbO.GeO_2$ glasses. A snapshot of the 39 pm

GeO_2 glass generated from the simulations is presented in Figure 4.1.1.8. The blue and green spheres represent germanium and oxygen ions, respectively.

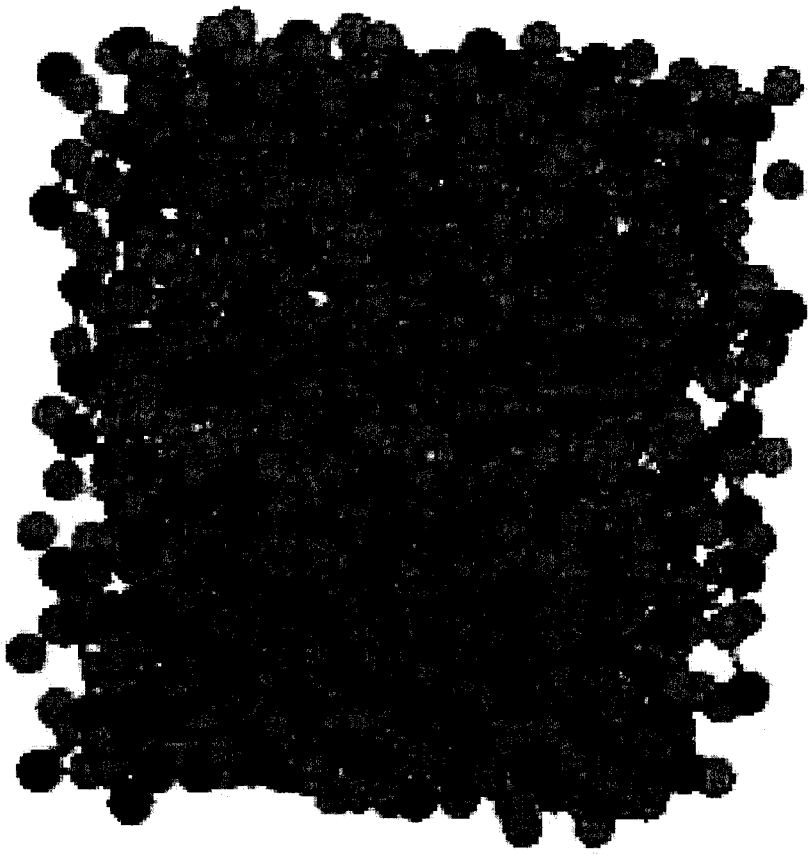

Figure 4.1.1.8 Pictorial representation of 39 pm GeO_2 glass.

4.2 Simulation of $PbO.GeO_2$ Glass using *Potential Model 1*

Once a good model for GeO_2 glass was generated, the next step involved simulation of $PbO.GeO_2$ glasses. We first focused on MD simulation of $xPbO.(1-x)GeO_2$ glasses with x = 0.50, a composition where the controversy around the 'germanate anomaly' does not exist, and there is more agreement on the structural detail of the glass among experimental studies. For simplicity reasons, we will refer to $xPbO.(1-x)GeO_2$ glass with x = 0.50 as 50/50 $PbO.GeO_2$ glass.

The initial set of atomic positions used to simulate the glass was obtained from the unit cell of crystalline alamosite $PbSiO_3$.[98] The crystal structure of $PbGeO_3$ has not yet been determined. The justification in using the atomic positions for $PbSiO_3$ is based on a study on lead germanium oxide single crystals[99] which showed that the germanium ion often replaces silicon ions to form isomorphous compounds in minerals. Based on the X-ray diffraction results from that study, $PbGeO_3$ and $PbSiO_3$ appear to be isomorphous.

The glass was simulated using *potential model 1* (described in section 3.2.1) using the Verlet algorithm. Ionic Radii of 0.39, 1.20, and 0.99Å were used for germanium, oxygen and lead ions, respectively. The

details of the simulation procedure are summarized in Figure 3.1.1.2 and Table 4.2.1.

Table 4.2.1 Simulation parameters for $PbO.GeO_2$ glass

Element	Ionic Radius, σ (Å)	Ionic Charge (q)	Number of Ions
O	1.20	- 2.0	3024
Ge	0.39	+ 4.0	1008
Pb	0.99	+ 2.0	1008
Hardness parameter, n :		8	
Simulated density (g/cm^3):		6.83	
Oxygen molar volume ($cm^3/mol\ O^{2-}$):		16.09	
Length of box side (Å):		43.23	

A snapshot of $xPbO.\ (1-x)GeO_2$ glass with x=0.50 generated from the simulation is presented in Figure 4.2.1. The blue, green and yellow spheres represent germanium, oxygen, and lead ions, respectively.

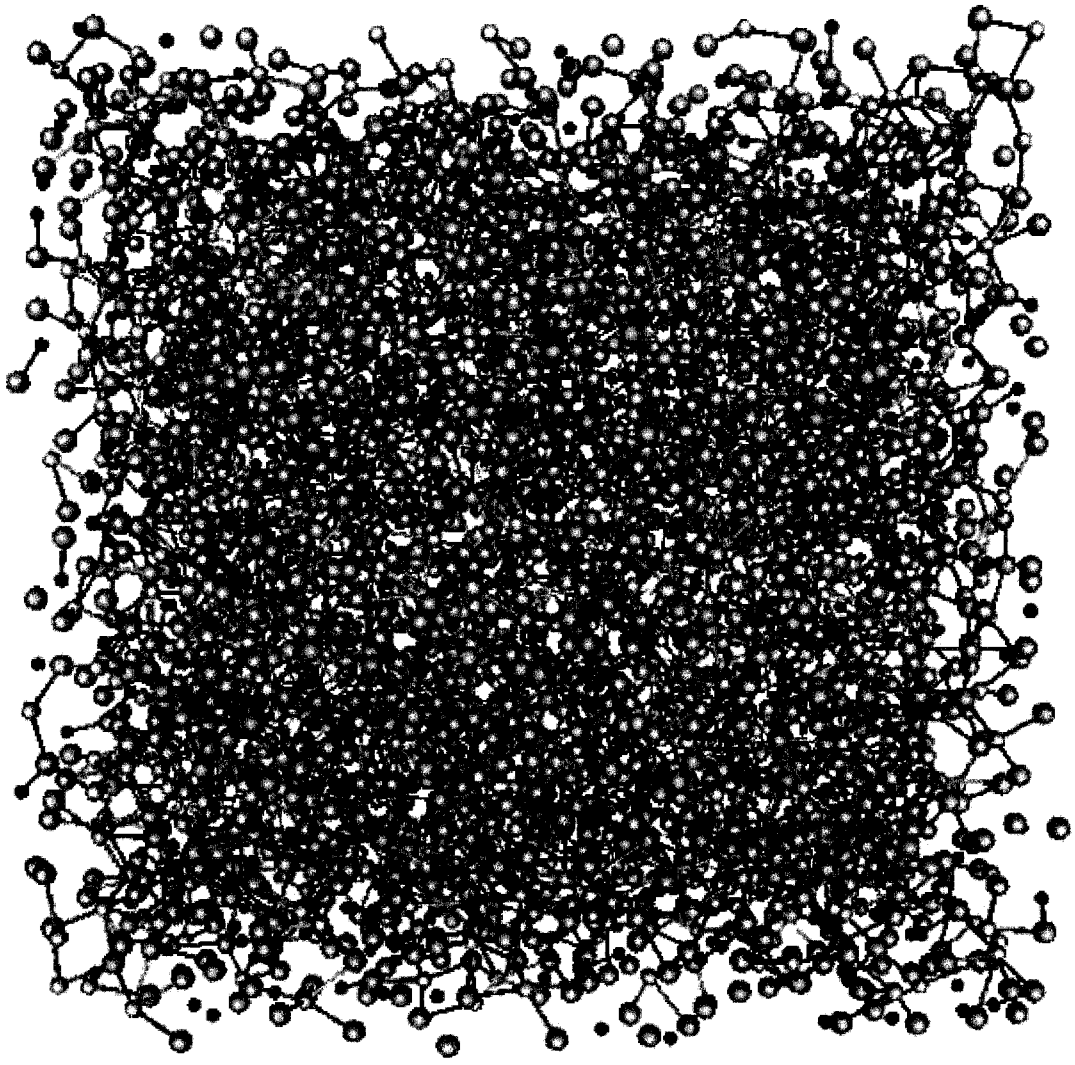

Figure 4.2.1 Pictorial representation of $xPbO.(1-x)GeO_2$ glass with x=0.50.

From the atomic positions obtained at 300K, the pair (PDF) and cumulative (CDF) distribution functions were calculated. For clarity purposes, the discussion will be separated into two main sections, the germanate framework and the environment of the lead atoms with respect to the germanate framework. A summary of the simulated interatomic distances and coordination numbers obtained from MD simulations is presented in Table 4.2.2.

Table 4.2.2 Structural parameters derived from the pair and cumulative distribution functions for 50/50 $PbO.GeO_2$ glass

	Simulated Results 50 mol% PbO			Experimental Results 50 mol% PbO [16, 19-22]	
Atomic pair	First Peak maxima (Å)	Width of First Peak (Å)	Average CN *	Interatomic Distance (Å)	Average CN
O-O	2.70	0.36	4.20 (3.7)	2.8	-----
Ge-O	1.72	0.15	4.02 (2.5)	1.74-1.78	4.1
Pb-O	2.37	0.21	5.64 (3.2)	2.21-2.42	6.0
Ge-Ge	3.27	0.29	2.10 (3.5)	2.93	1.9
Pb –Ge	3.80	1.27	5.20 (4.7)	------	-----
Pb –Pb	3.60	1.78	5.90 (5.8)	3.47-3.63	6.3

* The number in parentheses refers to the distance (in Å) at which the average coordination number is calculated.

4.2.1 The Germanate Framework

The room temperature equilibrated pair and cumulative distribution functions for the germanium-oxygen pair in simulated 50/50 $PbO.GeO_2$ glass are presented in Figure 4.2.1.1. The average Ge-O interatomic distance was found to be 1.72Å with FWHM of 0.15Å. The PDF for the Ge-O pair is sharp and narrow and returns to a null value after the first maximum which suggests that there is a good separation between the first and the second coordination shells.

From the CDF of the Ge-O pair (inset in Figure 4.2.1.1), the average number of oxygen atoms to germanium was determined to be 4.02 at a cut-off distance of 2.5Å. The CDF shows a flat plateau region which is indicative of a well defined short range environment with respect to germanium ions. The results for the Ge-O interatomic distance and coordination are in good agreement with the EXAFS studies by Yamamoto *et al.* [19] and Witkowska *et al.* [20]

In order to get a better idea of germanium-oxygen coordination, the percentage of different Ge-O coordinations present in the glass was calculated. The results of this calculation indicate that the 50/50 $PbO.GeO_2$ glass consists of 96% GeO_4 and 4% GeO_5 units.

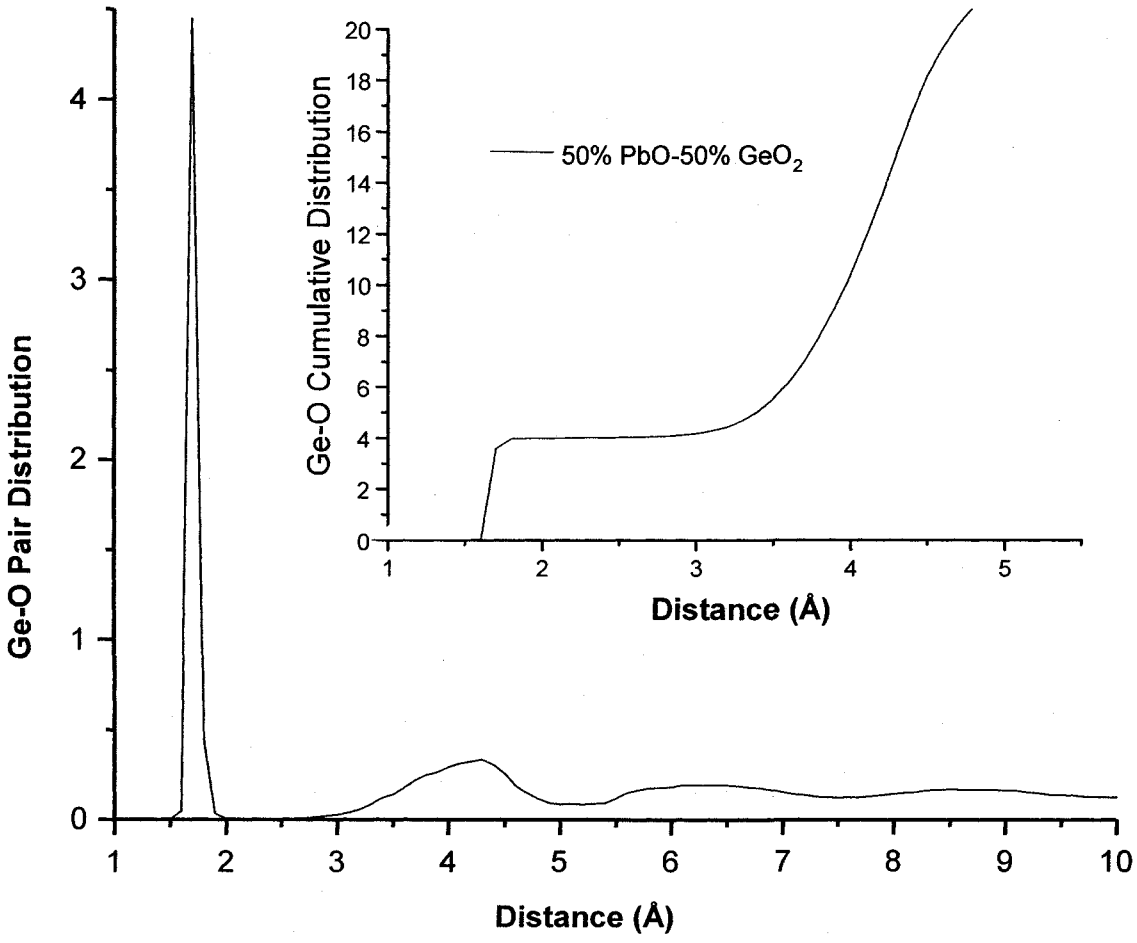

Figure 4.2.1.1 Pair and cumulative (shown in inset) distribution functions of the Ge-O atomic pair for the simulated 50mol% PbO.50mol% GeO_2 glass.

The pair and cumulative distribution functions for the oxygen-oxygen pair in the simulated 50/50 $PbO.GeO_2$ glass are presented in Figure 4.2.1.2. The average O-O interatomic distance was found to be 2.70Å with a FWHM of 0.36Å. The oxygen-oxygen pair distribution function is in good agreement with neutron diffraction results obtained by Umesaki *et al.*[18] The authors report an average interatomic distance of 2.8 Å. The PDF for the O-O pair in the simulated glass does not return to a null value after the first maximum which indicates that there is not a good separation between the first and the second coordination shells, i.e. the short range order is not well defined for the O-O pair. From the CDF of the O-O pair (inset in Figure 4.2.1.2), the average oxygen-oxygen coordination was determined to be 4.20 at a cut-off distance of 3.7 Å. The CDF for the O-O pair increases continuously without the presence of a clear defined flat plateau region. This is further indication that the short range environment is not well defined with respect to the O-O pair.

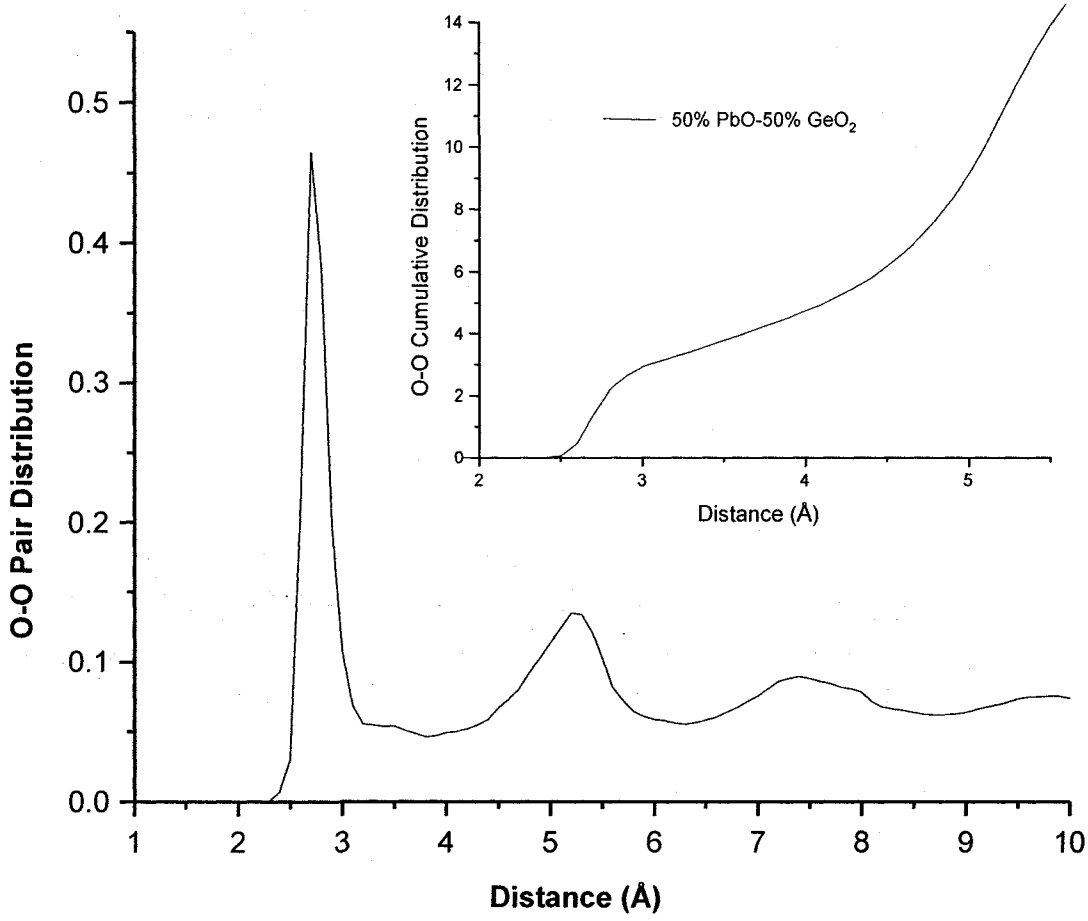

Figure 4.2.1.2 Pair and cumulative (shown in inset) distribution functions of the O-O atomic pair for the simulated 50mol%PbO.50mol%GeO_2 glass.

The germanium-germanium pair and cumulative distribution function for simulated 50/50 $PbO.GeO_2$ glass is presented in Figure 4.2.1.3. The average interatomic distance for the Ge-Ge pair was found to be 3.27Å with a FWHM of 0.35Å. The average number of germanium neighbours at a cut-off distance of 3.5Å was found to be 2.10 (inset in Figure 4.2.1.3). EXAFS study by Witkowska *et al.*[20] report a Ge-Ge interatomic distance of 2.93 Å and coordination number of 1.9. The MD results indicate that there is an overlap between the first and the second coordination shell. This is suggested by the observation that the PDF for the Ge-Ge pair does not return to a null value after the first maximum.

In order to investigate the structure of the germanate framework further, we examined the short range order of the germanium ions by identifying the different types of oxygen atoms present in the glass. This analysis is done by counting the types of oxygen atoms present within the first Ge-O coordination. This includes bridging oxygens (BOs), non-bridging oxygens (NBOs) and non-germanate anions (NGA). Bridging and non-bridging oxygens were previously described in section 1.1. In this thesis, an EXTRA refers to a germanium ion that has more than two bridging oxygen attached to it, and a non-germanate anion is an oxygen that is not connected to the germanate framework. Results from this study

indicate that the simulated 50/50 $PbO.GeO_2$ glass consists of 57.2 % BO, 42.6% NBO, and 0.2% EXTRA. The fact that 0% of the oxygen atoms are classified as non-germanate anions indicates that all of the germanium ions are part of the germanate framework. Furthermore, a high percentage of BOs and NBOs suggest that at high lead content, lead is depolymerizing the germanate framework by converting BOs to NBOs. This is consistent with the experimental observation that at high PbO content, lead acts as a network-former.[17, 21] The presence of a secondary lead framework was also observed in lead silicate glasses.[82]

To further investigate the germanate framework, the distribution of Q^n species was determined in order to identify the types of bonded oxygen for each individual germanium atom. The Q^n species were previously described in section 2.2 and illustrated in Figure 2.2.1 of this thesis. The MD results indicate that the 50/50 $PbO.GeO_2$ glass consists of 3.6% Q^0, 18.2% Q^1, 37.2% Q^2, 29.4% Q^3, and 11.6% Q^4 species. These results are consistent with the glass forming ability of lead at high PbO content. The large percentage of higher Q^n species might be due to the presence of a secondary lead framework. This would also explain the presence of a lower percentage of non-bridging oxygen atoms compared to bridging oxygens present in the 50/50 $PbO.GeO_2$ glass. It is worth mentioning that if

lead acted as a true modifier, then one would expect the non-bridging oxygens to dominate, and a high percentage of lower Q^n species.

The Ge-O-Ge and O-Ge-O bond angle distributions will further enhance the understanding of the local environment of the glass system and will enable us to monitor the presence and/or creation of corner-sharing and edge-sharing polyhedra. A corner-sharing GeO_4 polyhedron would exhibit a O-Ge-O bond angle of 109°, whereas a shoulder at 90° indicates edge-sharing GeO_6 units. The O-Ge-O and Ge-O-Ge bond angle distributions for the simulated 50/50 $PbO.GeO_2$ glass are presented in Figure 4.2.1.4. The average O-Ge-O and Ge-O-Ge bond angles for the simulated 50/50 $PbO.GeO_2$ glass were found to be 109° with FWHM of 12.1° and 144° with FWHM of 36.2°, respectively. These distributions are typical of corner-sharing polyhedra.

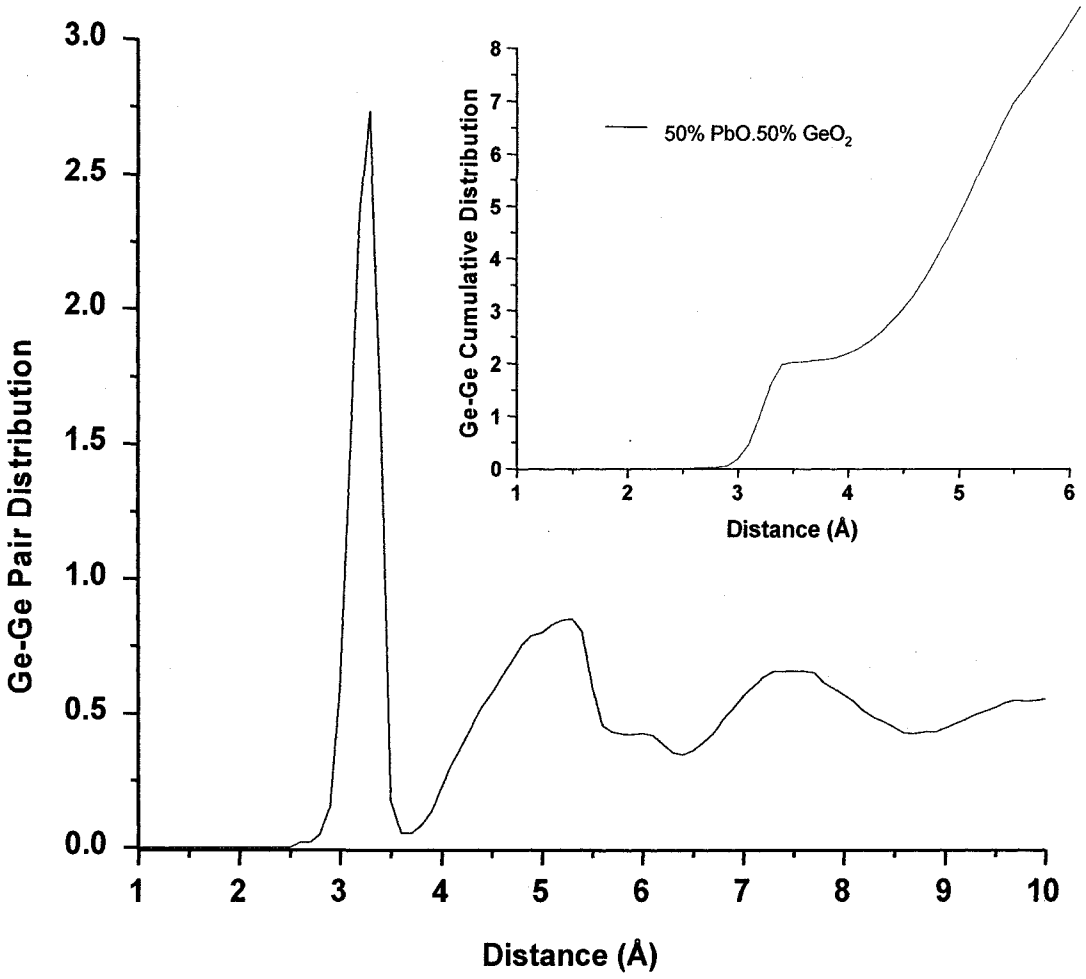

Figure 4.2.1.3 Pair and cumulative (shown in inset) distribution functions of the Ge-Ge atomic pair for the simulated 50mol%PbO.50mol%GeO_2 glass.

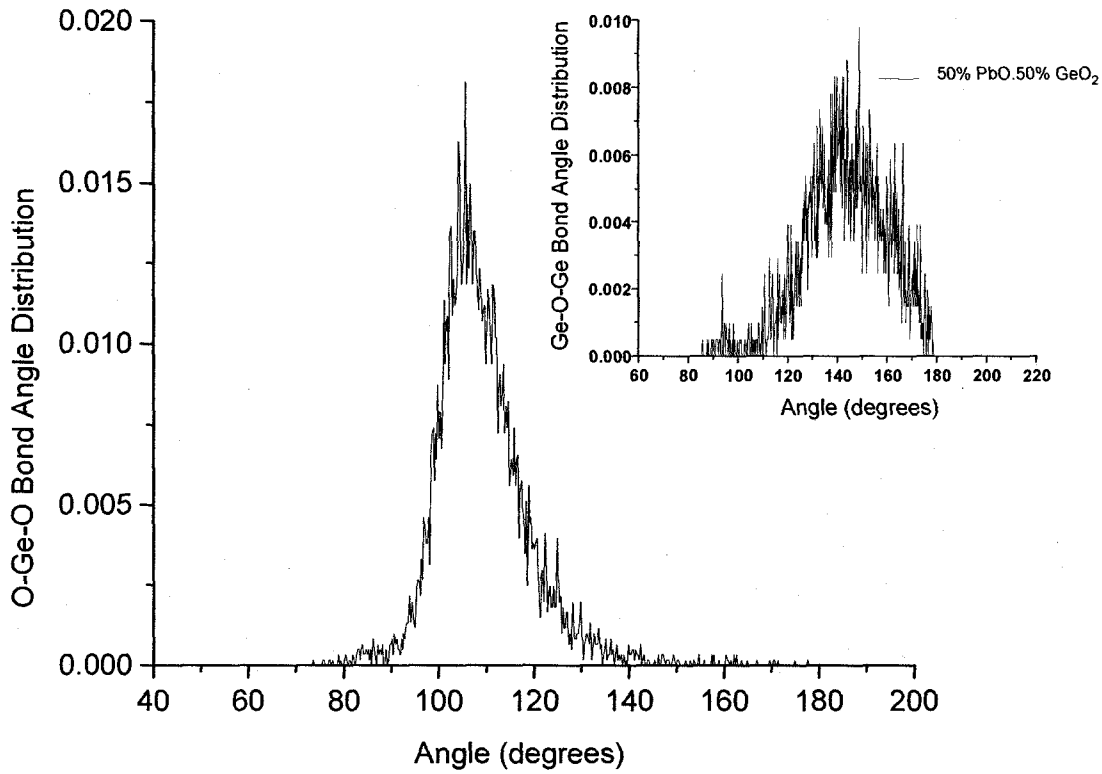

Figure 4.2.1.4 O-Ge-O and Ge-O-Ge (shown in inset) bond angle distribution for the simulated 50mol%PbO.50mol%GeO_2 glass.

4.2.2 The Lead Environment

The room temperature equilibrated pair and cumulative distribution functions for the lead-oxygen pair for the simulated 50/50 $PbO.GeO_2$ glass are presented in Figure 4.2.2.1. The Pb-O interatomic distance was found to be 2.37Å with FWHM of 0.21Å. These results are in agreement with experimental results obtained by EXAFS study[20] which reports a Pb-O nearest neighbour distance of 2.39Å . Also, neutron diffraction data[18] for $PbO.GeO_2$ glass indicate a Pb-O interatomic distance of 2.21-2.42Å for orthorhombic and 2.33Å for tetragonal systems. The PDF is sharp and narrow, although to a lesser degree in comparison to the PDF for the Ge-O atomic pair, discussed earlier. Also, the PDF for the Pb-O pair shows a small tail suggesting the presence of odd coordinated species in the structure, and does not return to a null value after the first maximum which indicates that there is not a clear separation between the first and the second coordination shells. The average number of oxygen neighbours with respect to lead (inset in Figure 4.2.2.1) was found to be 5.64 at a cut-off distance of 3.2 Å. This result is consistent with the orthorhombic structure exhibiting a coordination of 6.0. [60]

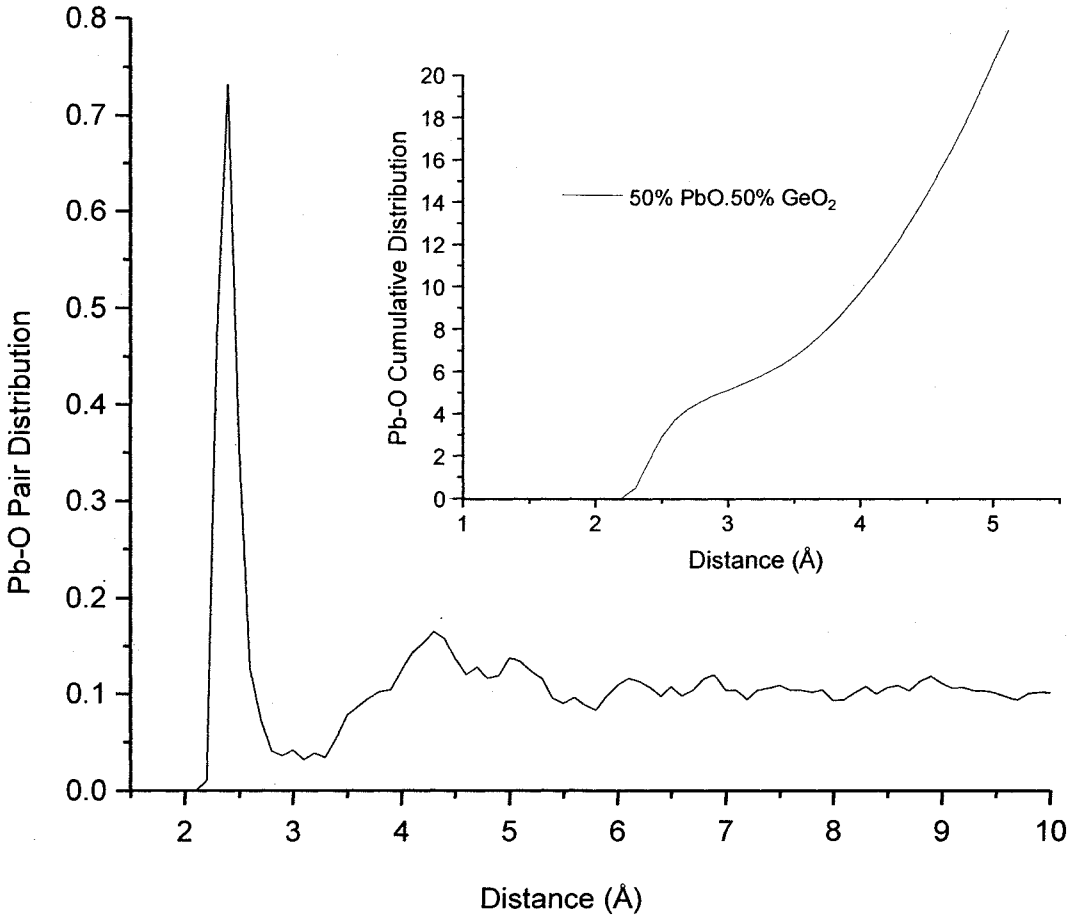

Figure 4.2.2.1 Pair and cumulative (shown in inset) distribution functions of the Pb-O atomic pair for the simulated 50mol% PbO.50mol% GeO_2 glass.

The lead-lead pair distribution function was found to be broad and asymmetric. The Pb-Pb interatomic distance was found to be 3.60Å with FWHM of 1.78Å. The average lead-lead coordination number at a cut-off distance of 5.8Å was found to be 5.90. The values for the Pb-Pb interatomic distance in the simulated 50/50 $PbO.GeO_2$ glass compares well with neutron diffraction study by Umesaki *et al.*[18] The authors report a Pb-Pb interatomic distance of 3.47-3.63Å for the orthorhombic phase and 3.70-3.90Å for the tetragonal phase.

The lead-germanium pair distribution function is broad. The Pb-Ge interatomic distance was 3.80Å with FWHM of 1.27Å. An average coordination number of 5.20 was obtained at a cut-off distance 4.7Å for the simulated 50/50 $PbO.GeO_2$ glass.

In order to analyze the lead environment in the lead germanate glass, the oxygen atoms bonded to individual germanium atoms were examined with respect to the lead framework at a lead-oxygen cut-off distance of 3.2Å. These results are shown in Table 4.2.2.1 and indicate that approximately 27.9% of the oxygen atoms bonded to germanium ions are free of lead neighbours in the simulated 50/50 $PbO.GeO_2$ glass. This suggests the presence of two regions in the glass, a lead-rich and a germanium-rich region. The simulated glass shows a significant percentage of n_{Pb}=1 and 2 indicating that over 50% of the oxygen atoms

bonded to germaniums have one to two lead neighbours in the simulated glass. These results are in good agreement with the Q^n species analysis, and implies that in the simulated 50/50 $PbO.GeO_2$ glass lead ions act as network-formers.

Table 4.2.2.1 % speciation of oxygen in the first Ge^{4+} coordination shell with respect to the lead framework

Simulated Glass	$n_{Pb}=0$	$n_{Pb}=1$	$n_{Pb}=2$	$n_{Pb}=3$	$n_{Pb}=4$
50mol%PbO.50mol%GeO_2	27.9	26.6	24.9	18.9	1.7

In conclusion, we first focused on the MD simulation of $xPbO.(1-x)GeO_2$ glass with x=0.50, a composition where the controversy around the 'germanate anomaly' does not exist, and there is more agreement on the structural detail of the glass among experimental studies. The simulated glass was compared to and found to be in agreement with experimental results from EXAFS and neutron diffraction studies.[16,19 – 22] Furthermore, the simulated $PbO.GeO_2$ glass at 50 mol% PbO content indicates the presence of a secondary lead framework where lead acts as a network-former. In the next section, simulation results of a study of lead germanate glasses at different PbO content is discussed.

4.3 Composition Study on $PbO.GeO_2$ Glasses using *Potential Model 1*

The next set of simulations involved the composition study on $xPbO.(1-x)GeO_2$ glasses with x = 0.05, 0.1, 0.2, 0.25, 0.3, 0.33, 0.37, and 0.45 to investigate the mechanism of the 'germanate anomaly' and the influence of the PbO content on the GeO_2 framework. These glasses will be referred to as simulated 5/95, 10/90, 20/80, 25/75, 30/70, 33/67, 37/64, and 45/55 $PbO.GeO_2$ glasses, respectively.

The glasses were simulated using *potential model 1* (described in section 3.2.1) using the Verlet algorithm. Ionic Radii of 0.39 Å, 1.20Å, and 0.99Å were used for germanium, oxygen and lead ions, respectively. The details of the simulation procedure are summarized in Figure 3.1.1.2 and Tables 4.3.1.a and 4.3.1.b.

Furthermore, the simulated glass densities for 5/95, 10/90, 20/80, 25/75, 30/70, 33/67, 37/64, 45/55, and 50/50 $PbO.GeO_2$ glasses are presented in Table 4.3.1.b. The simulated glass densities are lower than the experimental glass densities.[61]

Table 4.3.1.a Simulation parameters for $PbO.GeO_2$ glasses

Element	Ionic Radius, σ (Å)	Ionic Charge (q)
O	1.20	- 2.0
Ge	0.39	+ 4.0
Pb	0.99	+ 2.0
Hardness parameter, n :	8	

Table 4.3.1.b Number of atoms and density for $PbO.GeO_2$ glasses

mol% PbO	Number of Atoms			Density (g/cm^3)	
	Ge	Pb	O	experimental[61]	simulated
5	1008	53	2069	3.97	3.85
10	1008	112	2128	4.29	4.07
20	1008	252	2268	5.00	4.89
25	1008	336	2352	5.48	5.39
30	1008	432	2448	5.80	5.65
33	1008	503	2519	5.91	5.86
37	1008	592	2608	6.00	5.90
45	1008	825	2841	6.54	6.35
50	1008	1008	3024	6.81	6.83

From the positions obtained at 300K, the pair (PDF) and cumulative (CDF) distribution functions were calculated. The discussion is separated in two main sections, the germanate framework and the environment of the lead atoms with respect to the germanate framework. A summary of interatomic distances and coordination numbers obtained from the simulations is presented in Table 4.3.2.

Table 4.3.2 Structural parameters derived from the pair and cumulative distribution functions for simulated $PbO.GeO_2$ glasses

mol% PbO	Interatomic Distance (Å)						Coordination Number					
	O-O	Ge-O	Pb-O	Ge-Ge	Pb-Ge	Pb-Pb	O-O	Ge-O	Pb-O	Ge-Ge	Pb-Ge	Pb-Pb
5	2.70	1.72	2.37	3.30	3.70	3.60	4.18	4.00	3.03	2.03	3.76	3.33
10	2.70	1.72	2.37	3.30	3.60	3.60	4.21	4.02	3.85	1.95	4.49	3.53
20	2.70	1.72	2.37	3.30	3.70	3.60	4.16	4.05	4.16	1.96	4.94	3.60
25	2.70	1.72	2.36	3.30	3.70	3.60	4.18	4.06	4.39	1.94	5.01	4.62
30	2.70	1.72	2.37	3.29	3.70	3.50	3.94	4.07	4.64	2.00	5.02	5.15
33	2.70	1.72	2.37	3.29	3.70	3.60	4.16	4.02	4.39	1.96	4.69	5.21
37	2.70	1.72	2.35	3.29	3.70	3.60	4.16	4.03	4.59	1.95	4.89	5.43
45	2.70	1.72	2.37	3.30	3.70	3.60	4.17	4.03	4.89	2.02	5.12	5.57
50	2.70	1.72	2.37	3.27	3.80	3.60	4.20	4.02	5.64	2.10	5.20	5.90

4.3.1 The Germanate Framework

The room temperature equilibrated pair and cumulative distribution functions for the germanium-oxygen pair in simulated $PbO.GeO_2$ glasses are presented in Figure 4.3.1.1. The average Ge-O interatomic distance was found to be 1.72Å and independent of the PbO content. This finding is in agreement with a recent EXAFS study on lead germanate glasses[20] indicating that the average Ge-O interatomic distance is independent of glass composition. The PDFs for the Ge-O pair are sharp and narrow and return to a null value after the first maximum for all glasses. This suggests that there is a good separation between the first and the second coordination shells.

From the CDFs of the Ge-O pair (inset in Figure 4.3.1.1), the average coordination number of oxygen atoms to germanium was determined to be four at a cut-off distance of 2.5Å. The CDFs show a flat plateau region which is indicative of a well defined short range environment with respect to germanium. According to the simulated results, the number of oxygens surrounding germanium ions in the first coordination shell reaches a maximum of 4.07 at 30 mol% PbO content.

In order to get a better idea of the number of oxygen ions surrounding the germanium ions in the first coordination shell, the distribution of the Ge-O coordination for the simulated glasses was

calculated. The results of this calculation are illustrated in the form of a histogram in Figure 4.3.1.2, and indicate that at glass compositions of 10 to 33 mol% PbO, up to 8% of germanium ions are coordinated to five oxygen ions. At glass composition of 33 mol% PbO, the glass consists of about 97% four-coordinated germanium ions. The percentage of five-coodinated germanium ions increases once again between glass compositions of 37 and 50 mol % PbO. As mentioned earlier, for the 50/50 $PbO.GeO_2$ glass, 96% of the germanium ions are four-coordinated, and 4% are five-coordinated to oxygen atoms. Hence, the simulations show that in the first coordination shell of $PbO.GeO_2$ glasses (PbO compositions of 5-50mol%), the germanium ions are predominantly coordinated to four oxygen atoms and discount formation of six-coordinated germanium-oxygen ions. However, formation of up to 8% five-coordinated germanium-oxygen ions are observed in the simulated glasses. As previously discussed in chapter 2, experimental results on structural detail of $PbO.GeO_2$ glasses at different PbO compositions are rather inconclusive. The simulated results for $PbO.GeO_2$ glasses are in agreement with experimental studies on alkali germanate glasses by Henderson *et al.*[73] and Weber [74] which suggest formation of five-coordinated germanium ions to oxygen ions with the addition of alkali oxide. Also, an MD study on sodium germanate glass by Karthikeyan *et al.*[77] determined that with the

addition of up to 18 mol% sodium oxide to the sodium oxide glass, a portion of GeO_4 units converted to GeO_5.

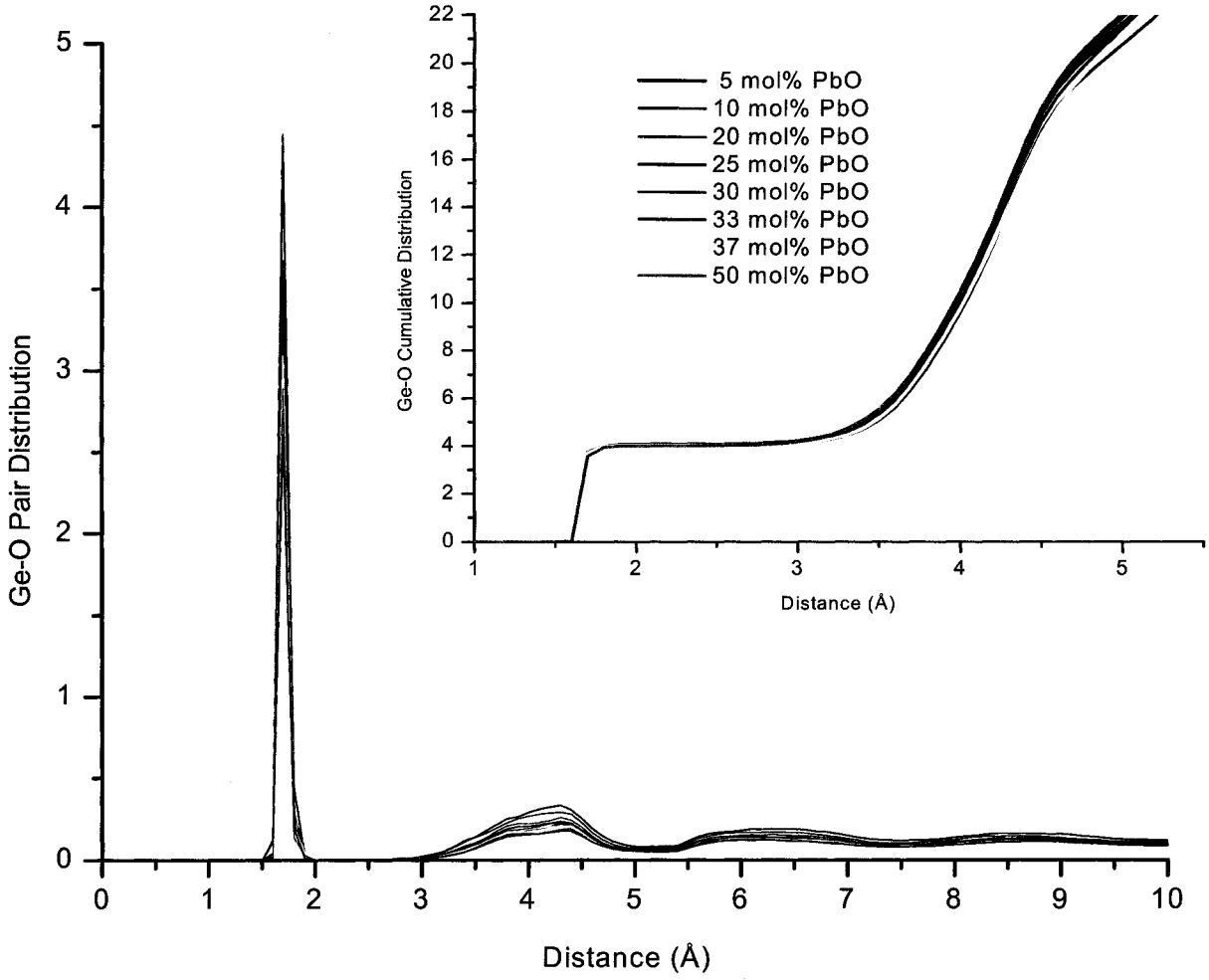

Figure 4.3.1.1 Pair and cumulative (shown in inset) distribution functions of the Ge-O atomic pair for the simulated $PbO.GeO_2$ glasses.

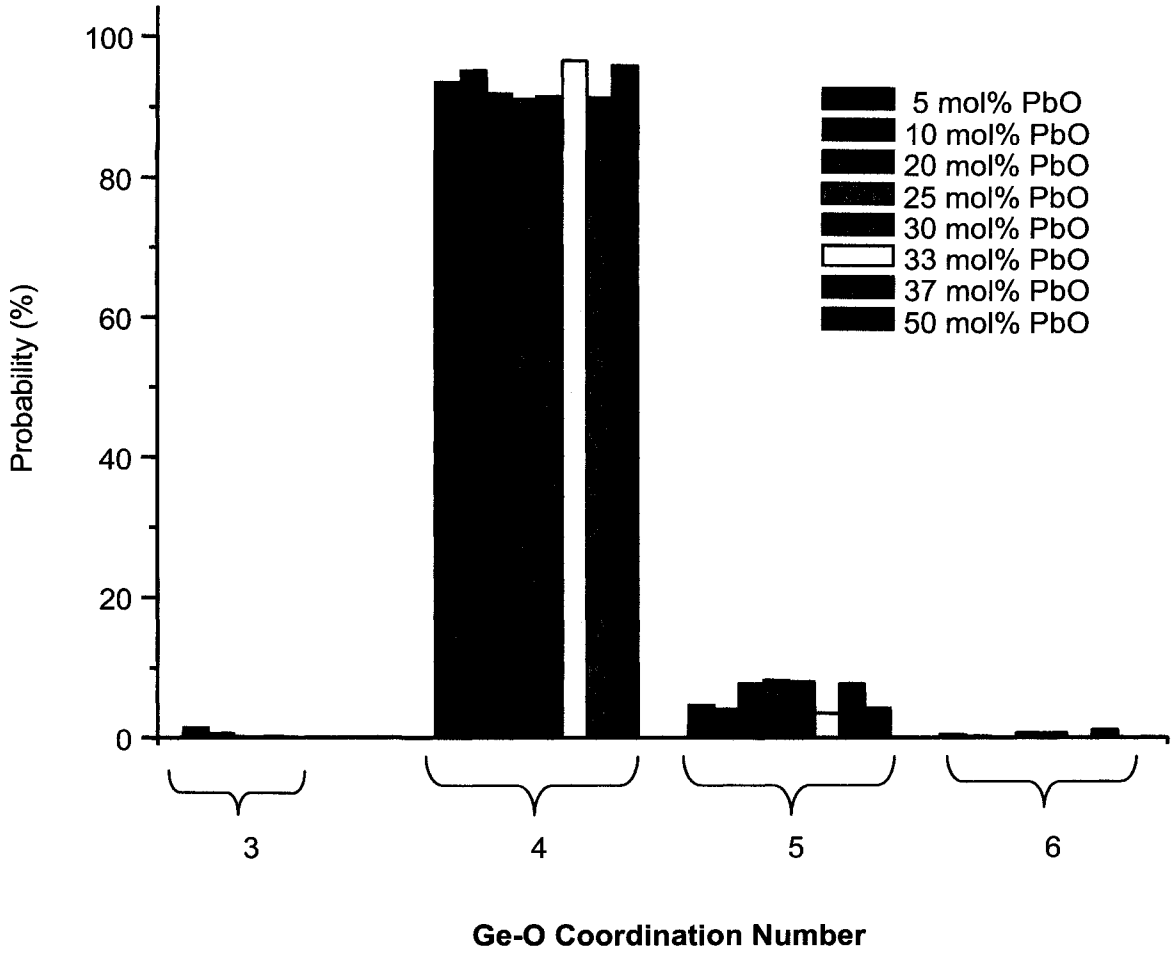

Figure 4.3.1.2 Percentage of the different types of Ge-O coordination present in simulated $PbO.GeO_2$ glasses.

The pair and cumulative distribution functions for the oxygen-oxygen pair in the simulated $PbO.GeO_2$ glasses are presented in Figure 4.3.1.3. The average O-O interatomic distance was found to be 2.70Å. The PDFs for the O-O pair in the simulated glasses does not return to a null value after the first maximum which indicates that there is not a good separation between the first and the second coordination shells. The average number of oxygen neighbours at a cut-off distance of 3.7Å (inset in Figure 4.3.1.3) was found to vary between 3.98 and 4.21. The CDFs for the O-O pair increases continuously without the presence of a distinct flat region. This is further indication that the short range environment is not well defined with respect to O-O pair.

The average interatomic distance for the Ge-Ge pair was found to vary between 3.27Å and 3.30 Å with the addition of 5-50 mol% PbO (Figure 4.3.1.4). The average number of germanium neighbours at a cut-off distance of 3.5Å shows slight variation between 1.95 and 2.10 for compositions of 5-50 mol% PbO. A EXAFS study on lead germanate glasses by Witkowska *et al.*[20] reports Ge-Ge interatomic distances of 2.93-2.96Å and Ge-Ge coordination of 1.9 - 2.3 between 10 and 50 mol% PbO contents. Furthermore, the MD results indicate that there is an overlap between the first and the second coordination shell. This is

suggested by the observation that the PDF for the Ge-Ge pair does not return to a null value after the first maximum.

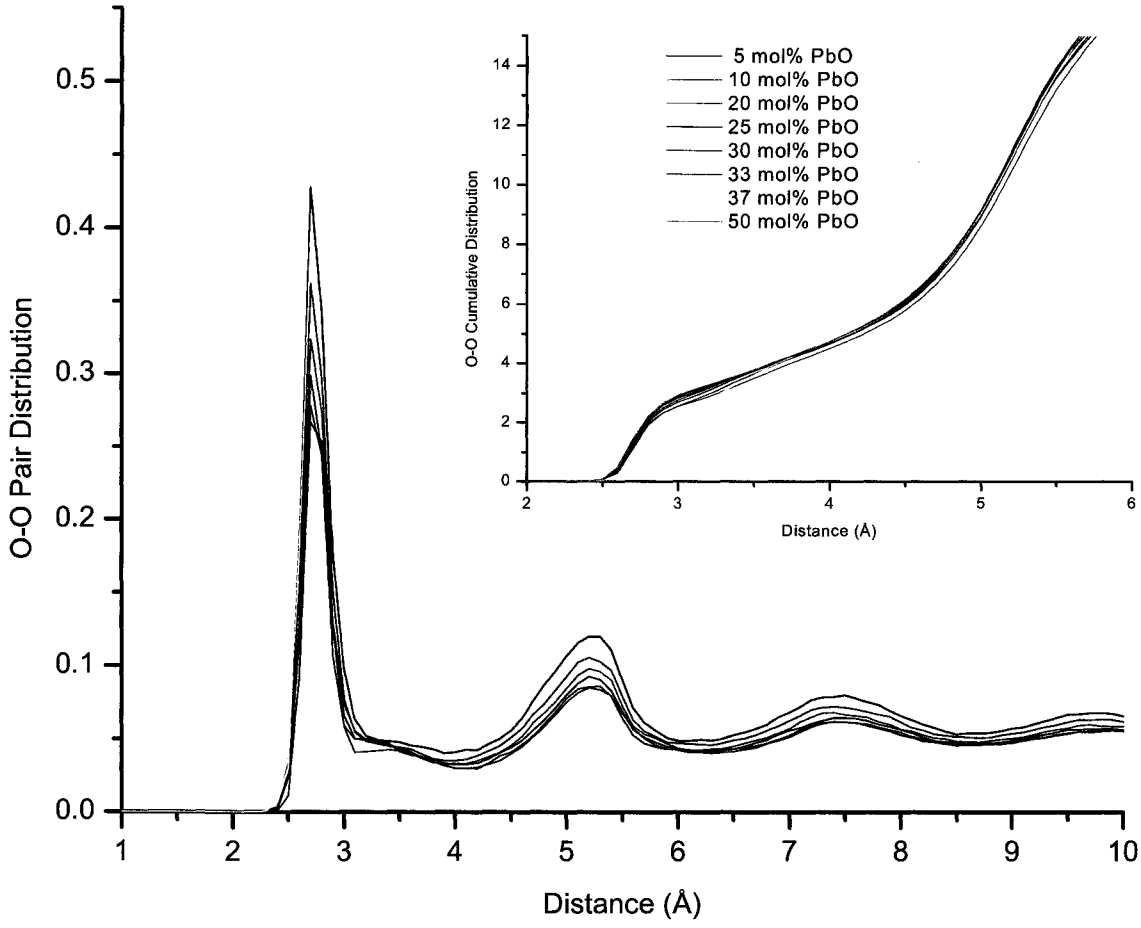

Figure 4.3.1.3 Pair and cumulative (shown in inset) distribution functions of the O-O atomic pair for the simulated $PbO.GeO_2$ glasses.

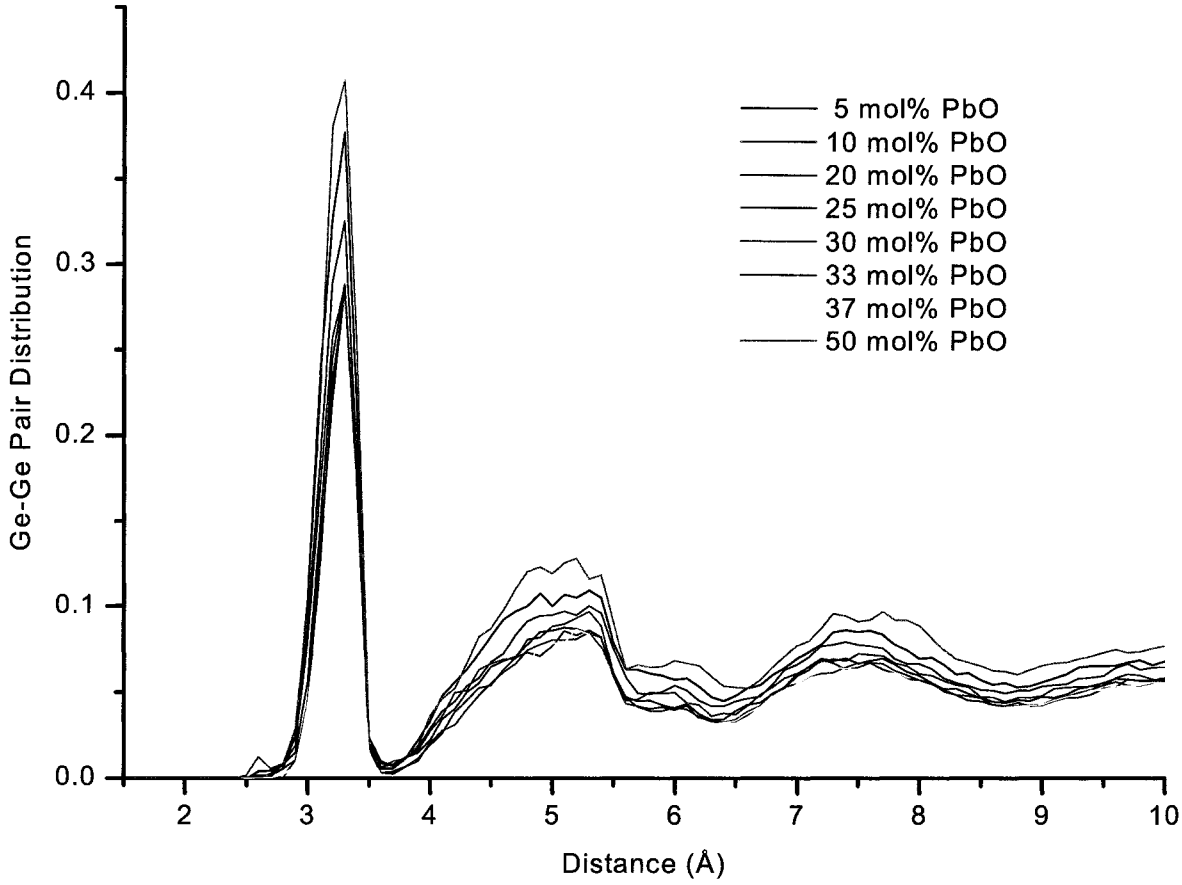

Figure 4.3.1.4 Pair distribution functions of the Ge-Ge atomic pair for the simulated $PbO.GeO_2$ glasses.

In order to further investigate the structure of the germanate framework, we examined the short range order of the germanium ions by identifying the different types of oxygen atoms present in the glass. The results from this study (summarized in Table 4.3.1.1) indicate that with the addition of PbO to the glass framework, there is continuous formation of NBOs, decrease in the percentage of BOs and EXTRA (germanium ion with more than two bridging oxygens attached to it). With the addition of PbO to the glass framework, non bridging oxygens form at the expense of bridging oxygens. This suggests that lead is depolymerising the germanate framework by converting BOs to NBOs. Continuous formation of NBOs (as opposed to formation of GeO_6 units) and a breakdown of the 3-dimensional germanate framework with the addition of PbO to lead germanate glasses has been suggested from EXAFS study.[17] Raman spectra of lead germanate glass have further shown that GeO_4 vibrations involving NBOs are observed at lower modifier contents in lead germanate glasses than in alkali germanate glasses.[64] The simulated results are consistent with the experimental observation that at high PbO content, lead acts as a network-former.[17] One has to also keep in mind that the large ionic radius of lead ion of 0.99Å might further result in deploymerization of the germanate framework. The size of the cation added to the germanate glasses might also effect the structural properties of the glass framework. Henderson *et*

al.[10] have shown that in the case of alkali germanate glasses, smaller alkali cations such as lithium, sodium, and potassium are easier to incorporate into the glass framework, whereas the larger alkali cations such as rubidium and cesium result in more rapid formation of NBOs, as they are more difficult to fit into the empty spaces of the GeO_4 rings.

Table 4.3.1.1 Types of oxygen ions present within the first Ge^{4+} coordination shell in simulated $PbO.GeO_2$ glasses

mol% PbO	EXTRA(%)	BO (%)	NBO (%)
5	8.2	87.5	4.3
10	3.9	90.2	5.9
20	2.9	85.9	11.2
25	3.1	82.1	14.8
30	1.8	79.6	18.6
33	0.3	77.0	22.7
37	1.2	73.5	25.3
45	0.5	63.4	36.1
50	0.2	57.2	42.6

The germanate framework was further studied by calculating the distribution of Q^n species. The Q^n species were previously described in section 2.2 and illustrated in Figure 2.2.1 of this thesis. The results of the MD simulations are summarized in Table 4.3.1.2. According to these results, with the addition of PbO to the germanate glass framework, the percentage of Q^4 species decreases steadily from 64.9% to 11.6%. The percentage of Q^3 species increases with the addition of up to 37mol% PbO from 29.8% to 40.6%. This is followed by a decrease in Q^3 species with further addition of PbO to the glass framework. The lower Q^n species, namely Q^2, Q^1, and Q^0, increase with the addition of PbO to the glass framework, however this increase is more pronounced in the case of Q^2 and Q^1 species. For the glasses with 5-50 mol% PbO content the Q^2 and Q^1 species increase from 5.1 to 37.2, and from 0.2 to 18.2, respectively. The decrease in Q^4 species is consistent with the decrease in BOs with the addition of lead oxide to the glass framework (see Table 4.3.1.1). The steady increase in Q^2, Q^1, and Q^0 species further validates the formation of NBOs with the addition of PbO to the germanate framework (see Table 4.3.1.1). As for the Q^3 species, it appears that two different mechanisms are responsible for the increase up to 37 mol% PbO and their subsequent decrease with further addition of lead oxide to the glass. One possible explanation is that with the addition of PbO, lead is acting as a modifier

filling void spaces in the glass and forming NBOs in the process. With further addition of PbO (~33-37mol%), lead starts to act as a network-former, in which case more NBOs are formed in the process. These results are consistent with the glass-forming capability of lead at high PbO content. Hence, the combined large percentage of higher Q^n species indicates the presence of a secondary lead framework.

Formation of Q^3 and Q^2 species have also been reported upon addition of alkali oxide to germanate glasses.[73]

Table 4.3.1.2 Types of bonded germaniums for each individual oxygen atom in simulated $PbO.GeO_2$ glasses

mol % PbO	Q^4 (%)	Q^3 (%)	Q^2 (%)	Q^1 (%)	Q^0 (%)
5	64.9	29.8	5.1	0.2	0.0
10	70.7	24.6	4.1	0.6	0.0
20	60.5	29.5	8.5	1.4	0.1
25	50.6	35.2	12.7	1.5	0.0
30	44.1	36.0	16.3	3.5	0.1
33	35.3	39.8	21.1	3.5	0.2
37	30.5	40.6	23.5	5.1	0.2
45	16.3	37.4	31.7	12.9	1.7
50	11.6	29.4	37.2	18.2	3.6

The Ge-O-Ge and O-Ge-O bond angle distributions will further help in characterization of the local environment of the glass system and will enable us to examine the presence and/or creation of corner-sharing and edge-sharing polyhedra. The O-Ge-O and Ge-O-Ge bond angle distributions for the simulated $PbO.GeO_2$ glasses are presented in Figure 4.3.1.5. The average O-Ge-O and Ge-O-Ge bond angles for the simulated glasses were found to be 109° and 144°, respectively. A corner-sharing GeO_4 polyhedron would exhibit a O-Ge-O bond angle of 109°, whereas a shoulder at 90° signifies edge-sharing GeO_6 units. Therefore, the simulated bond angle distributions are typical of corner-sharing polyhedra. This is not surprising, since the simulated $PbO.GeO_2$ glasses did not contain any GeO_6 units. The simulations indicate that the average simulated O-Ge-O and Ge-O-Ge bond angles are independent of the PbO composition. For clarity, the Ge-O-Ge bond angle distributions for 10/90, 30/70, and 50/50 glasses are shown separately in Figure 4.3.1.6 and show an average bond angle of 144° with similar FWHM of about 36 Å.

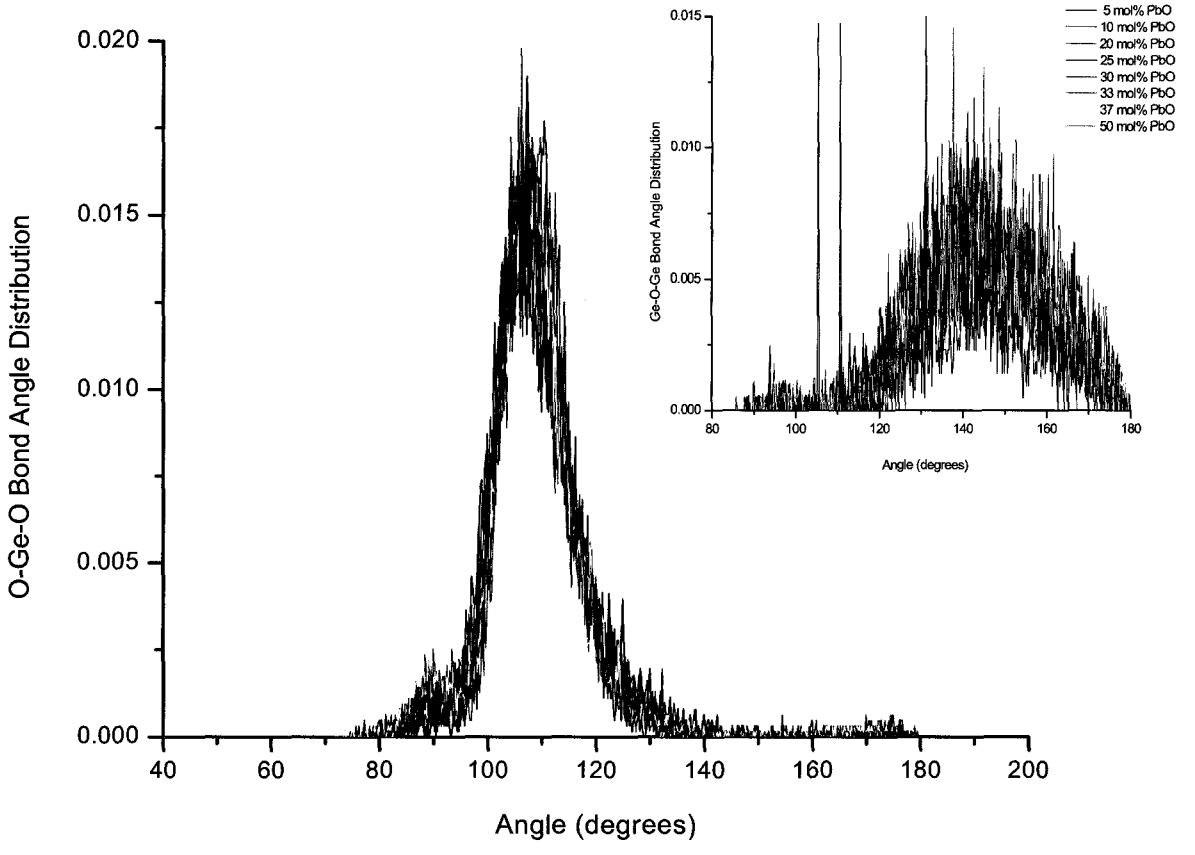

Figure 4.3.1.5 O-Ge-O and Ge-O-Ge (shown in inset) bond angle distribution for the simulated $PbO.GeO_2$ glasses.

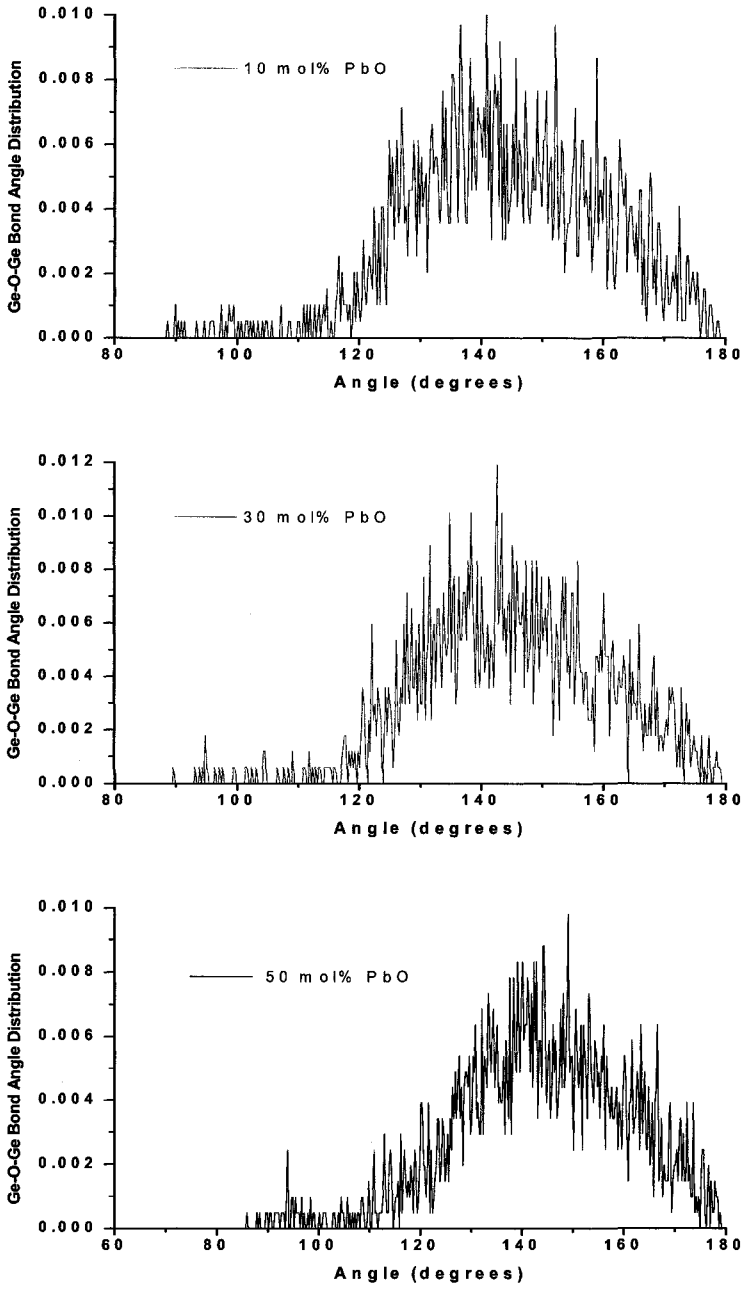

Figure 4.3.1.6 Ge-O-Ge bond angle distribution for the simulated 10/90 (in red), 30/70 (in turquoise), and 50/50 (in navy blue) $PbO.GeO_2$ glasses.

As it was mentioned earlier, Henderson *et al.*[10] have proposed the formation of three-membered GeO_4 rings without the creation of six-coordinated Ge^{4+} ions as alternative model for the mechanism of the germanate anomaly in alkali germanate glasses. In order to investigate the medium-range structure and connectivity of the simulated glasses, a ring analysis was performed (see Table 4.3.1.3). The addition of up to 30 mol% PbO to the germanate framework shows a 9% increase in three-membered GeO_4 rings. However, based on previously discussed results on the composition study of $PbO.GeO_2$ glasses, it appears that formation of three-membered GeO_4 rings is not the only change that occurs in the glass framework with the addition of PbO. For example, addition of PbO also resulted in continuous formation of NBOs. At this point, we will focus on the effect of PbO on the lead environment, as this will shed additional light on the simulated glass structures.

Table 4.3.1.3 Types of rings present in the simulated $PbO.GeO_2$ glasses

mol % PbO	2	3	4	5	6	7	8	9
5	6.2	3.4	15.9	29.8	22.6	13.4	5.8	2.9
10	6.9	7.0	16.0	28.8	20.1	10.7	6.4	4.1
20	7.2	10.6	15.8	22.9	17.9	13.6	7.9	4.1
25	6.9	12.1	14.0	22.9	16.9	14.4	8.5	4.3
30	7.7	12.3	13.9	21.3	15.9	15.6	8.9	4.4
33	7.3	10.9	13.9	20.5	18.0	15.8	9.6	4.0
37	8.2	11.1	13.4	19.8	18.0	16.4	8.8	3.3
45	8.5	10.9	13.0	18.7	19.3	18.9	8.4	2.3
50	8.3	9.9	13.6	18.3	21.4	19.6	7.6	1.3

4.3.2 The Lead Environment

The room temperature equilibrated pair and cumulative distribution functions of lead-oxygen pair for the simulated $PbO.GeO_2$ glasses are presented in Figure 4.3.2.1. The average Pb-O interatomic distance was found to be in the range of 2.35 - 2.37Å for the simulated glasses. This variation is statistically small, so that essentially the Pb-O interatomic distance is independent of the glass composition. This is in agreement with EXAFS[21], and Raman[16] studies on lead germanate glasses.

The PDFs for the Pb-O pair do not return to a null value after the first maximum which indicates that there is not a clear separation between the first and the second coordination shells. The PDFs are sharp and narrow, although to a lesser degree in comparison to the PDF for the Ge-O atomic pair, discussed earlier.

The average number of oxygen neighbours with respect to lead (inset in Figure 4.3.2.1) was found to increase continuously with the addition of PbO to the glass framework (see Table 4.3.2). For the 5/95 glass, the number of oxygens surrounding lead in the first coordination shell at a cut-off distance of 3.2Å is 3.03. The number of oxygen atoms at a cut-off distance of 3.2Å increases to 5.64 for the 50/50 glass. The addition of 10 mol% PbO to the germanate framework increases the Pb-O

coordination to 3.85. The simulated results suggest that at low PbO content, the lead environment consists predominantly of PbO_4 units. According to EXAFS[21], PbO_4 units are predominant at PbO compositions of up to 20 mol%. Both PbO_4 and PbO_3 units have been reported from this EXAFS[21] study with the addition of higher than 20 mol% PbO. Simultaneous occurrence of PbO_4 and PbO_3 units could also be inferred from the simulations, but must be confirmed with additional simulated structural features of the glass framework.

The average lead-lead and lead-germanium interatomic distances were found to be 3.60Å and 3.70Å for the major portion of the glass framework (see Table 4.3.2). The average Pb-Pb and Pb-Ge coordination number was found to continuously increase with the addition of PbO to the glass framework. According to the simulated results, the Pb-Pb coordination at cut-off distance of 5.8Å increased from 3.33 for the 5/95 glass to 5.90 for the 50/50 glass. The average number of germanium ions surrounding the lead atoms at a cut-off distance 4.7Å increased from 3.76 for the 5/95 glass to 5.20 for the 50/50 glass.

The experimental Pb-O and Pb-Pb interatomic distances are of 2.34Å and 3.70-3.90Å for the tetragonal structure[59] and 2.21-2.42Å and 3.47-3.63Å for the orthorhombic structure[60], respectively. It is important to note that the experimental values for Pb-O and Pb-Pb interatomic

distances overlap for the tetragonal (red PbO) and orthorhombic (yellow PbO) structures. Hence, the lead environment in the lead germanate glasses was further analyzed by examining the oxygen atoms bonded to individual germanium atoms with respect to the lead framework at a lead-oxygen cut-off distance of 3.2 Å. As mentioned earlier, the cut-off distance of 3.2Å for the lead-oxygen atomic pair was chosen from the PDF to reflect the atoms in the first coordination shell. These results are shown in Table 4.3.2.1 and indicate that the addition of lead oxide causes a decrease in the percentage of oxygen atoms bonded to germanium ions that are free of lead neighbours (n_{Pb} = 0). This confirms the presence of two networks in the glass.

The simulated glasses show an increasing percentage of n_{Pb}=1 and 2 with the addition of PbO to the glass. This increase in percentage of the higher n_{Pb} with addition of lead oxide to the glass indicates connectivity of the two networks via BOs. As discussed earlier, the addition of lead oxide resulted in a continuous decrease in the percentage of BOs and an increase in percentage of NBOs (see Table 4.3.1.1). However, at PbO content of 50 mol%, the glass consisted of 57.2% BOs. These results are in good agreement with the Q^n species analysis (see Table 4.3.1.2).

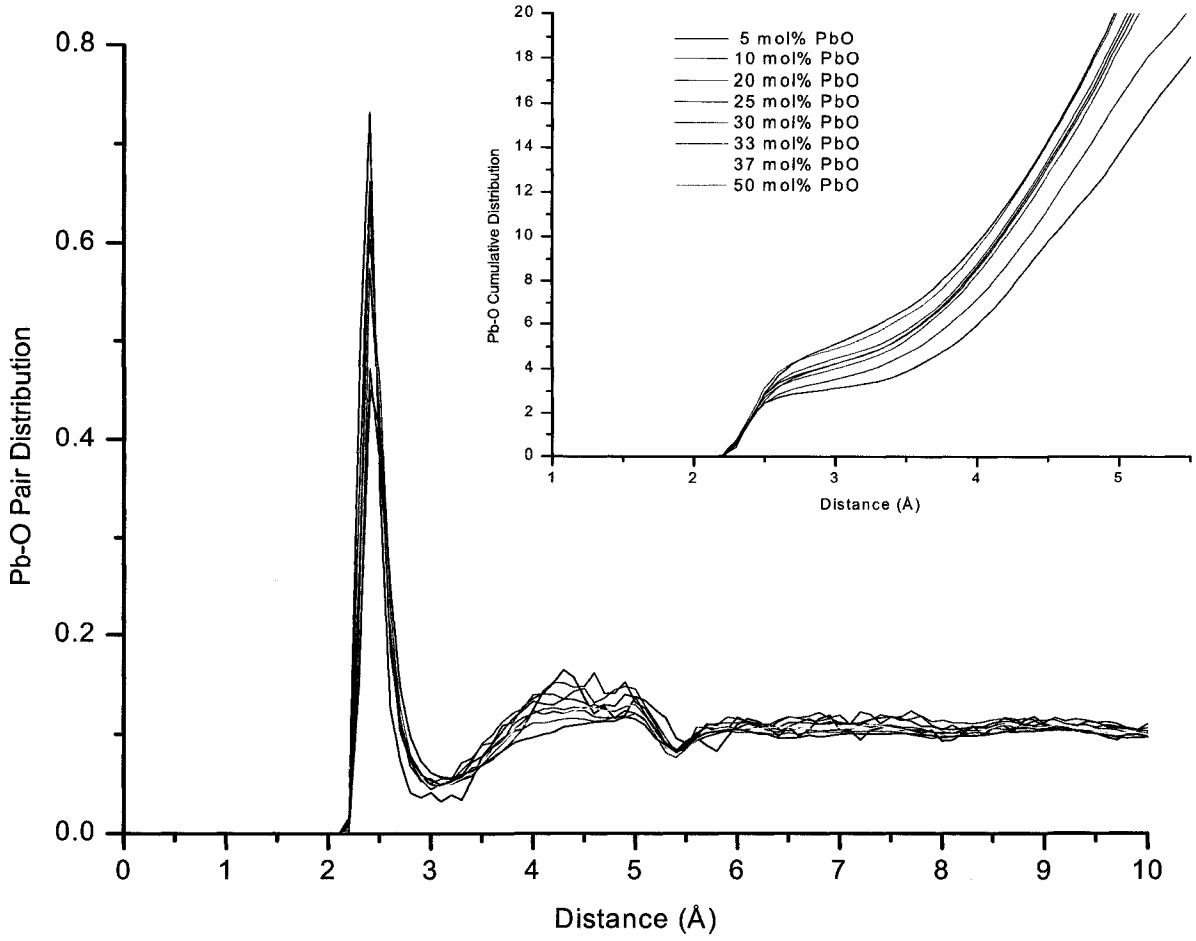

Figure 4.3.2.1 Pair distribution functions of the Pb-O atomic pair for the simulated $PbO.GeO_2$ glasses.

Table 4.3.2.1 % speciation of oxygen in the first Ge^{4+} coordination shell with respect to the lead framework

mol% PbO	$\%n_{Pb}=0$	$\%n_{Pb}=1$	$\%n_{Pb}=2$	$\%n_{Pb}=3$	$\%n_{Pb}=4$
5	95.1	4.6	0.3	0.0	0.0
10	87.8	10.4	1.7	0.1	0.0
20	72.4	21.1	5.8	0.7	0.0
25	65.3	23.9	9.4	1.4	0.0
30	55.8	28.8	12.7	2.6	0.1
33	57.7	24.2	14.8	3.2	0.1
37	45.5	30.8	18.2	5.3	0.2
45	32.6	30.5	24.4	11.7	0.8
50	27.9	26.6	24.9	18.9	1.7

In conclusion, we performed a composition study on $xPbO.(1-x)GeO_2$ glasses with x = 0.05, 0.1, 0.2, 0.25, 0.3, 0.33, 0.37, 0.45, and 0.50 to investigate the structural mechanism of the 'germanate anomaly' and the influence of the PbO content on the GeO_2 framework. The results of these simulations indicate the continuous formation of NBOs with addition of PbO, and conversion of 9% of five-membered to three-membered GeO_4 rings with addition of up to 30 mol% PbO.

As for the proposed coordination change of Ge-O with respect to the 'germanate anomaly,'[18, 22] formation of six-coordinated Ge^{4+} ions was not observed with the addition of PbO. However, formation of up to 8% five-coordinated germanium-oxygen ions is observed in the simulated glasses.

At low PbO content, germanium ions are linked to 4 BOs and a high percentage of Q^4 species is obtained from simulations indicating that the germanate framework is highly polymerized. At high PbO content, the germanate framework becomes depolymerized and is made of GeO_4 units with one to four NBOs and high percentage of Q^3 to Q^0 species. A summary of interatomic distances and coordination numbers for simulated glasses is presented in Table 4.3.2.

In order to further analyze the lead environment, the oxygen atoms bonded to individual germanium atoms were examined with respect to the lead framework. The simulations indicate a decrease in percentage of $n_{Pb=0}$ (representing oxygen atoms connected to germanium ions that are free of lead neighbours) in these simulated glasses with addition of lead oxide which confirms the presence of two distinct regions in the glass, a lead-rich region and a germanium-rich region. Furthermore, the increased % of higher n_{Pb} confirms the connectivity of lead-rich regions via BOs. As for the role of lead in the glass framework, at low PbO content it acts as a network-modifier with predominance of PbO_4 units and at high PbO content, lead acts as a network-former consisting of PbO_4 and PbO_3 units.

The presence of a secondary lead framework has also been observed in lead silicate glasses.[82] In the case of alkali germanate glasses, Henderson states that "the structural mechanism responsible for

the anomaly remains inconclusive, but appears to involve a complex interaction between the formation of five-fold Ge^{4+}, generation of Q^3 and Q^2 species, and formation of small three-membered GeO_4 rings.[73] This structural trend is also observed for the simulation of $PbO.GeO_2$ glasses at PbO compositions of 5-50 mol%.

Chapter 5

5.1 Simulation of GeO_2 Glass using *Potential Model 2*

The second potential model includes a combination of 2- and 3-body BMH potential. The initial set of atomic coordinates was derived from the crystalline unit cell for α-quartz-like GeO_2.[96] The first step involved the development of the potential parameters for the GeO_2 crystal by adjusting the atomic force pair interactions to yield the proper interatomic distances. For example, the Ge-O potential curve was generated to yield the interatomic distance of 1.73 Å reported for the α-quartz-like GeO_2.[96] This was done by modifying the Born-Mayer-Huggins potential parameters, A_{ij}, β_{ij}, and ρ_{ij} described previously in section 3.2.2 of this thesis. It is important to note that although each of the three parameters influences a certain part of the potential curve, they are dependent on one another, and hence a change in one parameter usually alters the other parts of the potential curve as well. Due to lack of Ge-O and Ge-Ge potential curves in the literature, we used the previously derived Si-O and Si-Si potential parameters [82, 93] as the initial guide to derive the Ge-O and Ge-Ge potential curves. The justification in comparing the Ge-O potential curve to the Si-O potential curve follows from a study on lead germanium oxide single crystals[99] where the germanium ions replace the silicon ions to form

isomorphous compounds in minerals. However, in employing the Si-O potential curve as guide, we considered the fact that germanium is less electronegative than silicon. This decrease in electronegativity would theoretically result in decreasing the repulsion between germanium and oxygen ions, and therefore possibly yield a steeper potential curve for Ge-O pair, compared to Si-O atomic pair. Figure 5.1.1 is a representation of the derived potential curves for the Ge-O, O-O, and Ge-Ge atomic pairs of GeO_2 crystal.

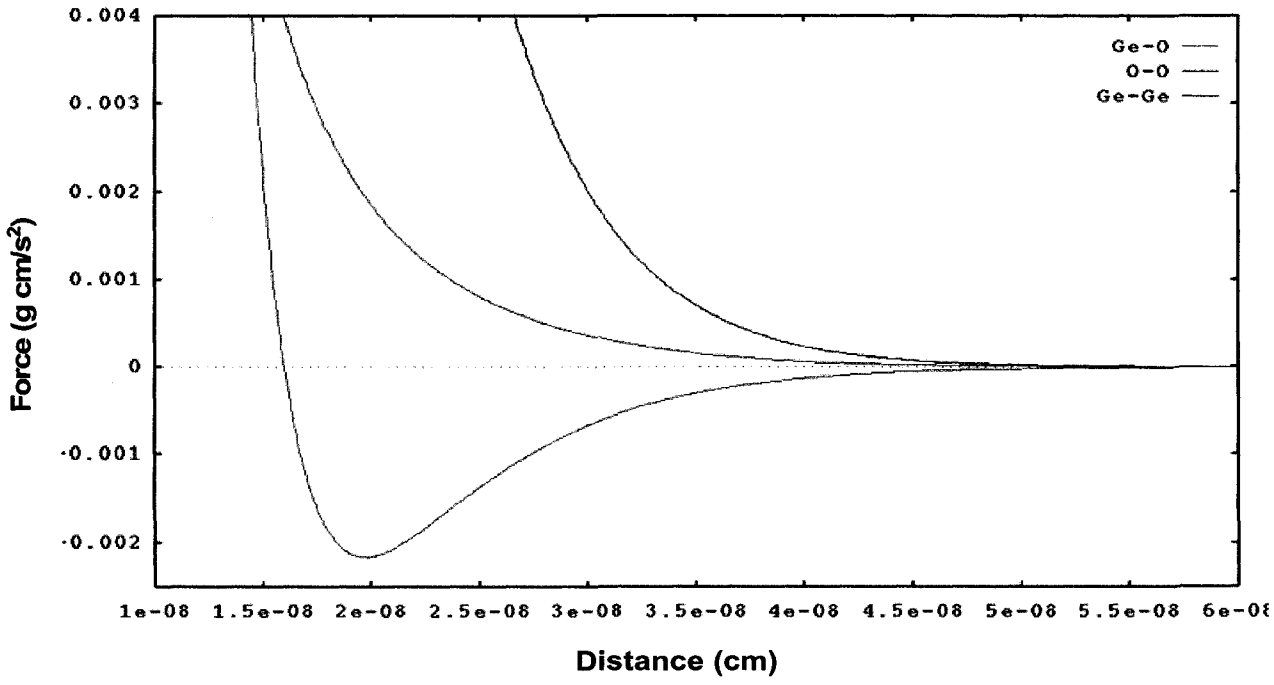

Figure 5.1.1 Representation of the Ge-O (red curve), Ge-Ge (blue curve) and O-O (green curve) force curves.

To verify the derived potential parameters, the MD simulation of the GeO_2 crystal at constant energy was performed for 10,000 time steps at room temperature. A good set of potential parameters for the ionic pairs would result in only a slight displacement in the position of the crystal caused by vibrations and would not cause any bond rearrangements. It is also important to note that the potential parameters developed for the crystal should result in identical interatomic distances, coordination and bond angles before and after it is run through the MD simulation. From the data generated by this test MD run, one could instantly check the crystalline system for its stability by simply looking at its temperature and pressure. Stable temperatures and pressures are further indications of good potential parameters for the ionic pair in the crystalline system. Figure 5.1.2 shows an example of potential parameters for the GeO_2 crystal that resulted in total bond breakage after it was run through the MD simulation, whereas Figure 5.1.3 represents more suitable potential parameters for the GeO_2 crystal. With the use of numbered arrows we have brought to attention the regions where bond rearrangements have occurred. Both arrows 1 and 2 in Figure 5.1.3 show how bond rearrangement occurred as the potential parameters ran through the MD simulation. Once suitable potential energy curves for the interionic pairs of

the GeO_2 crystal were obtained (summarized in Table 5.1.1), GeO_2 glass was simulated.

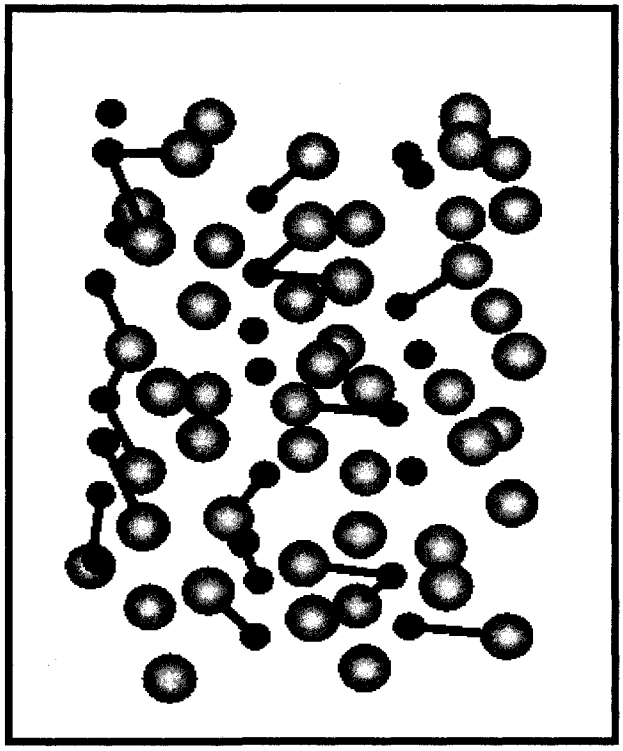

Figure 5.1.2 Pictorial representation of GeO_2 crystal with unsuitable 3-body potential parameters. The smaller spheres represent germanium and larger spheres represent oxygen.

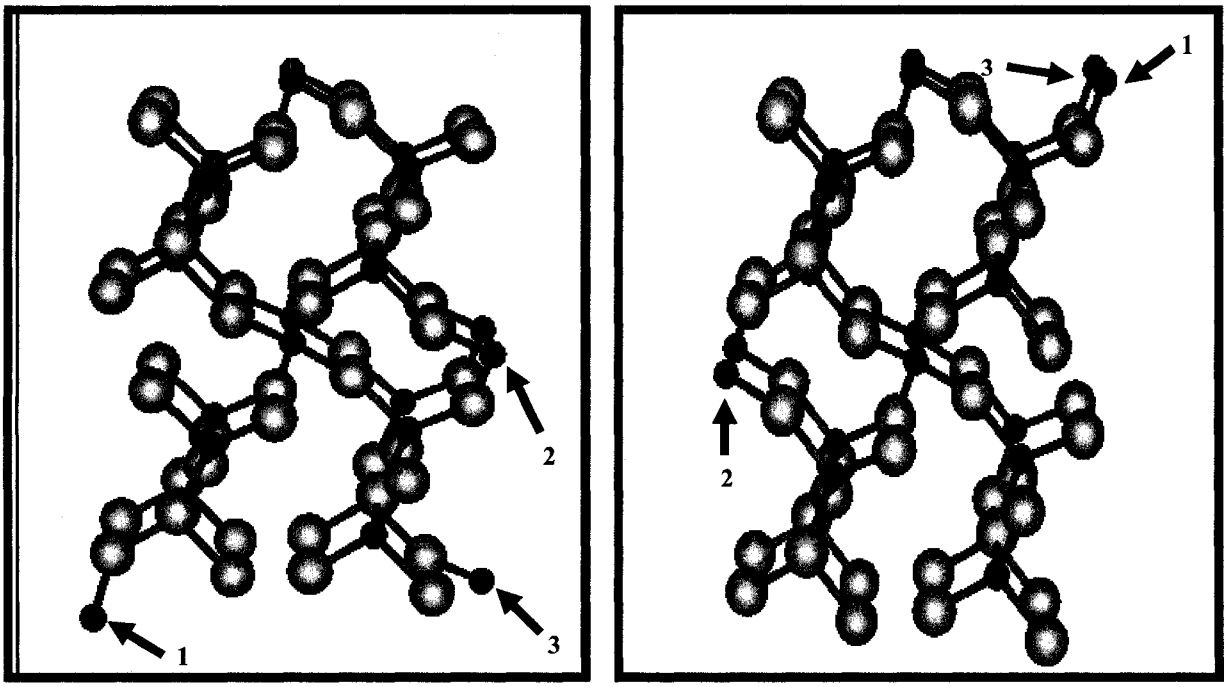

Before MD run

After MD run

Figure 5.1.3 Pictorial representation of GeO_2 crystal with more suitable 3-body potential parameters before MD run (on the left) and after MD run (on the right). The smaller spheres represent germanium and larger spheres represent oxygen.

Table 5.1.1 Simulation parameters for GeO_2 crystal

BMH pair potential parameters			
Atomic pair	A_{ij} (x 10^{8} erg)	β_{ij} (x 10^{7} cm)	ρ_{ij} (x 10^{8} cm)
O-O	0.0725	0.2340	0.2900
Ge-O	2.9300	0.2200	0.2050
Ge-Ge	0.2800	0.1900	0.5000

Three-body potential parameters			
Bond Angle	r_i^c (Å)	λ_i (x10^{11} erg)	γ_i (Å)
O-Ge-O	2.6	1.0	2.0
Ge-O- Ge	3.0	24.0	2.8

The room temperature equilibrated pair function for the germanium-oxygen pair is shown in Figure 5.1.4. The average Ge-O interatomic distance was found to be 1.73Å with a full width half maximum (FWHM) of 0.11Å. The PDF for the Ge-O pair is sharp and narrow, and returns to a null value after the first maximum, which indicates a good separation between the first and the second coordination shells. From the cumulative distribution function of the Ge-O pair (inset of Figure 5.1.4), the average number of oxygen around germanium ions at a cut-off distance of 2.5Å was determined to be 4.0. The CDF shows a flat plateau region, which is

indicative of the well-defined short-range environment for the germanium ions. These results are in excellent agreement with the experimental neutron diffraction studies and X-ray diffraction [36 – 48] on GeO_2 glass which reported a Ge-O interatomic distance of 1.70 to 1.74 Å and a Ge-O coordination of four.

The average interatomic distance for the oxygen-oxygen (Figure 5.1.5), and germanium-germanium (Figure 5.1.6) pairs was found to be 2.81Å with FWHM of 0.46Å and 3.39Å with FWHM of 0.17Å, respectively. The oxygen-oxygen interatomic distance for the simulated glass appears to be in good agreement with experimental results of 2.82 - 2.85Å (see Table 2.1.1.1). However, the Ge-Ge interatomic distance of 3.39Å is overestimated compared to experimental values. [38– 48]

The average O-Ge-O bond angle (Figure 5.1.7) for the simulated GeO_2 glass was found to be 110° with FWHM of 29°. The simulated O-Ge-O bond angle distribution seems to be bimodal with O-Ge-O angles of 100° and 115°. Experimentally, a O-Ge-O bond angle distribution of 106.1-113.1° has been reported.[35,100] A value of 109° corresponds to a tetrahedral angle and is in agreement with the four-coordinated Ge-O found in the simulated GeO_2 glass.

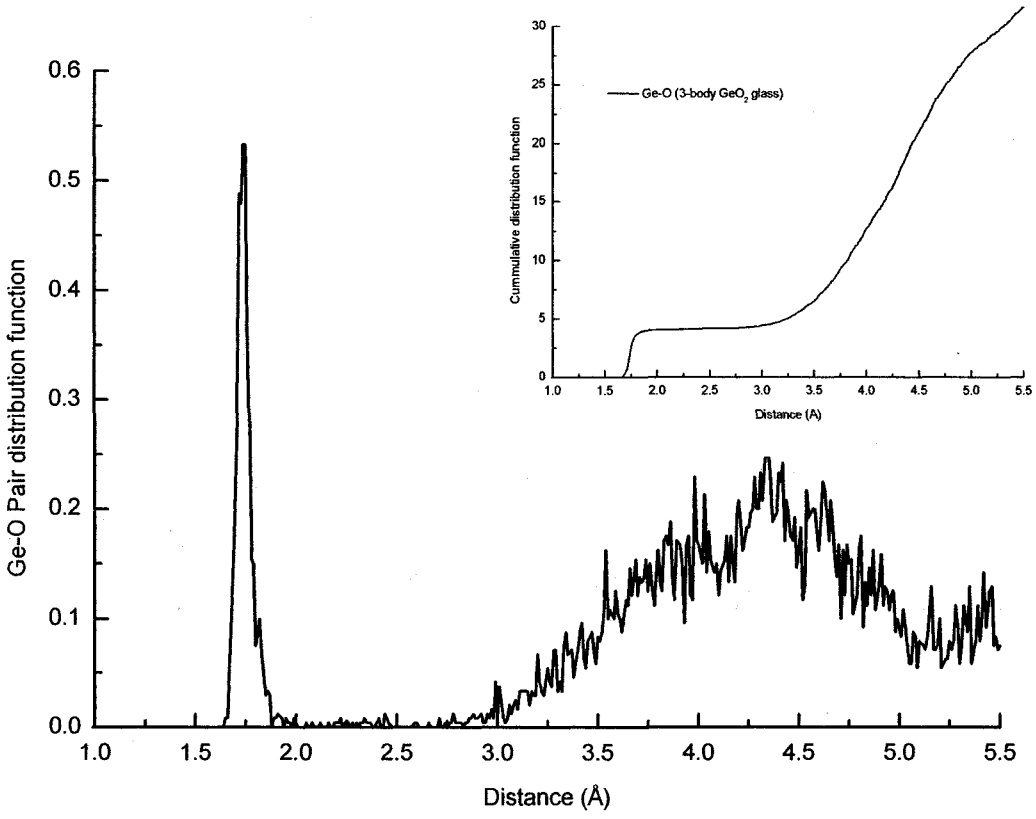

Figure 5.1.4 Pair and cumulative (inset) distribution function of the Ge-O atomic pair in the GeO_2 glass using *potential model 2*.

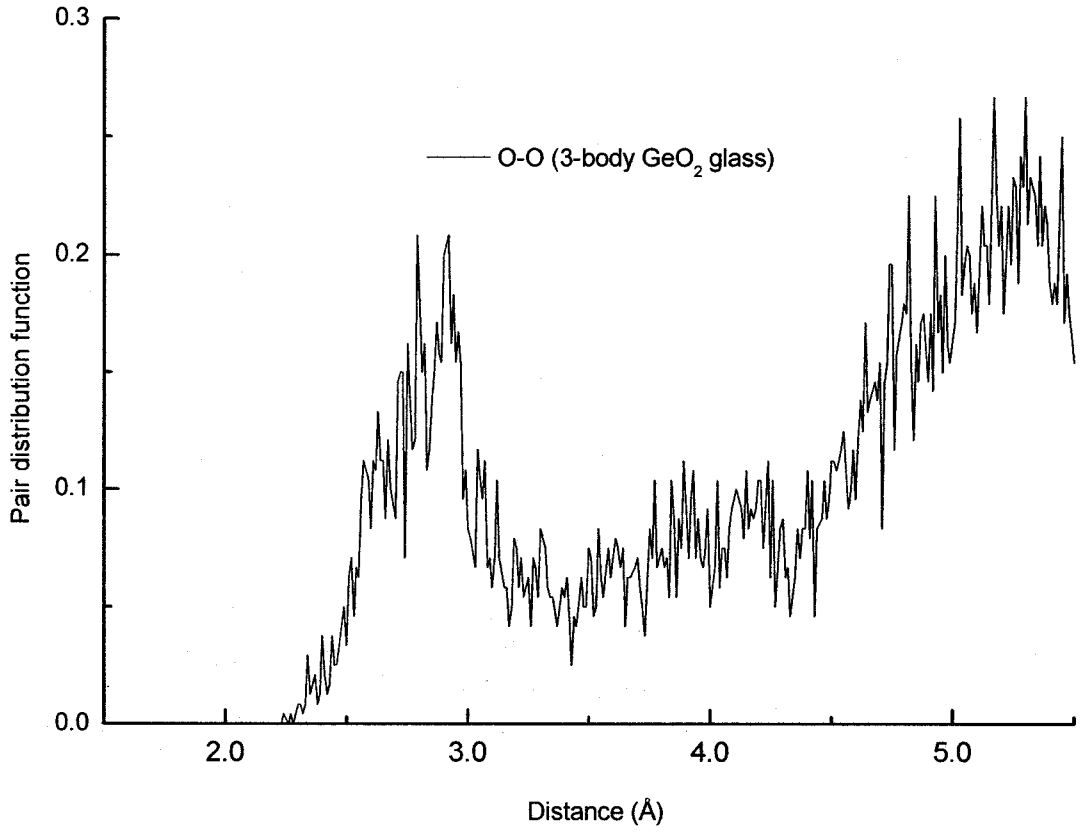

Figure 5.1.5 Pair distribution function of the O-O atomic pair in the GeO_2 glass using *potential model 2*.

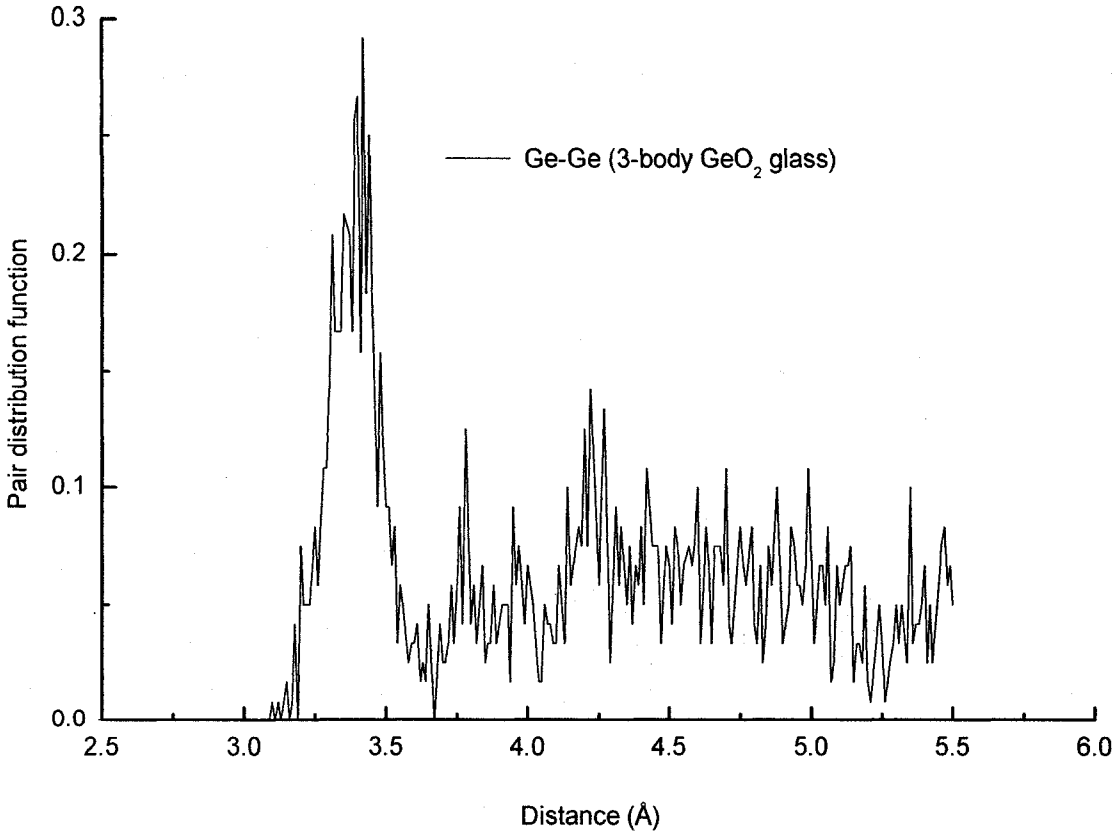

Figure 5.1.6 Pair distribution function of the Ge-Ge atomic pair in the GeO_2 glass using *potential model 2*.

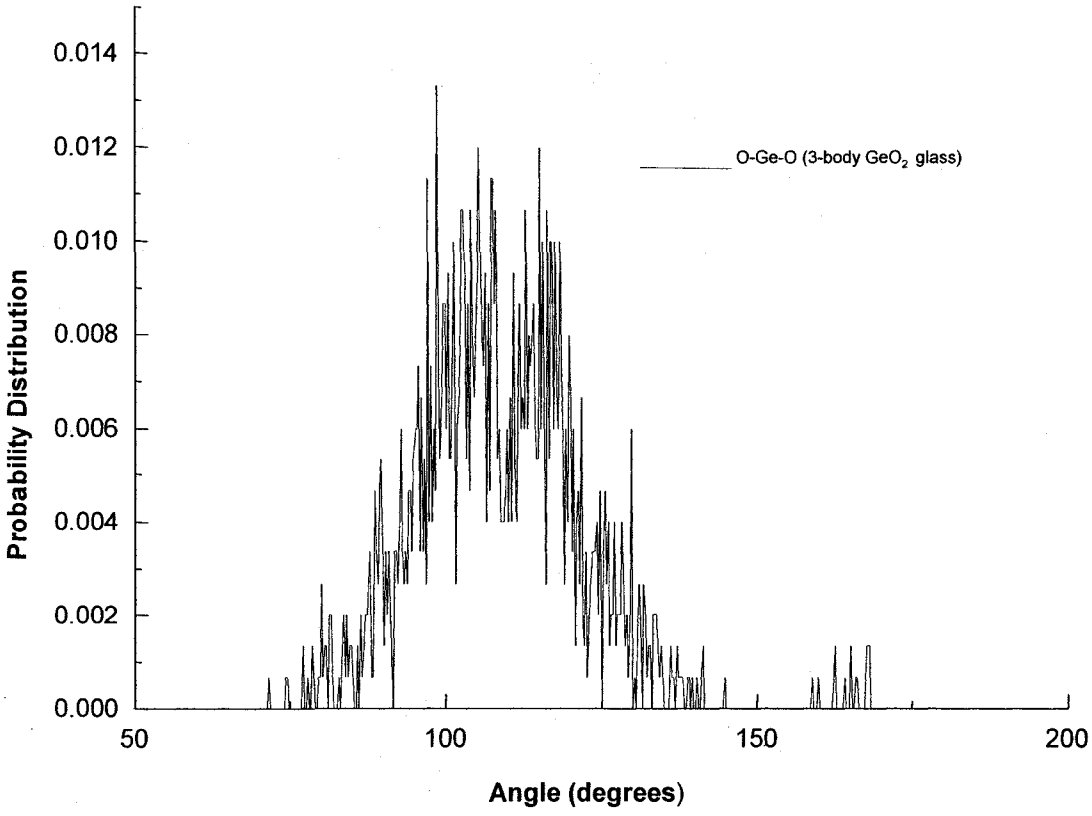

Figure 5.1.7 O-Ge-O bond angle distribution for the simulated GeO_2 glass using *potential model 2*.

A snapshot of the 3-body GeO_2 glass generated from the simulations is presented in Figure 5.1.8. The smaller spheres represent germanium and larger spheres represent oxygen.

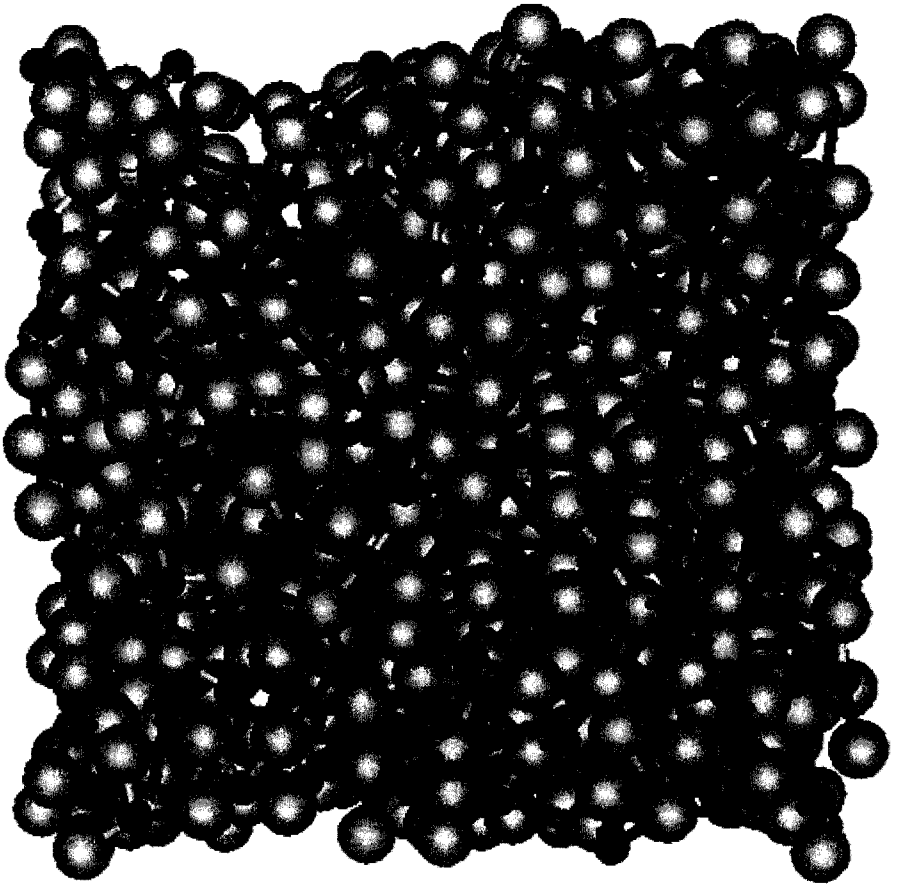

Figure 5.1.8 Pictorial representation of the simulated 3-body GeO_2 glass.

5.2 Comparison of Simulated GeO_2 Glasses using *Potential Models 1* and *2*

A comparison of the simulated GeO_2 glasses using the 2-body potential model by Mitra *et al.* [90] (*potential model 1*) and 2- and 3-body potential model by Feuston *et al.*[93] (*potential model 2*) is presented.

The pair distribution functions of the Ge-O pair are shown in Figures 5.2.1 and 5.2.2. The PDF for both glasses are sharp, narrow, and return to the null value indicating a good separation between the first and second coordination shell. It is important to note that a narrower pair distribution is observed for the simulated glass using *potential model 2*. Furthermore, the experimental Ge-O interatomic distance of 1.70-1.74 Å [36 – 48] is obtained from both potential models.

The cumulative distribution functions of the Ge-O pair are shown in Figures 5.2.3 and 5.2.4. The CDFs for both glasses show a flat plateau region confirming that the first and second coordination shells are well separated. Both CDFs indicate the expected Ge-O coordination of 4.

The O-Ge-O angles obtained from the simulations (Figures 5.2.5 and 5.2.6) are in good agreement with the four-coordinated Ge-O and the experimental O-Ge-O angle distribution of 106.3°-113.1°. The inclusion of a 3-body bending term, however, did not improve the short range GeO_2 glass structure significantly.

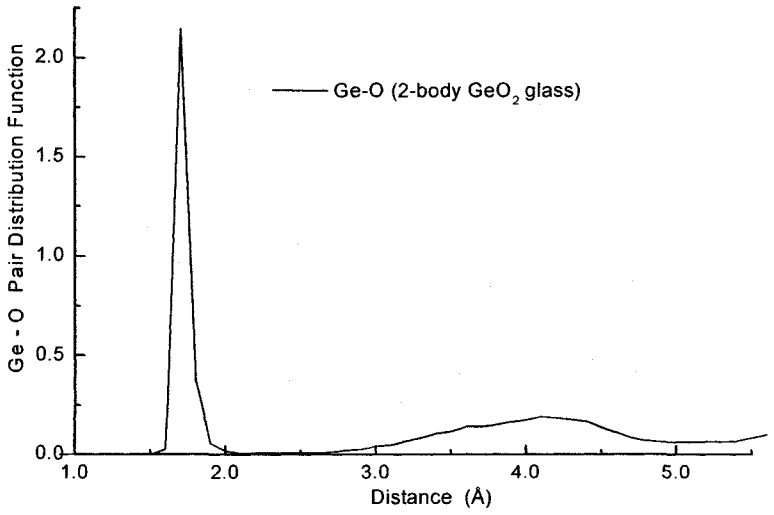

Figure 5.2.1 Pair distribution function of the Ge-O atomic pair for simulated GeO_2 glass using *potential model 1*.

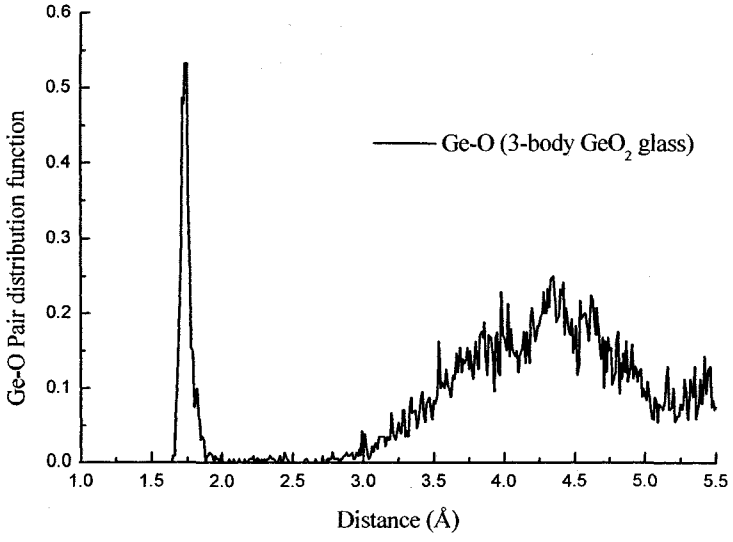

Figure 5.2.2 Pair distribution function of the Ge-O atomic pair for simulated GeO_2 glass using *potential model 2*.

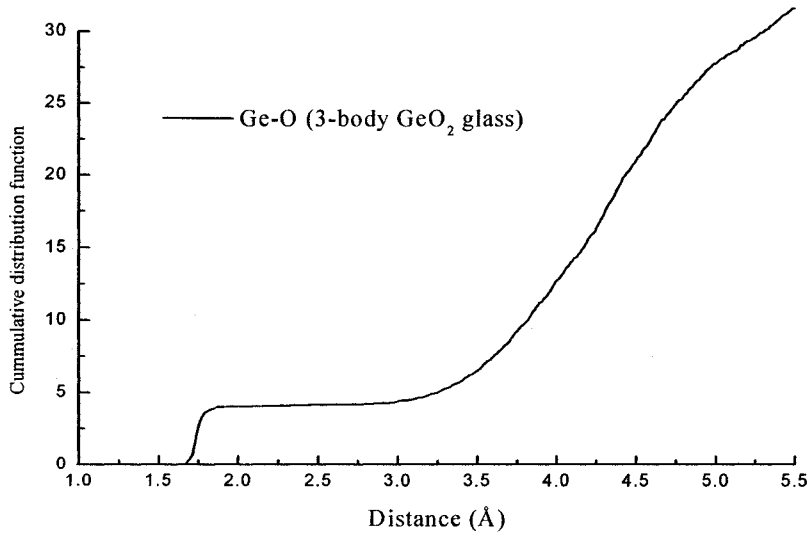

Figure 5.2.3 Cumulative distribution function of the Ge-O atomic pair for simulated GeO_2 glass using *potential model 1.*

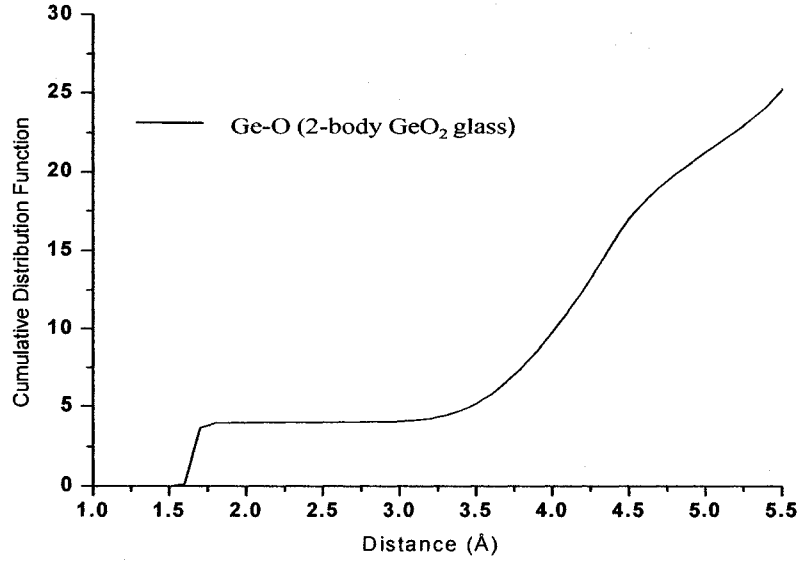

Figure 5.2.4 Cumulative distribution function of the Ge-O atomic pair for simulated GeO_2 glass *using potential model 2.*

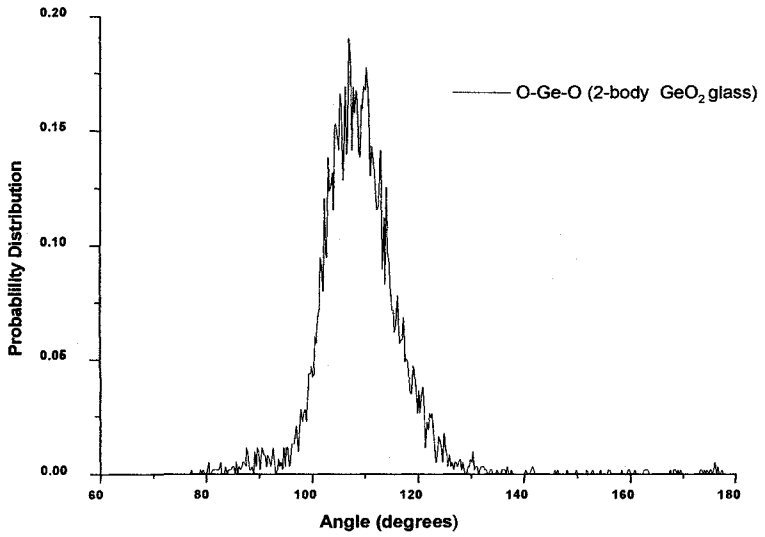

Figure 5.2.5 O-Ge-O bond angle distribution for simulated GeO_2 glass using *potential model 1*.

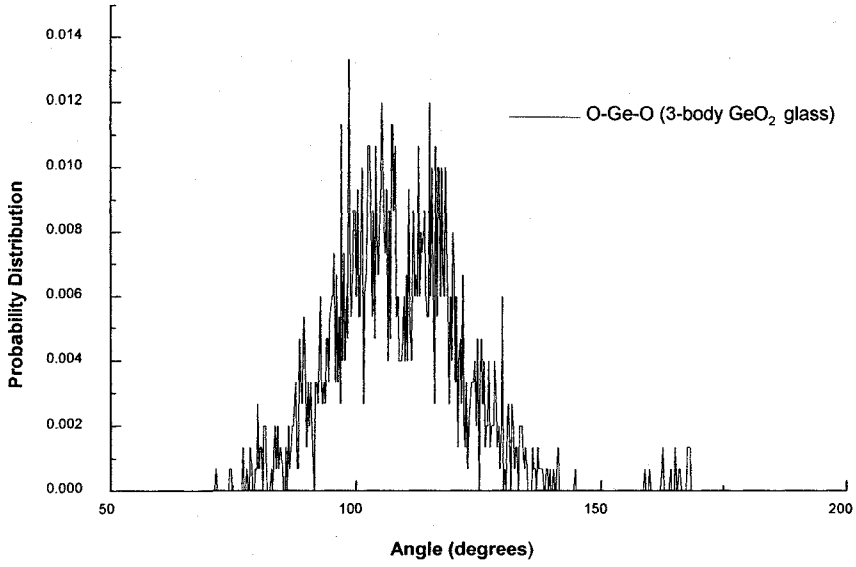

Figure 5.2.6 O-Ge-O bond angle distribution for simulated GeO_2 glass using *potential model 2*.

Chapter 6

6.1 Lattice Dynamics Simulation of GeO_2 Crystal using *Potential Model 3*

In search of an improved potential model to study the germanate anomaly in lead germanate glasses, we used a combination of 2- and 3-body potential with a shell-model in the interaction potential. The details of *potential model 3* are described in section 3.2.3 of this thesis. As mentioned earlier, the inclusion of polarizability allows for calculation of additional structural information (such as infrared frequencies, lattice energy, bulk modulus, elastic constants, static dielectric constants, high frequency dielectric constants, and heat capacity at constant volume) and results in improved simulated properties that are closer to experimental results. One of the drawbacks of including polarizability in the interaction potential has been associated with the added computing time required versus the projected improvements in the results.[101] This assumption is no longer valid due to advances in computer technology in recent years.

The starting point was to focus on the development of potential parameters for α-quartz-like GeO_2 crystal. Lattice energy minimization calculations at constant pressure with respect to both atomic coordinates and cell dimensions was performed. The computational package GULP [101] was used to carry out the calculations. The initial potential parameters

used in this study to model the interaction between lattice ions were reported by Catlow *et al.*[102] We modified these parameters further by empirically fitting the bond bending constant, K_{ijl}, as well as the A_{ij} parameters for the oxygen-oxygen and germanium-oxygen pairs to the structure in order to obtain crystal properties that were in better agreement with experimental results. The potential parameters were adjusted via a least squares fitting method and are presented in Table 6.1.1.

Table 6.1.1 Potential parameters for α-quartz-like GeO_2 using *potential model 3*

Parameter	O(shell) - O(shell)	Ge(core)-O(shell)
A_{ij} (eV)	0.00365	1946.065
ρ_{ij} (Å)	0.149	0.3172
C_{ij} (eV/Å^6)	27.88	53.66
Ge core charge (e)		4.000
O shell charge (e)		- 2.869
O core charge (e)		0.869
Core/shell spring constant (eV/Å^2)		74.92
Bond bending constant (eV/radians^2)		2.272

In order to test the validity of the developed potential parameters for the α-quartz-like GeO_2 crystal, infrared frequencies, lattice energy, bulk modulus (resistance of a material to compression and deformation), elastic constants (represented by a 6x6 matrix which contains the second derivatives of energy density with respect to external strain), static dielectric constants, high frequency dielectric constants, and heat capacity at constant volume were calculated and compared to available experimental results. In Tables 6.1.2 and 6.1.3, we compare the calculated crystal properties of α-quartz-like GeO_2 with those obtained from experiment.[96, 103–108] The model is also capable of producing dielectric and elastic constants that are in most part in agreement with experimental results.[104 – 106] It is important to note that one of the limitations of pair potentials is that the elastic constants are difficult to model. Typically, calculated elastic constants deviate 10-30% from experimental values.[107]

According to literature, one of the best-calculated values for the bulk modulus of α-GeO_2 is 27.4 GPa [106], the potential parameters derived in this study produced a value of 29.147 GPa, which is closer to the experimental values of 32.8-34.7 GPa. [106,109]

In order to further test the validity of the developed potential parameters for the α-quartz-like GeO_2 system, the infrared frequencies of the crystal were calculated. In Table 6.1.4 we compare the calculated

infrared frequencies for the α-quartz-like GeO_2 crystal with previously calculated[110] and experimental results.[111] The simulated infrared frequencies for the α-quartz-like GeO_2 presented in this thesis are in better agreement with experimental values[111] in comparison to previously calculated infrared frequencies.[110]

Table 6.1.2 Observed and calculated crystal parameters for α-quartz-like GeO_2 crystal

	Calculated	Experimental
Lattice parameters		
a , b (Å)	5.028	4.985 [96]
c (Å)	5.553	5.645 [96]
α, β	90.00	90.00 [96]
γ	120.0	120.0 [96]
Volume (Å^3)	121.553	121.500 [96]
Ge-O(core) distance (Å)	1.68	1.73 [96] & 1.65[105]
O-Ge-O bond angle (degrees)	107.5 – 115.9	106.3-113.1
		106.0-109.1
Lattice energy (kJ/mole)	-11960.4	-12828.0 [103]
Density (g/cm^3)	4.28	4.28 [104]
Bulk modulus (GPa)	29.1	32.8[106] & 34.3[115]

Table 6.1.3 Observed and calculated crystal properties for α-quartz-like GeO_2 crystal

	Calculated	**Experimental** [104,105,108]
Elastic constants (10^{11} Dyne/cm^2)		
C_{11}	6.99	6.64 & 6.48
C_{33}	9.16	11.8
C_{44}	3.84	3.68 & 3.74
C_{66}	3.07	2.25
C_{13}	0.41	3.20
C_{12}	0.84	2.13
Static dielectric constants		
ε_{11}°	6.00	7.43
ε_{33}°	6.26	6.65 & 7.44
High frequency dielectric constant		
$\varepsilon_{11}^{\infty}$	2.05	
Heat capacity-const volume (J/(mol.K)	45.09	58.77
Entropy J/(mol.K)	35.44	
Helmholtz free-energy (kJ/mol)	-11942.82	

Table 6.1.4 Infrared frequencies for α-quartz- like GeO_2 crystal at room temperature

Our Calculated values		Experimental peak position [111] (cm^{-1})	Previously Calculated peak position [110] (cm^{-1})
peak position (cm^{-1})	intensity		
130.9	0.129	122	144.2
152.1	0.092	164	193.5
349.3	0.122	372	391.3
485.8	0.215	456	380.0
511.6	0.289	514	525.4
565.2	0.098	595	561.3
932.1	0.337	949	896.7
969.5	0.300	970	977.1

Since the development of valid and transferable potential models is very crucial, it is important that the potential model and its parameters are able to reproduce all the existing phases of the crystal. For this reason, we tested the derived potential parameters by calculating the elastic constants (see Table 6.1.5) and infrared frequencies (see Table 6.1.6) for rutile-like GeO_2 crystal at room temperature. The calculated infrared frequencies for

rutile-like GeO_2 crystal compare well with available experimental data. In general, the calculated elastic constants for rutile-like GeO_2 crystal is in good agreement with experimental results[112], but also show an improvement over previously calculated values.[113, 114]

Table 6.1.5 Elastic constants for rutile- like GeO_2 crystal at room temperature

Elastic Constants (10^{11} Dyne/cm^2)	Our Calculated Values	Experimental Values (Ref. 112)	Previously Calculated Values (Ref. 113)	(Ref . 114)
C_{11}	326.0	337.2	300	492
C_{12}	145.2	188.2	97	238
C_{13}	240.5	187.4	143	239
C_{33}	610.9	599.4	474	679
C_{44}	159.8	161.5	150	197
C_{66}	232.4	258.4	93	165

Table 6.1.6 Infrared frequencies for rutile- like GeO_2 crystal at room temperature

Our Calculated peak position (cm^{-1})	Experimental peak position [65]
331	Broad band at 347 cm^{-1}
347	
351	
409	403 cm^{-1}
456	435 cm^{-1}
525	Broad band at 570 cm^{-1}
591	
609	
673	Broad band at 700 cm^{-1}
734	
788	

In conclusion, the lattice dynamics study described in this section suggests that it is possible not only to model, but also to predict various crucial properties of crystals by the use of appropriate potential models and computer modeling codes. The published results [89] for α-quartz-like GeO_2 crystal (presented in Tables 6.1.2, 6.1.3, and 6.1.4) are generally

in good agreement with the experimental data and show an improvement over previously developed potential parameters by another research group.[102] Furthermore, the potential parameters are also capable of reproducing the infrared frequencies, and elastic constants of rutile polymorph of GeO_2 crystal.

Conclusion

The present thesis has been motivated by the need to shed additional light on the structure of lead germanate glasses and the mechanism by which the 'germanate anomaly' occurs using MD. The specific goal of this thesis was to perform MD simulations of $xPbO.(1-x)GeO_2$ glasses with $x = 0.05 - 0.50$ to investigate the structural causes of the 'germanate anomaly', and to study the structural features of the germanate framework and the lead environment, including interatomic distances, coordination numbers, bond angle distributions, ring statistics, and percentage of NBOs at each composition.

Once we were confident that the 2-body potential model was able to reproduce the structure of GeO_2 glass consistent with experimental results, we concentrated on MD simulation of $xPbO.(1-x)GeO_2$ glasses with $x=0.50$. This is a composition where the controversy around the 'germanate anomaly' does not exist, and there is better agreement on the structural detail of the glass among experimental studies. The simulated glass was compared and found to be in agreement with experimental results from EXAFS and neutron diffraction studies.[16,19–22] Furthermore, the simulated $PbO.GeO_2$ glass at 50 mol% PbO content indicated the

presence of a secondary lead framework where lead acts as a network-former.

Molecular dynamics studies of xPbO. (1-x)GeO_2 glasses with x = 0.05, 0.1, 0.2, 0.25, 0.3, 0.33, 0.37, 0.45, and 0.50 were performed to investigate the influence of the PbO content on the GeO_2 framework. The results of these simulations indicated the continuous formation of NBOs with addition of PbO, and conversion of 9% of five-membered to three-membered GeO_4 rings with addition of up to 30 mol% PbO.

As for the proposed coordination change of Ge-O[18, 22] with respect to the 'germanate anomaly', formation of six-coordinated Ge^{4+} ions was not observed with the addition of PbO. However, formation of up to 8% five-coordinated germanium-oxygen ions is observed in the simulated glasses. At low PbO content, germanium ions are linked to four BOs and a high percentage of Q^4 species is obtained from simulations indicating that the germanate framework is highly polymerized. At high PbO content, the germanate framework becomes depolymerized and is made of GeO_4 units with one to four NBOs and high percentage of Q^3 to Q^0 species.

In order to further analyze the lead environment, the oxygen atoms bonded to individual germanium atoms were examined with respect to the lead framework. The simulations indicate a decrease in percentage of $n_{Pb=0}$ in these simulated glasses with addition of lead oxide which confirms the

presence of two regions in the glass, a lead-rich region and a germanium-rich region. Furthermore, the increased % of higher n_{Pb} confirms the connectivity of lead-rich regions via BOs. As for the role of lead in the glass framework, at low PbO content it acts as a network-modifier with high proportion of PbO_4 units and at high PbO content, lead acts as a network-former consisting of PbO_4 and PbO_3 units. Hence, the results of molecular dynamics simulations of xPbO. (1-x)GeO_2 glasses with x = 0.05–0.50 presented in this thesis show no evidence of the germanate anomaly in the simulated lead germanate glasses.

One of the criticisms of the use of a 2-body potential model has been that the lack of a multibody bonding term might result in bond defects and discrepancies in the O-Ge-O bond angle distributions. For this reason, we incorporated a combination of 2- and 3-body potential model in the simulation of GeO_2 glass. The inclusion of a 3-body bending term, however, did not improve the short range GeO_2 glass structure significantly.

In search of an improved potential model to study the germanate anomaly in lead germanate glasses, we used a combination of 2- and 3-body potential with a shell-model in the interaction potential. In order to test the validity of the developed potential parameters for the α-quartz-like GeO_2 crystal, infrared frequencies, lattice energy, bulk modulus, elastic

constants, static dielectric constants, high frequency dielectric constants, and heat capacity at constant volume were calculated and compared to available experimental results. The lattice dynamics study on α-quartz-like GeO_2 suggests that it is possible not only to model, but also to predict various crucial properties of crystals by the use of appropriate potential models and computer modeling codes. The potential was also capable of reproducing the infrared frequencies, and elastic constants of rutile-like GeO_2 crystal.

Future Work

Three-Body Simulation

The goal of this thesis has been to find the best potential model, as simple or complex as it might be, to simulate the structure of lead germanate glasses and to study the causes of the 'germanate anomaly.' One of the shortcomings of the simple 2-body simulation is the lack of 3-body bending term creates a large number of bond defects. The inclusion of a 3-body term has been shown to remove odd coordinated species in the structure and to give narrower PDFs and bond angle distributions. Although, no significant improvement in the short range order of the simulated 2-body (see section 4.1) compared to the simulated 2- and 3-body (section 5.1) GeO_2 glass was observed, the lead environment might greatly benefit from inclusion of a 3-body term and BMH potential model. The use of this potential model has been shown to improve the simulation of the lead environment of $PbO.SiO_2$ glasses and give a better separation of the first and second coordination shell with respect to Pb-O, Pb-Pb and Pb-Ge PDFs and CDFs.[82]

Hence, the first proposed study would involves MD simulation of lead germanate glasses using combination of 2- and 3-body BMH potential model described in section 2.3.2 of this paper. Glasses with compositions

of xPbO. (1-x)GeO_2 with x = 0.05, 0.1, 0.2, 0.25, 0.3, 0.33, 0.37, 0.45, 0.50 will be simulated. The results will be divided into two sections, the germanate framework and the lead environment. The results of these simulations will also be compared to the previous 2-body simulations of lead germanate glasses (section 4.3).

The characterization of the germanate framework would be done by calculation of Ge-O, Ge-Ge, O-O interatomic distances from PDF and coordination numbers from CDF. This would enable us to further study the existing controversy in the literature concerning the dominant coordination number of germanium ions at different PbO compositions and the mechanism for the 'germanate anomaly'. In order to get a better idea of Ge-O coordination, the percentage of all the different coordinations present in lead germanate glass at each specific PbO composition will be calculated enabling us to verify the formation of five- or six-coordinated Ge ions upon addition of PbO.

We would examine the short range order of the germanium ions by identifying the different types of oxygen atoms present in the glass, namely the percentage of BOs , NBOs and non-germanate anions (oxygen atoms that are not connected to the germanate framework).

To further examine the germanate framework, the distribution of Q^n species would be determined to identify the types of bonded germaniums for each individual oxygen atom.

The lead environment would be analyzed by determination of Pb-O, Pb-Pb interatomic distances and coordination numbers from PDFs and CDFs, respectively. In order to analyze the lead environment in the lead germanate glass, the oxygen atoms bonded to individual germanium atoms will be examined with respect to the lead framework.

Lattice Dynamics Simulation

In one of the previous studies[89], the implementation of a shell-model in the interaction potential and simulation of polarization enabled us, among other things, to simulate the Raman and infrared spectra of the GeO_2 crystal. A limitation of the Buckingham potential model is "the energy tends to minus infinity as the distance goes to zero. This can be overcome by the use of a four range Buckingham which also introduces a further degree of freedom by being able to specify the position of energy minimum." [101]

We would like to test the validity of this potential model for the simulation of glasses by first performing MD simulation of GeO_2 glass using a combination of 2- and 3-body Buckingham potential as described in section 2.3.3. Upon successful simulation of the base glass, the next study will involve the MD simulation of xPbO. (1-x)GeO_2 glasses with x = 0.05, 0.1, 0.2, 0.25, 0.3, 0.33, 0.37, 0.45, 0.50. The germanate framework and the lead environment will be characterized as previously described. We will also be able to compare the Raman and infrared spectra of the simulated glasses with available experimental studies in order to shed additional light on the mechanism of the 'germanate anomaly' and further validate the simulated structural properties.

Simulation of Doped PbO.GeO_2 Glasses

Rare earth doped glasses have important applications in optical devices and laser technology.[116] Er^{3+}-doped glasses have been of interest since a room temperature laser was developed at 1.5 μm, an excellent wavelength for optical communications. Erbium-doped lasers are also practical sources of short wavelength radiation for display and data storage applications.[117] For these applications, it has been determined that the

composition of the glass host plays an important role in the properties of the laser.[118] In the case of inorganic glasses, the Eu^{3+} ion is one of the most useful spectroscopic probes due to its simple electronic structure, and has been studied in combination with several classes of oxide and halide hosts.[119] Hence the MD simulation and detailed study of the local environment of Eu^{3+} and Er^{3+} doped ions in $PbO.GeO_2$ glass at different dopant concentrations is also of interest. The purpose of the simulations would be to investigate the effect of the dopant on the structure of $PbO.GeO_2$ glasses, and to examine the degree of dopant-dopant clustering at different dopant concentrations. In previous MD simulations of Er^{3+}-doped lead silicate glass performed by a member of our group, Er-Er clustering was observed at dopant concentrations $\geq 2\%$.[120] Dopant-dopant clustering affects the energy transfer by quenching the signal and its absence is crucial for application of glasses in fibre optics.

Appendix

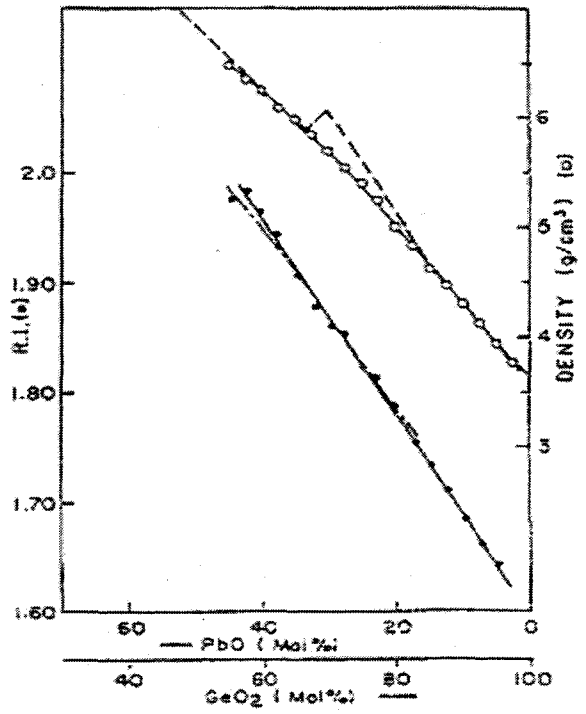

Figure A1: Compositional variation of density and refractive index for $PbO.GeO_2$ glasses (reproduced from reference. 14). *Dashed line* represent data from reference 63; *dot-dash* line represent data from reference 62.

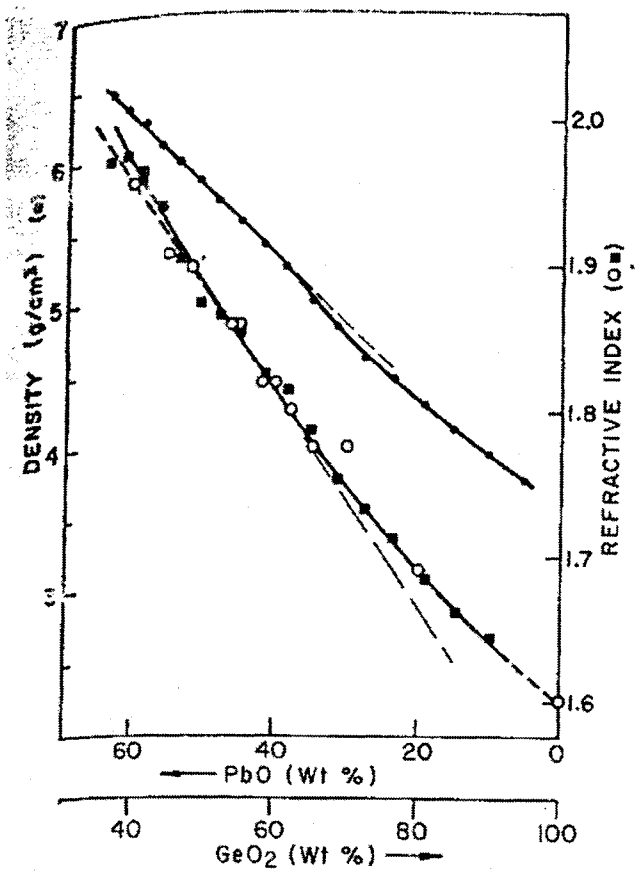

Figure A2: Compositional variation of density and refractive index for $PbO.GeO_2$ glasses (reproduced from reference 14); open circles represent data from reference 62; dark circles represent data from reference 14.

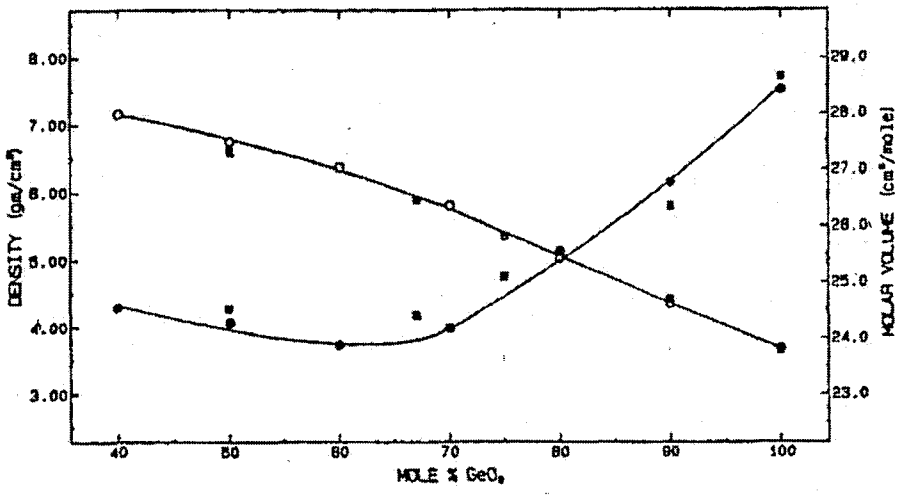

Figure A3: Compositional variation of density and molar volume for $PbO.GeO_2$ glasses (reproduced from reference 61); *open circles* represent data from reference 61; *dark squares* represent data from reference 4.

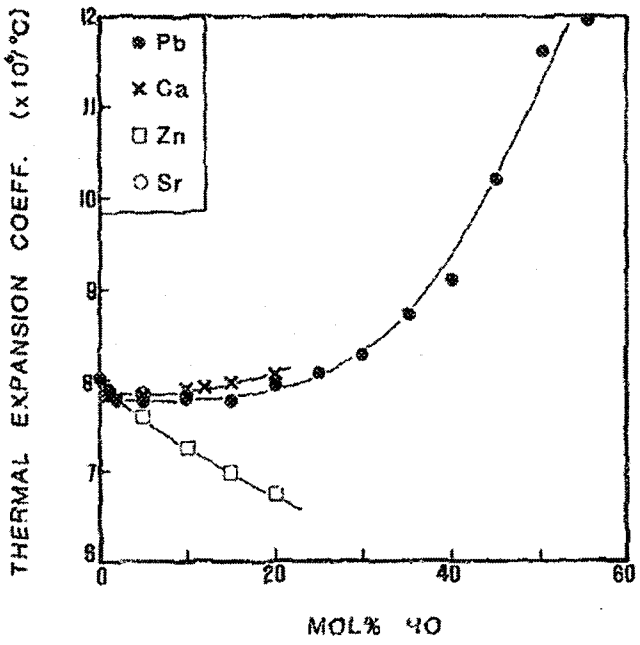

Figure A4: Compositional variation of thermal expansion coefficient for germante glasses (reproduced from reference 8).

Bibliography

1. M.B. Volf, Chemical Approach to Glass , Elsevier, N.Y. **7** (1984) 153.

2. J. Zarzycki, Glasses and the vitreous state, Cambridge University Press, N.Y. 1991, p. 11.

3. G.S. Henderson and D.R. Baker, The application of synchrotron radiation to the study of amorphous materials, In Synchrotron Radiation: Earth, Environmental and Material Sciences Applications, Mineralogical Association of Canada Short Course, 30 (2002) 159.

4. K. Nassau and D.L. Chadwick, J. Am. Ceram. Soc. **65** (1982) 195.

5. O. Ohtaka, A. Yoshiasa, H. Fukui, K. Murai, M. Okube, H. Takebe, Y. Katayama, W. Utsumi, J. Phys. Condens. Matter. **14** (2002) 10521.

6. J. Haines, J. M. Leger, C. Château, A.S. Pereira , Phys. Chem. Miner. **27** (2000) 575.

7. L. Huang and J. Kieffer, Phys. Rev. B **69** (2004) 224204.

8. J.E. Shelby, J. Am. Ceram. Soc. **66** (1983) 414.

9. H. Verweij and J. H. J. M. Buster, J. Non-Cryst. Solids **34** (1979) 81.

10. G. S. Henderson and H. M. Wang, Eur. J. Mineral **14** (2002) 733.

11. P. Rino and I. Ebbsjö, Phys. Rev. B **47**(1993) 3053.

12. C. Lin, J. Opt. Commun **4** (1983) 2.

13. D. Lezal, J. Pedlíková and J. Horák, J. Non-Cryst. Solids **196** (1996) 178.

14. J.A. Topping, I.T. Harrower and M.K. Murthy, J. Am. Ceram. Soc. **57** (1974) 209.

15. M. Imaoka, J. Ceram. Assoc. Jpn. **67** (1959) 364.

16. V.N Sigaev, I. Gregora, P. Pernice, B. Champagon, E. N. Smelyanskaya, A. Aronne and P.D. Sarkisov, J. Non-Cryst. Solids **279** (2001)136.

17. J.L. Ribeiro, J. Dexpert-Ghy, B. Piriou and V.R. Mastelaro, J. Non-Cryst. Solids **159** (1993) 213.

18. N. Umesaki, T. M. Brunier, A.C. Wright, A.C. Hannon and R.N. Sinclair, Physica B **213** (1995) 490.

19. H. Yamamoto, K. Kamiya, J. Matsuoka and H. Nasu, J. Ceram. Soc. Japan **101** (1993) 949.

20. Witkowska, B. Sikora, K. Trzebiatowski and J. Rybicki, J. Non-Cryst. Solids **352** (2006) 4356.

21. Witkowska, A. Madecka, K. Trzebiatowski, J. Kziedzic and J. Rybicki, Rev. Adv. Mater. Sci. **12** (2006) 112

22. L. Červinka, J.Bergerová, V.N. Sigaev and F. Rocca, J. Non-Cryst. Solids **293-295** (2001) 502.

23. J.P. Itie, A. Polian, G. Calas, J. Petiau, A. Fontaine and H. Tolentino, Phys. Rev.Lett. **63** (1989) 398.

24. A.W.Laubengayer and D.S.Morton, J. Am. Chem. Soc. **54** (1932) 2303.

25. W.H. Bauer and A.A. Kahn, Acta Cryst. B**27** (1971) 2133.

26. W.H. Bauer, Acta Cryst. **9** (1956) 515.

27. J.F. Sarver and F.A. Hummel, J. Am. Ceram. Soc. **43** (1960) 336.

28. W.Zachariasen, Z.Krist. **67** (1928) 226.

29. G.S. Smith and P.B. Isaacs, Acta Cryst. **17** (1964) 842.

30. K. M. Ault and R.A. Secco, Solid State Commun **98** (1996) 449.

31. K.J. Seifert, H. Nowotny and E. Hauser, Mh. Chem. **102** (1971) 100.

32. G. Gutierrez and J. Rogan, Phys. Rev. E **69** (2004) 031201.

33. M. Micoulaut , J. Phys.: Condens. Matter **16** (2004) L131.

34. A. Meyer, H. Schober and J. Neuhaus, Phys. Rev. B **63 (**2001) 212202.

35. J.A.E. Desa, A.C. Wright and R. N. Sinclair, J. Non-Cryst. Solids **99** (1988) 276.

36. E.A. Lorch, J. Phy. C. **2** (1969) 229.

37. J. F. Sarver and F.A. Hummel,J. Am. Ceram. Soc. **43** (1960) 336.

38. R.N Sinclair and A.C. Wright, The Physics of Non-Crystalline Solids (Aedermannsdorf: Trans Tech) 1977.

39. U. Hoppe, R. Kranold, H. J. Weber and A.C. Hannon, J. Non-Cryst. Solids **248** (1999) 1.

40. C.E. Stone, A.C. Hannon , T. Ishirawa , N. Kitamura, Y.Shirakawa , R. N. Sinclair, N. Umesaki and A. Wright, J. Non-Cryst. Solids **293-295** (2001) 769.

41. D. L. Price, M. L. Saboungi, A. C. Barnes, Phys. Rev. Lett. **81** (1998) 3207.

42. J. Zarzycki, Verres Refract. **11** (1957) 3.

43. A.J. Leadbetter and A.C. Wright, J. Non-Cryst. Solids **7** (1972) 37.

44. P. Bondot, Phys. Stat. Sol. **A 22** (1974) 511.

45. P. Bondot, Acta Cryst. **A30** (1974) 470.

46. M. Okuno, C.D. Yin, H. Morikawa and F. Marumo, J. Non-Cryst. Solids **87** (1986) 312.

47. D.E. Sayers, E. A. Stern and F.W. Lytle, Phys. Rev. Lett. **35** (1975) 584.

48. J. Neuefield and K.D. Liss, Ber. Bunsenges. Phys. Chem, **100** (1996) 1341.

49. A. Bodapati, M.M.J. Treacy, M. Falk, J. Kieffer and P. Keblinski, J. Non-Cryst. Solids, **352** (2006) 116.

50. W.H. Zachariasen, J. Am. Chem Soc. **54** (1932) 3841.

51. R. L.Mozzi and B.E. Warren, J. Appl. Crystallogr. **2** (1969) 164.

52. J.H. Konnert, J. Karle and G.A. Ferguson, Science **179** (1973) 177.

53. J.C. Phillips, J. Non-Cryst. Solids **63** (1984) 347.

54. J.C. Phillips, Solid State Commun. **60**(1986) 299.

55. F.L.Galeener, Solid state Commun. **44** (1982) 1037.

56. M. Micoulaut, Y. Guissani and B. Guillot, Phys. Rev. E **73** (2006) 31504.

57. V. Van Hoang, J. Phys.: Condens. Matter **18** (2006) 777.

58. A. F. Wells, structural inorganic chemistry, 4th ed., Clarendon, Oxford 1975.

59. B. Dickens, J. Inorg. Nucl. Chem. **27** (1965) 1495.

60. R. Soderquist and B. Dickens, J. Phys. Chem. Solids **28** (1967) 823.

61. J.E. Canale, R.A. Condrate, Sr., K. Nassau and B.C. Cornilsen, J. Can. Ceram. Soc. **55** (1986) 50.

62. B. Phillips and M. Scroger, J. Am. Ceram. Soc. **48** (1965) 398.

63. K.S. Evstropiev and A. O. Ivanov, Advances in Glass Technology Part II, edited by F.R. Matson and G.E. Rindone, Plenum Press, New York, 1963, p.79-85.

64. J.E. Canale, R.A. Condrate, Sr., K. Nassau and B.C. Cornilsen, J. Can. Ceram. Soc. **55** (1986) 50.

65. M. Madon, P. Gillet, C. Julien and G.D. Price, Phys Chem Mineral **18** (1991) 7.

66. V.N. Morozov, Neorganicheskie Materialy **5** (1969) 979.

67. V. N. Morozov, G. P. Tikhomirov, L.A. Kartseva and B.D. Matsoyan, Neorganicheskie Materialy **7** (1971) 296.

68. V.A. Kolesova, Fizika i Khimiya Stekla, **9** (1983) 257.

69. C.A. Worrell and T. Henshall, J. Non-Cryst. Solids **29** (1978) 283.

70. Z. Pan, D.O. Henderson and S.H. Morgan, J. Chem. Phys. **101** (1994) 1767.

71. J. Zarzycki, Glasses and the vitreous state, Cambridge University Press, N.Y. 1991, p. 43.

72. G. S. Henderson and H. M. Wang, Eur. J. Mineral **14** (2002) 733.

73. G.S. Henderson, J. Non-Cryst. Solids , **353** (2007) 1695.

74. H-J Weber, J. Non-Cryst. Solids **243** (1999) 220.

75. C.B. Azzoni, D. Di Martino, A. Paleari and R. M. Almeida, J. Non-Cryst. Solids **278** (2000) 19.

76. D. Di Martino, L.F. Santos, A.C. Marques and R. M. Almeida, J. Non. Cryst.Solids **293-295** (2001) 394.

77. A. Karthikeyan and R.M. Almeida, J. Non-Cryst. Solids **281** (2001) 152.

78. G. Cormier, T. Peres and J.A. Capobianco, J. Non-Cryst. Solids **195** (1996) 125.

79. A.C. Hannon, D. Di Martino, L. F. Santos, R. M. Almeida, J. Non-Cryst. Solids **353** (2007)1688.

80. C.R.A. Catlow, R.G. Bell and J.D. Gale, J. Mater. Chem. **4** (1994) 781.

81. G. Cormier, "Molecular Dynamics Simuation and Crystal-Field Theory: Predicting the optical spectra and structure of rare-earth doped inorganic glasses", PhD. Thesis, Concordia University, 1993.

82. T. Peres, Application of a Three-body Potential Model and Crystal Field Calculation to the Simulation of Eu^{3+}, Er^{3+} and Yb^{3+} Environments in $PbO.SiO_2$ glass, PhD. Thesis, Concordia University, 1999.

83. E. Sourial, Molecular Dynamics Simulation: An Investigation into the Short Range Structure of Metaphosphate Glasses, MSc. Thesis, Concordia University, 1998.

84. K.S. Evstropiev and A. O. Ivanov, Advances in Glass Technology part II, edited by F.R. Matson and G.E. Rindone, Plenum Press, New York, 1963, p.79-85.

85. L.V. Woodcock, C.A. Angell and P. Cheesman, J. Chem. Phys. **65** (1976) 1565.

86. L.Verlet, Phys. Rev. **159** (1967) 98.

87. A. Nordsieck, Math. Comput., **16** (1962) 22.

88. J. M. Haile, Molecular Dynamics Simulation, Elementary Methods, John-Wiley and Sons Inc., New York ,1992.

89. E. Ghobadi and J.A. Capobianco, Phys. Chem. Chem. Phys. **2** (2000) 5761.

90. S.K. Mitra and R.W. Hockney, philos.Mag . B**48** (1983) 151.

91. R.D. Shannon and C.T. Prewitt, Acta Cryst. B**25** (1969) 925.

92. E.J.W. Whittaker, R. Muntus, Geochimica et Cosmochimica Acta **34** (1970) 945.

93. B.P. Feuston and S.H. Garofalini, J. Chem Phys. **89** (1988) 5818.

94. J.D. Gale, Phil. Magazine B **73** (1996) 3.

95. B.G. Dick and A.W. Overhauser, Phys. Chem. Solids **3** (1958) 20.

96. J.D. Jorgensen, J. appl. Phys. **49** (1978) 5473.

97. R. L.Mozzi and B.E. Warren, J. Appl. Crystallogr. **2** (1969) 164.

98. J. Huheey , Inorganic Chemistry , Principles of Structure and Reactivity , Harper Collins College, N.Y. fourth edition, 1993.

99. K.Sugii, H. Iwasaki and S. Miyazawa, Journal of Crystal Growth **10** (1971) 127.

100. M. Micoulaut, L. Cormier and G.S. Henderson, J. Phys: Condens. Matter **18** (2006) R753.

101. J.D. Gale and A.L. Rohl, Mol. Simul. **29** (2003) 291.

102. A.R. George and C.R.A. Catlow, J. Solid State Chem.**127** (1996) 137.

103. CRC handbook of chemistry and physics, Cleveland , Ohio, 2007.

104. Balitskil O. Yu. Sil'vestrova, Crystallography Reports **45** (2000) 145.

105. M. Grimsditch, A. Polian, V. Brazhkin and D. Balitskii, J. Appl. Phys. **83** (1998) 3018.

106. Y. Yashiro, A. Yoshiasa , O. Kamishima, T. Ishii and H. Maeda, J. Phys IV France **7** (1997) 1175.

107. K. De Boer, A. P.J Jansen, R. A. Van Santen, G. W. Watson S.C. Parker, Phys. Rev. B. **54** (1996) 826.

108. N. Suresh, G. Jyoti, S.C. Gupta, S.K. Sikka, Sangeeta and S.C. Sabharwal, J. Appl. Phys., **76** (1994) 1530.

109. N.Soga, J. Geophys. Res. **76** (1971) 3983.

110. T. Sato and J. Suda, J. Phy. Soc. Japan. **67** (1998) 3809.

111. Ph. Gillet, A. Cleach and M. Madon, J. Geophys. **95** (1990) 21635.

112. H. Wang and G. Simmons, J. Geophys. Res. **78** (1973) 1262.

113. R. D. Oeffner and S.R. Elliott, Phy. Rev. B **58** (1998) 14791.

114. T. Tsuchiya, T. Yamnak and M. Matsui, Phys. Chem. Miner. **25** (1998) 94.

115. B. Houser, N. Alberding, R. Ingalls and E.D. Corzier, Phys. Rev. B. **7** (11), 6513, 1988.

116. M.J. Weber, J. Non-Cryst. Solids **123** (1990) 208.

117. P.Xie and S.C. Rand, Appl. Phys. Lett. **63** (1993) 3125.

118. S. Zemon, G. Lambert, L.J. Andrews, W.J. Miniscalco, B.T. Hall, T. Wei and R. C. Folweiler, J. Appl. Phys. **69** (1991) 6799.

119. W.M. Yen and P.M. Selzer, Laser Spectroscopy of Solids, Springer- Verlag, Berlin, 1981, p.189.

120. T. Peres, D.A. Litton, J.A. Capobianco and S.H. Garofalini, J. Non-Cryst. Solids **221** (1997) 34.